PROTEIN STRUCTURE AND ION BINDING
IN POTASSIUM SELECTIVE CHANNELS

APPROVED BY SUPERVISORY COMMITTEE

Youxing Jiang, Ph.D.

Paul Blount, Ph.D.

Philip Thomas, Ph.D.

Elizabeth Goldsmith, Ph.D.

In memory of Dr. Harry John Sauer Jr.

And dedicated to the family, friends and colleagues who have made this possible. Most especially I want to thank Nathan DeCarolis, Scott Younger, Greg Kunkel, and Juan Mendoza who were compatriots on this journey and Jennifer Hovis who helped me with my first steps on this path.

PROTEIN STRUCTURE AND ION BINDING IN POTASSIUM SELECTIVE CHANNELS

by

David Bryant Sauer

DISSERTATION

Presented to the Faculty of the Graduate School of Biomedical Sciences
The University of Texas Southwestern Medical Center at Dallas
In Partial Fulfillment of the Requirements
For the Degree of

DOCTOR OF PHILOSOPHY
The University of Texas Southwestern Medical Center at Dallas

Dallas, Texas
August, 2012

PROTEIN STRUCTURE AND ION BINDING
IN POTASSIUM SELECTIVE CHANNELS

DAVID BRYANT SAUER, Ph.D.
The University of Texas Southwestern Medical Center at Dallas, 2012

Youxing Jiang, Ph.D.

Potassium channels play a central role in a number of biological processes, most classically the action potential of excitable cells in multicellular organisms. These channels are defined by their selective conduction of potassium to the exclusion of other monovalent ions as governed by a common sequence and structural motif, the selectivity filter. This structure, made of backbone carbonyls and threonine side chains, directly coordinates the ions as they diffuse through the channel and appears central to this sub-angstrom discrimination between cations. Utilizing the non-selective Sodium and Potassium conducting channel (NaK) as a structural scaffold the mechanisms of both ion selectivity and formation of this selective structure are examined.

Table of Contents

Prior Publications

Liao J, Li H, Zeng W, **Sauer DB**, Belemares R, Jiang YX (2012) Structural Insight into the Ion Exchange Mechanism of Sodium/Calcium Exchanger. *Science* 335: 686-690

Sauer DB, Zeng W, Raghunathan S, Jiang YX (2011) Protein Interactions Central to Stabilizing the K+ Channel Selectivity Filter in a 4-sited Configuration for Selective K+ Permeation. *Proc Natl Acad Sci USA* 108:16634-16639.

Derebe MG, **Sauer DB**, Zeng W, Alam A, Shi N, Jiang YX (2011) Tuning the Ion Selectivity of Tetrameric Cation Channels by Changing the Number of Ion Binding Sites. *Proc Natl Acad Sci USA* 108:598-602.

Hull MC, **Sauer DB**, Hovis JS (2004) The Influence of Lipid Chemistry on the Osmotic Response of Cell Membranes: Effect of Non-Bilayer Forming Lipids. *J Phys Chem B* 108:15890 -15895.

List of Figures

List of Tables

List of Appendices

List of Abbreviations

KcsA	Potassium channel from *Streptomyces lividans*
NaK	Sodium and Potassium conducting channel from *Bacillus cereus*
eag	Ether-a-go-go gene encoding a potassium channel
hERG	Human Ether-a-go-go Related Gene
CNG	Cyclic Nucleotide Gated
HCN	Hyperpolarization-activated Cyclic Nucleotide gated
Na_V	Voltage-gated Sodium channels
Ca_V	Voltage-gated Calcium channels
K_V	Voltage-gated Potassium channels
K_{ir}	Inwardly Rectifying Potassium channels
K_{2P}	Two-Pore Potassium Channels
K_{Ca}	Calcium-activated Potassium channels
MthK	Potassium channel from *Methanothermobacter thermautotrophicus*
K_{ir}Bac	Bacterial orthologs of Inwardly Rectifying Potassium channels
P_X/P_K	Relative permeability of substrate X relative to potassium
NaK2K	Potassium selective NaK channel mutant
NaK2CNG	CNG channel mimicking mutant of the NaK channel

Chapter 1. Introduction

Membrane Structure and Permeability

The boundaries of all cells are defined by a lipid membrane which envelops the cellular volume. (Fig 1.1) The phospholipids that make up this membrane have both a hydrophilic moiety and some number of hydrophobic acyl tails and with this amphipathic nature these lipids spontaneously form multi-molecular structures to achieve an energetically stable state in aqueous solution. Specifically, those lipids that make up a cell membrane form a two-dimensional sheet termed a bilayer. This structure, with hydrophilic portions facing the aqueous milieu and the acyl chain tails forming a hydrophobic core, presents a strong energetic barrier against the spontaneous diffusion of polar or charged solutes (1).

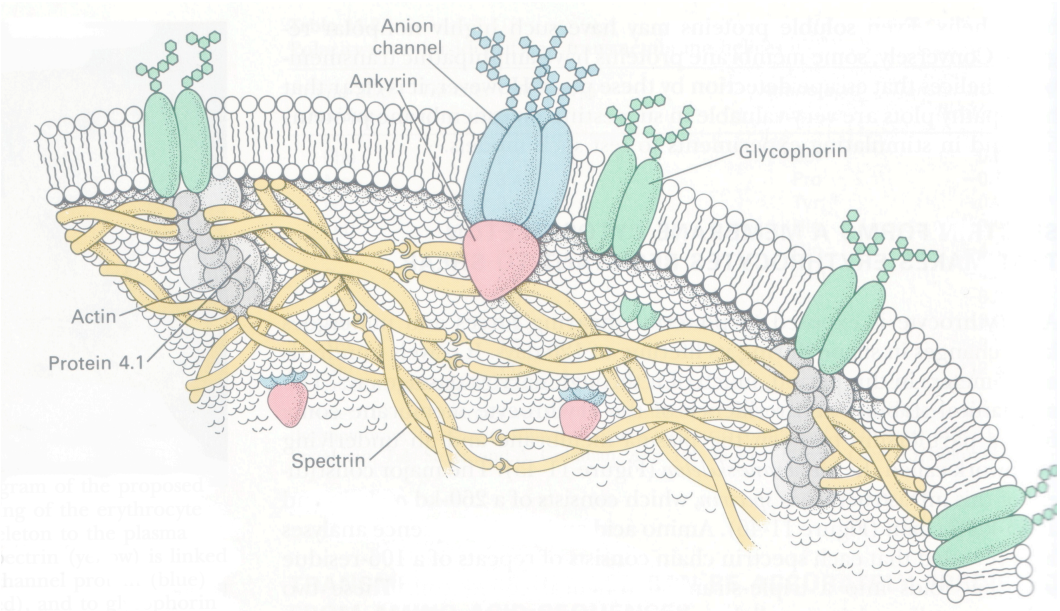

Figure 1.1. Structure of a eukaryotic cell membrane. The membrane is made up of lipids, primarily phospholipids, though it also includes cholesterol, sphingolipids and glycolipids. Within the membrane reside membrane proteins which act to transport signals and substrates across the bilayer. Figure reproduced from (2).

These membranes defines the boundaries of both the cell and its internal compartments and the hydrophobic barrier segregating biochemical reactions within the cell (3). Organisms both utilize and need to overcome the diffusional impediment this membrane presents to the movement of solutes. Notably nutrients, waste products and information all need to be moved across these membranes. To overcome this barrier organisms have evolved a number of strategies to allow for the regulated import and export of substrates and signals of biological importance. Membrane proteins that reside within the membrane catalyze and control these processes (4). A number of mechanisms have been devised, some specific only to single domain or kingdom of life, while others are maintained throughout evolution from bacterial to mammals. In humans an estimated 27% of the human proteome is made up of alpha-helical membrane proteins (5). These include receptors for carrying information, transporters to import or export substrates, and enzymes to catalyze chemical reactions near or within the membrane.

Organisms have evolved to use membranes as a means to store energy, in addition to acting as an organizational structure (6). The asymmetric partitioning of solutes, ions or small molecules, gives rise to both chemical and in some cases electrical gradients that the cell can use both as an energy store and in information signaling. For example, in mammalian skeletal muscle sodium, calcium, and chloride are notably more concentrated outside while potassium is concentrated within the cell; these ionic differences giving rise to a resting potential below -60mV. (Table 1.1) Similar electrochemical gradients are found in all kingdoms of life and can further be differentially used within the organelles of a single organism. In multicellular organisms, these gradients are most classically used in the efficient long distance transmission of information by electrically excitable cells, notably in nervous tissues. However, within those same cell types asymmetric calcium partitioning into the ER and

proton gradients across the membrane of the mitochondrion are fundamental aspects of the function of those organelles. Exploiting the energy invested and biological need for this solute asymmetry, a number of toxins, including antibiotics, act by neutralizing this electrochemical gradient to the detriment of the target organism (7, 8).

Ion	Extracellular concentration (mM)	Intracellular concentration (mM)	$\frac{[Ion]_o}{[Ion]_i}$
Na^+	145	12	12
K^+	4	155	0.026
Ca^{2+}	1.5	100 nM	15,000
Cl^-	123	4.2	29

Table 1.1. The resting free ion concentration in Mammalian skeletal muscle. Figure reproduced from (3).

Channels and Transporters

The transport proteins that reside within the membrane were classically first identified by their functional role in model organisms, characterized by their functional behaviors, and then further studied in model systems as the specific genes were identified. Grossly, transport proteins are separated into channels and carriers, where channels simply open a hole in the membrane which allows substrate to diffuse down its electrochemical gradient while carriers must undergo discrete binding and unbinding events, each with an associated conformational change. (Fig 1.2)

Among the carriers, there is a further series of subdivisions based on the need and source of energy for ligand transport. While uniporters simply move a ligand by simple diffusion, there are a number of discrete energy coupled transporter families where the substrate can be concentrated against its electrochemical gradient using the free energy associated with a coupled second reaction. (Fig 1.2B) Symporters link the

transport of the desired cargo to the co-tranport of a second energetically favored ligand. (Fig 1.2C) Conversely, antiporters couple ligand movement to the flow of a second substrate in the opposite direction; again with a net decrease in free energy. (Fig 1.2D) Alternatively, the ABC Transporters and P- and V-type ATPases use the energy of ATP hydrolysis to drive ligand transport. (Fig 1.2E) While it can be convenient to generally describe gene families discretely as either channels or carriers these divisions are occasionally blurred by cases of transporter family members having evolved into channels and the reverse (9, 10).

Given the differences of mechanism for transporting ligands across this lipid barrier, the kinetics of moving ligands across the membrane couple to the energetic source. Grossly these differences in mechanism give rise to discrete regimes of activity, where the kinetics of the energetic source, substrate binding, and necessary protein rearrangement limit the rate of transport and the ability to accumulate substrate (3). ATPases generally are the slowest but can generate the greatest ligand asymmetry, while channels only allow energetically favored substrate movement but do so the quickest, at up to diffusion limited rates.

A common feature noted as being of biological importance and correspondingly frequently used as a means of discriminating between membrane transporters is ion selectivity. This selectivity is defined as the relative flux of ions to relative to some reference ion. The biological role of some transporters clearly depends upon their ability to recognize the appropriate substrate with high fidelity, while in other cases an indiscriminate nature is central to their function, as is the Na/K-ATPase and multi-drug resistance transporters, respectively (11, 12). Gradations in selectivity may underly the physiological role of some transporters whose selectivity is diminished relative to their evolutionary ancestors, as in the cases of theCyclic Nuclotide Gated (CNG) and Hyperpolarization activated Cyclic Nucleotide gated (HCN) channels (3, 13, 14).

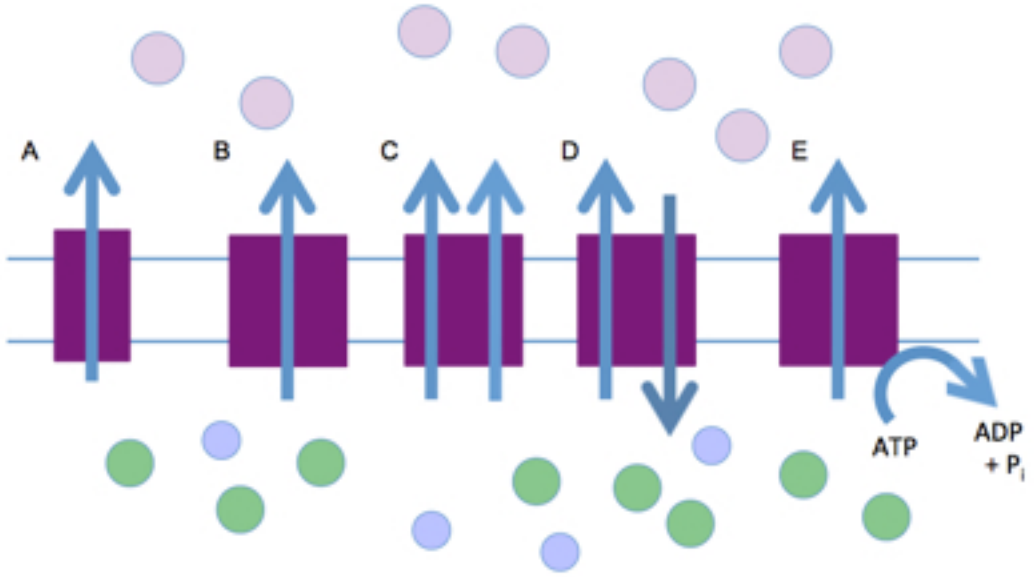

Figure 1.2. Cartoon of major membrane transporter classes, demonstrating the distinct mechanisms of substrate transport. Depicted are the (A) channel and (B) Uniporters which transport without an energetic source. (C) Symporters and (D) Exchangers/Antiporters couple transport of the ligand to another, energetically favored, substrate. (E) ATPases, including the V- and F-type and ABC transporters, couple transport to the hydrolysis of ATP.

Chapter 2. Ion Channels

Channels

In contrast to the slower kinetics of carriers, channels rapidly conduct ions down their electrochemical gradient (3). This flux can be orders of magnitude higher than the carrier rates. Channels accomplish this fast ionic flux by providing a continuous pathway across the membrane which the ions traverse by simple diffusion. While the overall gating process can be kinetically complex, the open state is usually generalized as a single conductive state, in contrast to carriers' multi-step transport cycle.

Within electrically excitable tissues it is the coordination of multiple ionic currents that give rise to the action potential. (Fig 2.1) This depolarization and repolarization wave is mediated by a number of ion channel genes with varying selectivity and kinetic properties. Generally, some external stimuli depolarizes the local membrane from the resting potential. If the depolarization is above a threshold potential it activates voltage gated sodium and calcium channels, which rapidly open and allow sodium and calcium into the cytosol, further depolarizing the membrane. These sodium channels then rapidly inactive. This change in the local electric field activates adjacent voltage gated sodium channels, propagating the signal down the cell body. Restoration of the membrane potential begins with the opening of voltage gated potassium channels, which open with slower kinetics and allow potassium to flow out of the cell. Finally, these voltage gated potassium channels inactivate and ATPases and transporters restore the resting ionic concentrations across the plasma membrane. Mis-regulation of these signals, in selectivity or gating, can be caused by either drug effects or naturally occurring mutations and lead to a number of diseases in humans including long QT syndrome, adenomas and blindness (15-17).

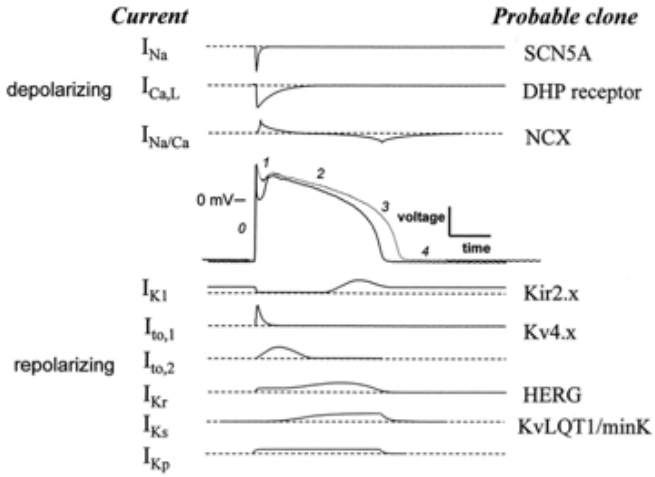

Figure 2.1. The action potential is composed of discrete currents mediated by a number of selective ion channels. Depolarizing currents respond to the initial stimulus and depolarize the local membrane and rapidly inactivate. Subsequent channels and transporters repolarize the membrane and restore the electrochemical gradients. Figure reproduced from (18).

Channels, including voltage-gated channels, have been found in all kingdoms of life, though their biological role in prokaryotic and archaeal organisms is not well understood where action potential like signaling is unexpected (19-22). However, as proteins in microbes tend to be smaller and more readily expressed in standard protein expression systems they usually are more amenable to experimentation and have served as valuable models for the study of basic channel biophysics (23, 24).

When initially identified by a variety of genetic, biochemical or pharmacological studies channels were organized into families based upon substrate specificity and gating mechanism. With further genetic information, some of the disparate families have been further organized into larger superfamilies. The largest of these is the tetrameric cation channel family which includes the notable branches of Na^+, K^+, Ca^{+2}, CNG and HCN channel families (5, 25). (Fig 2.2)

The tetrameric cation channel superfamily was recognized based on a common topology and domain structure within channels of diverse function (26). Minimally, this superfamily contains a pore domain defined as two transmembrane helices linked by a sequence termed the P-loop (27). (Fig 2.4A) It is this P-loop which contains a sequence characteristic for each family that is believed to define selectivity (Fig 2.3) with four domains being required to form a single ion conduction pathway (28). These domains can be encoded on a single polypeptide or multiple peptides, including separate genes forming a single heterotetramer pore. While channels within this superfamily are quite diverse with differences in selectivity, size, and mechanism of gating; this single domain structure is common throughout. Genes encoding the channel domain alone are commonly seen in prokaryotes, though eukaryotic channels usually have additional domains that regulate channel gating in response to stimuli such as membrane voltage or ligand binding (25, 29).

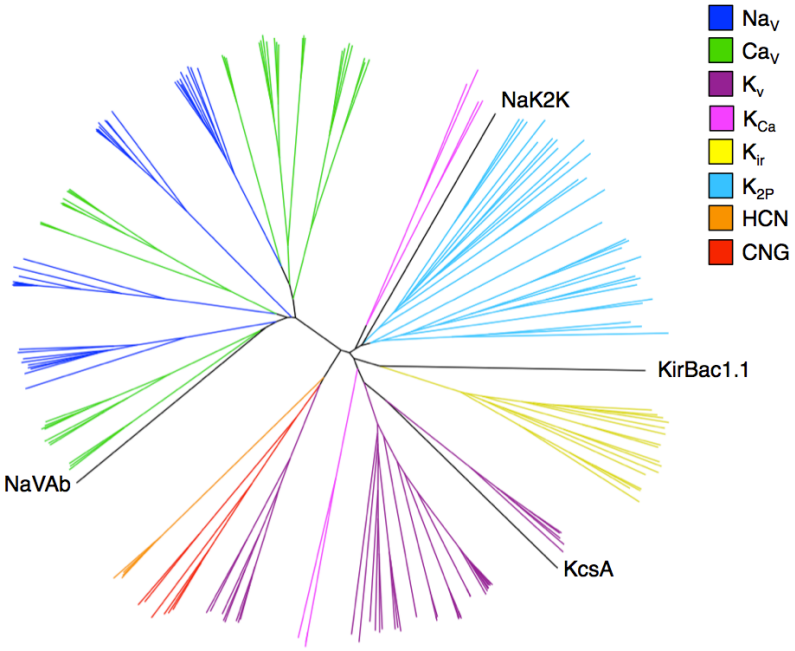

Figure 2.2. The NaK2K channel is most similar to potassium selective channels. Phylogenetic tree of tetrameric cation channels. Phylogenetic tree constructed with the pore domains only of representative tetrameric cation channels and bacterial homologs with crystal structures.

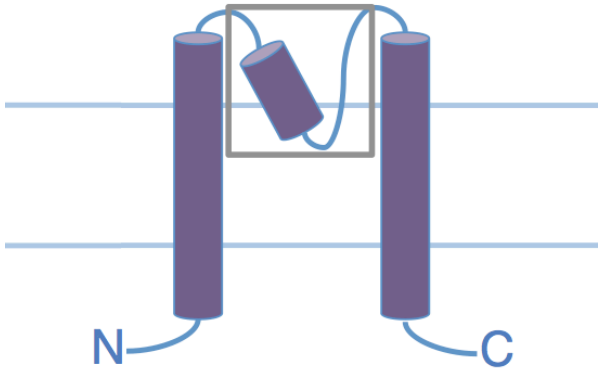

Figure 2.3. The secondary structural context of the P-loop. The P-loop (boxed) is between the transmembrane helices of the pore domain of tetrameric cation channels.

These P-loop sequences are conserved in each family and distinct between channels of differing selectivity, belying their central role in ion discrimination (13). (Fig 2.3) Variations in this sequence, either by natural differences or experimental mutation, frequently alter selectivity in these channels, further underlining their central role in selectivity (30). It should be noted that while the potassium channel P-loops are frequently 4-fold symmetric this is not necessarily the case for all of the tetrameric cation channels, most notably sodium and calcium channels where the filter is asymmetric by differences in the sequences contributing to the tetrameric pore. Such asymmetry can arise from non-identical pore subunits encoded on a single polypeptide or hetreotetramerization of differing channel subunits.

K^+ Channels

Within the potassium channels there are three major sub-families, organized by sequence, predicted structure, and physiological behavior. (Fig 2.2) These are the Voltage gate (K_v) and Calcium gated Potassium

channels (K_v and K_{Ca}) [31, 32], the Inward Rectifier Potassium channels (K_{Ir}) [33], and the Two Pore Potassium channels (K_{2P}) [34]. Within the K_{Ir} and K_{2P} channel families the protein frequently contains additional extra-membrane domains but generally do not have additional transmembrane domains. (Fig 2.4B & C) However in the K_v and K_{Ca} families can have voltage gating domains, or analogous domains that may be vestigial, which add an additional 4-5 transmembrane helices, in addition to soluble regulatory domains. (Fig 2.4B, D & E) In contrast, prokaryotic orthologs tend to be smaller, with out any additional transmembrane helices [24]. (Fig 2.4 A &B)

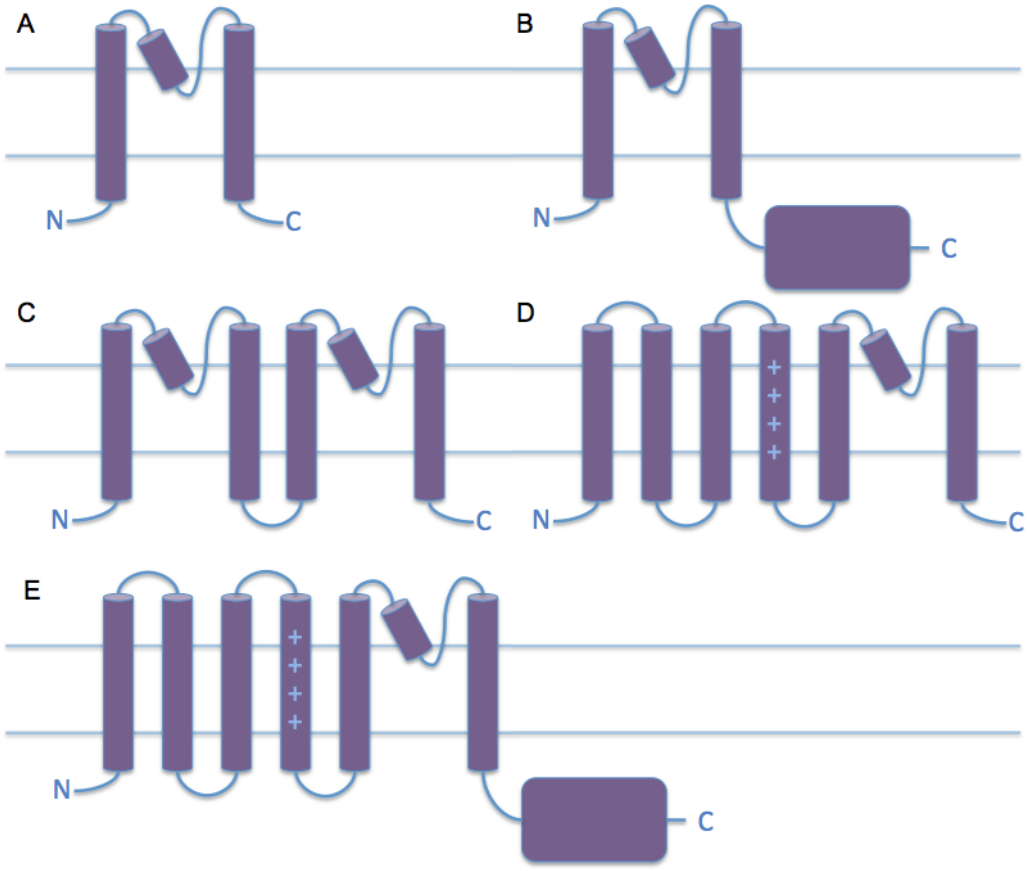

Figure 2.4. Domain organization of K^+ channels. Potassium channels have divergent domain organization but share a common pore domain. (A) The pore domain of K^+ channels, minimally required for potassium selectivity. (B) K^+ channel domain with C-terminal regulatory domain. Examples include wild-type KcsA and MthK [35, 36]. (C) Two pore potassium channels where the complete channel pore is believed to form by dimerization. Examples include TWIK and TRAAK [37, 38]. (D) Voltage gated potassium channels. The N-terminal voltage sensing domain regulates channel opening in response to membrane voltage, such as in the shaker channel and K_vAP [39, 40]. (E) Potassium channels with both a voltage sensing domain and ligand binding domain. These channels include BK and MlotiK1 [41, 42].

All of these potassium channels have a common conserved sequence motif within the P-loop connecting a short pore helix and the second transmembrane helix, termed the signature sequence (13, 30). (Fig 2.3) Generalized as TVGYG, it has been shown that mutations within this sequence lead to variations in selectivity or a conductively dead channel suggesting a central role for this sequence in ion conduction. In particular, both absolutely conserved glycine residues are particularly sensitive to mutation. In distantly related HCN and CNG channels the signature sequence has clear variations from the canonical potassium channel sequence, corresponding their lack of selectivity between sodium and potassium (13, 14). (Figs 2.2 and 2.3)

	Delayed rectifier			Inward rectifier	M current	BK K(Ca)
Ion	Frog node	Frog muscle	Snail neuron	Starfish egg	Frog neuron	Rat muscle
Tl^+	2.3	—	1.29	1.5	—	1.2
K^+	1.0	1.0	1.0	1.0	1.0	1.0
Rb^+	0.91	0.95	0.74	0.35	0.94	0.67
NH_4^+	0.13	—	0.15	0.035	0.11	0.11
Cs^+	<0.077	<0.11	0.18	<0.03	0.10	<0.05
Li^+	<0.018	<0.02	0.09	—	<0.004	<0.02
Na^+	<0.010	<0.03	0.07	<0.03	<0.004	<0.01
$H_2NNH_3^+$	<0.029	—	—	—	—	—
Methylammonium	<0.021	—	—	—	<0.004	—

Table 2.1. Relative ion permeability of K^+ channels. Potassium channels have markedly low sodium permeability to sodium, though less selectivity agains rubidium and cesium. Table of relative ion permeabilities (P_X/P_K) of Potassium Channels, reproduced from (3).

Using this characteristic signature sequence potassium channels are able to discriminate with high precision and accuracy between sodium and potassium, the most highly concentrated cations found at the plasma membrane of animals, despite the smaller ionic radius of sodium. (Tables 1.1 and 2.1) Potassium channel selectivity is usually described as a permeability ratio relative to K^+ (P_X/P_K, where X is the second ion for

comparison) and P_{Na}/P_K is typically less than 0.01 in canonical potassium channels (43). The mechanism by which the K^+ channels select their substrate is unknown as, in addition to size, there are differences in the related charge density and dehydration energy between the two ions. Despite this stringent selectivity, potassium ions can pass through some K^+ channels at near diffusion limited rates (3, 44). However, these same potassium channels are typically unable to exclude larger monovalent cations, with Thallium, Rubidium and Cesium having permeabilities greater than 0.1 relative to potassium.

The first theories of selectivity, before individual channels were identified functionally, were descriptions of channels as molecular sieves, where ions were selected by size exclusion (3). With the identification of the potassium channel and others, new theories were devised to account for selective conduction of larger ions to the exclusion of small ions. The initial model of selectivity was an equilibrium electrostatic model, where selectivity depends on the electric field strength of the ion binding site within the channel (45). Another theory of selectivity in potassium channels was the snug-fit model, where the distances of the coordinating ligands within the pore were thought to be optimized to the distance of a water molecule in the first hydration shell of a potassium ion (46). As the sodium ion is smaller, with a correspondingly smaller hydrations shell, its binding within a binding site of the a potassium channel would be energetically unfavorable.

With the first structure of the tetrameric cation channel, the pore domain of the potassium channel from *Streptomyces lividans* (KcsA), many previously inferred features of tetrameric channels were directly observed (47). Representing only the ion conduction pathway, the channel polypeptide contains two transmembrane helices connected by a helix-loop structure, over a portion of which the ion is directly coordinated by the polypeptide and is termed the selectivity filter. (Fig 2.5B) In the case of

KcsA four polypeptides come together to form a single, four-fold symmetric ion conduction pathway. (Fig 2.5A) In the initial KcsA crystal structure the channel is clearly in a closed state, where the internal gate is closed with the second transmembrane helices forming a bundle crossing too narrow for an ion to pass. A consequence of this closed structure is an enclosed aqueous volume contained within the pore domain termed the cavity. Notably, the selectivity filter is formed by the $_{75}$TVGYG signature sequence which adopts a novel structure where permeating ions were coordinated largely by the carbonyls of the peptide backbone. These ion binding sites were identified initially by discrete binding of rubidium or cesium, used as a more strongly diffracting surrogates for potassium.

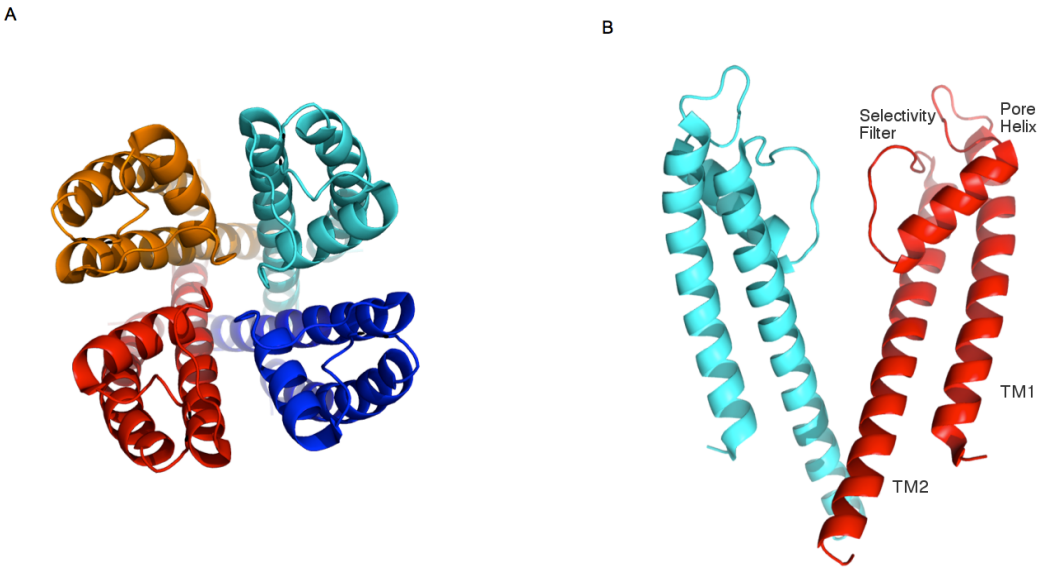

Figure 2.5. The secondary and tetrameric quarternary structure of the KcsA channel pore (47). (A) View from the extracellular solution of the KcsA tetramer. (B) View from the membrane plane of the KcsA fold. The front and back subunits have been removed for clarity. Though crystallographically equivalent each symmetry related subunit is colored uniquely for clarity.

Following on this work, the high resolution structure of KcsA was solved (48). While again in a closed state, the selectivity filter with bound potassium ions can now be unambiguously described. (Fig 2.6) Clearly seen are four ion binding sites, formed by the backbone carbonyls of the

signature sequence and hydroxyl side signature sequence's conserved threonine. Labeled sites 1-4, from the external to cytoplasmic sides, each of these binding sites contains a well ordered potassium ion; in addition to partially dehydrated ions seen at the extracellular face of the filter and a fully hydrated potassium ion within the cavity. In the presence of a low concentration of potassium, and therefore the predominant ion within the crystallization solution is sodium, the filter of KcsA adopts a "collapsed" structure where the filter structure significantly changes and no longer forms a continuous pathway for ions to traverse.

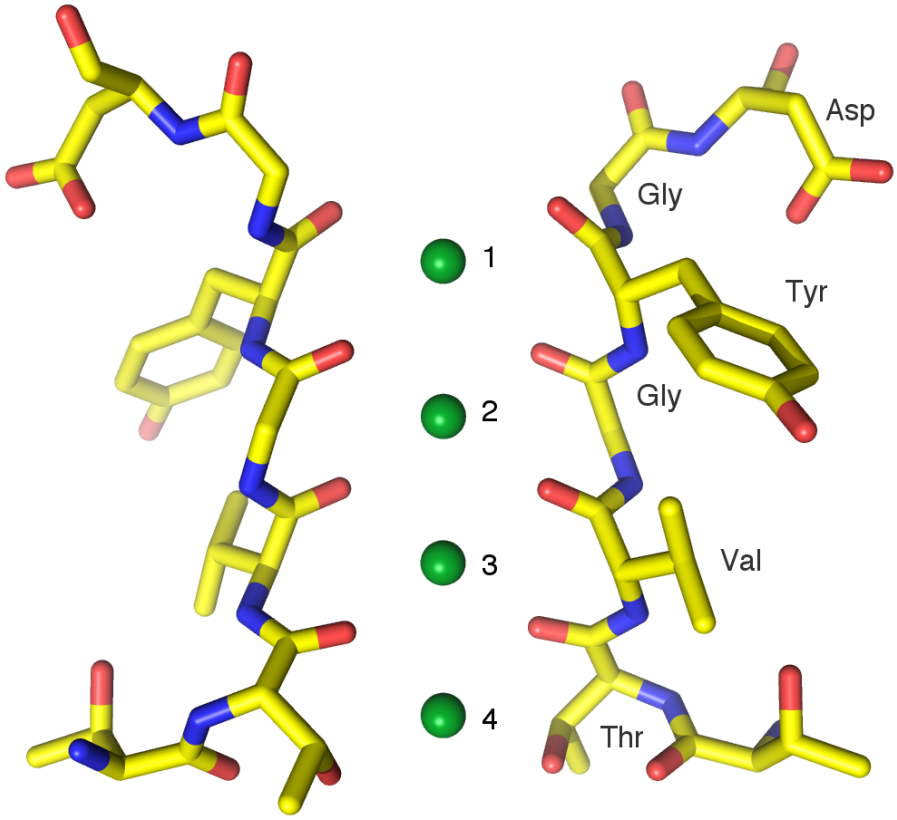

Figure 2.6. Structure of the KcsA ion selectivity filter (48). Structure of the KcsA selectivity filter with K^+ ions drawn as green spheres. The four potassium ions within the filter are bound completely dehydrated by backbone carbonyls of residues 75-78 and the Thr75 side-chain hydroxyls. The front and back subunits removed for clarity.

Interestingly, the filter collapse of KcsA can be abrogated by a synthetic mutation within the channel filter (49). Replacing the central glycine (Gly77) of the signature sequence with a D-Ala amino acid locks the channel in a conductive state when crystallized in a low potassium environment. This synthetic mutation is necessary as glycine, the only achiral amino acid, is in a left handed configuration within the KcsA filter (50). The mutant channel remains potassium selective demonstrating that selectivity is intrinsic to the non-collapsed filter structure.However, in the absence of potassium the synthetic channel can conduct sodium, suggesting that selectivity arises through competition of ions within the filter.

It is notable that that the electron density within the filter was not equivalent between potassium and rubidium in the high resolution KcsA structures, though both ion are known to conduct through the channel (44). Despite similar ion profiles within the filter at low K^+ or Rb^+ concentration, the electron density is relatively uniform for potassium at higher concentrations with equivalent intensity at all four ion binding sites. In contrast, density was notably absent at site 2 in KcsA crystals at even at 300mM rubidium concentrations. These results correlate well the fact that both ion have similar currents at low concentration but increasing potassium concentration results in higher flux while rubidium flux saturates with increasing concentration. These combined structure and function results suggest that with high concentration potassium ions can move through the four energetically equivalent sites, with two ions occupying site 1 and 3 or sites 2 and 4. Such an equivalence is not see with rubidium, resulting in an energetic barrier for rubidium ions traversing the pore and resulting in the slower kinetics of ion conduction.

With the high resolution KcsA structure and those of other potassium channels the mechanism of potassium selectivity, most notably the robust conduction of potassium to the exclusion of sodium, began to

be directly examined. Structures of a number of prokaryotic and eukaryotic potassium channels have been solved, illustrating a number of different protein architectures (36, 39-41, 51, 52). Most of these structures highlighted different mechanisms for gating, such as voltage or ligand dependent gating. Pertinent to the issue of selectivity, however, all contain a similar signature sequence (TVGYG) and adopt similar filter structures. This common sequence and structure appears to underly a common mechanism of selectivity.

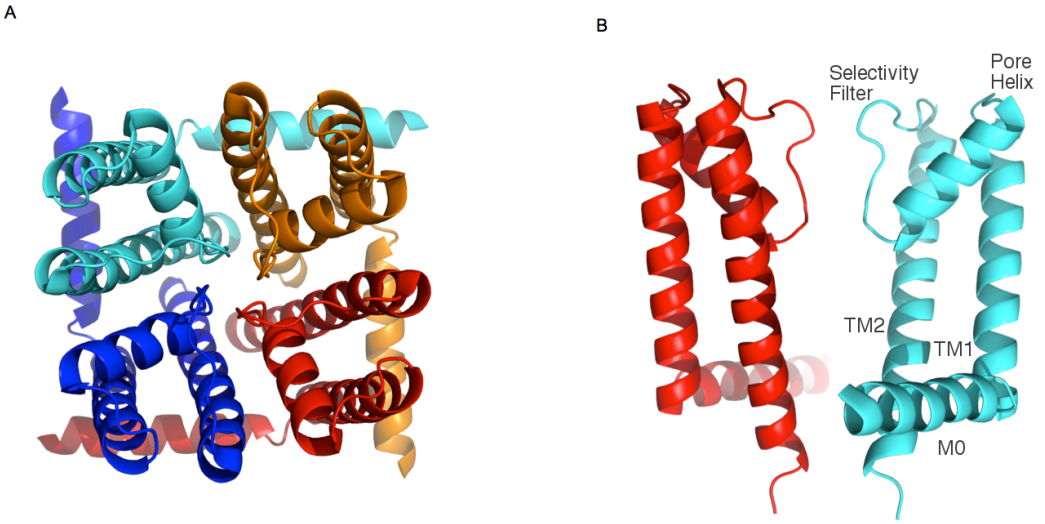

Figure 2.7. The tetrameric quarternary and secondary structure of the NaK channel (53). (A) View from the extracellular solution of the NaK tetramer. (B) View from the membrane plane of the NaK fold. The front and back subunits have been removed for clarity. Though crystallographically equivalent each subunit is colored uniquely for clarity.

The first non-potassium selective tetrameric cation channel crystallized was the Sodium and Potassium conducting channel (NaK) cloned from *Bacillus cereus* (53). Initially proposed as a CNG channel pore homolog, the overall pore fold is similar to that of the previous potassium channels. (Fig 2.7) The signature sequence of $_{63}$TVGDG contains an acidic amino-acid, distinct from the classic potassium channel and reminiscent of the CNG channel filter sequence. (Fig 2.3) In addition to this sequence difference the filter structure of the NaK is clearly distinct

from those of potassium selective channels. (Fig 2.8) The two most intracellular ion binding sites are maintained, corresponding to the conserved TVG filter sequence of both NaK and K^+ channels, but sites 1 and 2 are remodeled to form an enlarged vestibule and external ion binding site. Electrophysiological and flux assays of the radioactive tracer $^{86}Rb^+$ show this channel to be non-selective between sodium and potassium. (Fig 2.9) However, structurally there is no change in the filter structure in the presence of either sodium or potassium. With a higher resolution structure it became apparent that within the two ion binding sites of the NaK channel the potassium ions bound via the classical K^+ channel like coordination chemistry (Fig 2.8A), while sodium ions bound to different sites within the same filter structure. (Fig 2.8B) This was direct structural evidence contradicting the snug fit model of selectivity as it demonstrated that the ion binding sites could be used by smaller ions without necessitating a change in the filter structure.

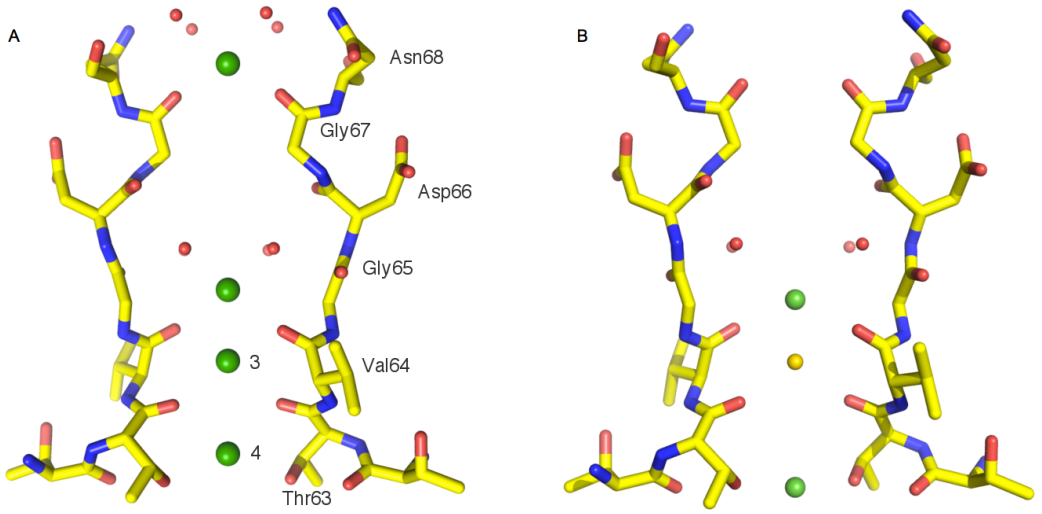

Figure 2.8. Structure of the NaK selectivity filter (54). (A) The structure of NaK crystallized in potassium. Potassium ions bind at sites 3 and 4 in a similar mode to KcsA. In the vestibule and at the external binding site potassium ions bind coordinated by backbone carbonyls and four symmetry related water molecules. (B) The structure of NaK crystallized in sodium. Sodium binds in plane with the hydroxyl of Thr63 and backbone carbonyls of Val64. Bound within site 3 is a strongly diffracting contaminant ion modeled as cesium. K^+, Na^+ and Cs^+ ions drawn as dark green, light green and yellow spheres, respectively.

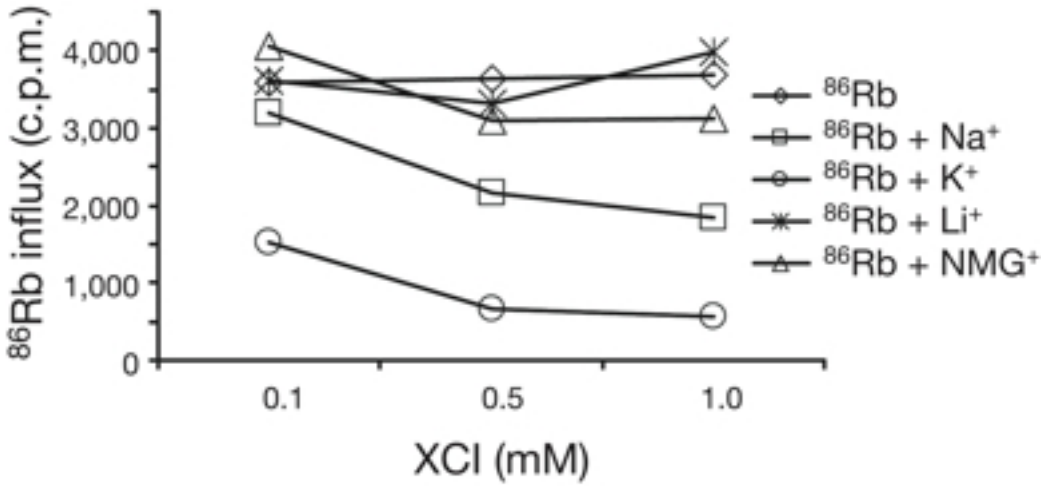

Figure 2.9. The NaK channel conducts both sodium and potassium, as demonstrated by $^{86}Rb^+$ flux competition assay (53). Rubidium permeation is decreased by the flux of the permeant potassium and sodium ions, while the impermeant lithium and NMG have no effect.

Similarly, the high resolution structure of the MthK pore domain in the presence of only sodium also demonstrated a potassium selective channel could bind sodium within the canonically potassium filter without a structural change in the protein (55). (Fig 2.10) Sodium is seen to bind in plane with the carbonyls of Gly63 (site 4) of MthK soaked in 100% NaCl. Interestingly, while the merged diffraction data of crystals soaked in 99% NaCl/1% KCl indicates equivalent density across all four binding sites, the anomalous difference peaks show markedly weaker potassium binding at site 2 and less so at site 4. This demonstrates some amount of in-equivalence in sodium versus potassium competition for each of the filter binding sites. Corresponding to this maintained filter structure in the absence of potassium, sodium currents were observed in the absence of potassium, similar to the results of the KcsA D-Ala channel (49).

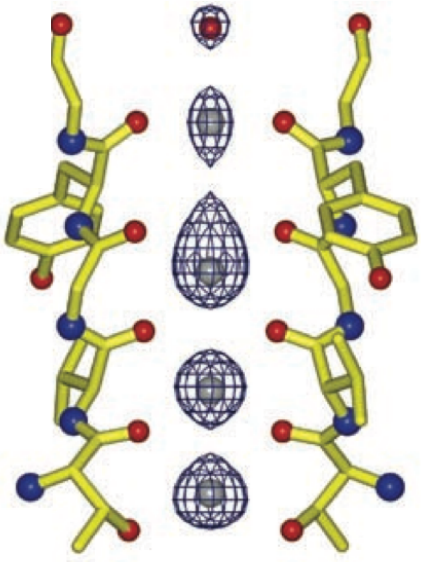

Figure 2.10. Sodium binds in the MthK pore with distinct binding sites from potassium (55). MthK pore structure and Fo-Fc ion omit map of the MthK pore soaked in 100mM Na^+, 0mM K^+. The ion omit map is contoured at 5σ.

The recently available structure of a sodium selective channel Na_VAb from *Arcobacter butzleri* illustrates the differences between sodium and potassium selective channels (56). While the overall fold of the pore domain is grossly similar to potassium selective channels, there is are some notable difference in the structure. A helix-loop-helix motif links the pore lining transmembrane helices, where two anti-parallel pore helices are connected by a loop forming the selectivity filter. This selectivity filter is shorter and wider overall than that of potassium channels suggesting incomplete dehydration of the permeant ions and a distinct mechanism of selectivity from K^+ channels where a single high field strength site determines the preferential Na^+ to K^+ conduction.

Mechanisms of Selectivity

With the availability of the potassium channel filter structure a number of theories were developed for selectivity based on biophysical properties and computational simulations (57-62). While many propose mechanisms for potassium versus sodium selectivity, it should be noted that some proposals are not mutually exclusive and may represent some of the multiple requirements of K^+ selectivity.

Initial study of the KcsA structure lent credence to some proposed mechanisms of potassium selectivity and unambiguously invalidated others. The static K^+ crystallized structure agrees well with the sung-fit model as the potassium ions observed in the filter are at the center of square anti-prism binding sites, with ion-oxygen distance similar to what would be expected for the first hydration shell of potassium in water (46, 48, 63). (Fig 2.6) Such a result explains how potassium channels can conduct at high rates, with minimal energetic cost of the ion transferring from water to the filter. Additionally, these ligand-ion distances were though to reflect a role of distance restraints in selectivity, as they are ideal for coordinating potassium but not the shorter distance expected to coordinate the smaller sodium. To coordinate a sodium ion was

hypothesized to require a structural change in the filter, with an associated energetic cost. Correspondingly, when KcsA was crystallized in the presence of sodium the selectivity filter structure changes significantly, adopting a non-conductive state. This change to the collapsed state is believed to reflect the necessity of potassium to stabilize KcsA in a conductive configuration.

The primary direct criticism of the snug-fit hypothesis, as it applies to KcsA and other potassium channels, is that the thermal motion of the protein is greater than the size difference between sodium and potassium (64). As there is only a 0.38Å difference in Pauling radius between sodium and potassium a snug-fit mechanism of selectivity seems implausible as the high resolution structure of KcsA has filter B-factors corresponding to a positional root mean square deviation of ~0.75Å and similarly large movements are modeled in molecular dynamics simulations. In addition, other K^+ selective channels and channel mutants can conduct sodium in the absence of potassium, suggesting the filter collapse cannot be the sole mechanism of selectivity.

In molecular dynamics simulations of the KcsA filter suggested differences in the free energy of solvation between sodium and potassium which were found to favor sodium when the repulsion between carbonyl backbone coordinating ligands is removed (64). An extension of the field strength principle of selectivity, these results suggested that while the free energy of binding sodium was lower than potassium with the high field strength carbonyls, the carbonyl-carbonyl repulsion of the more tightly packed ligands disfavors such a binding event. Further molecular dynamics studies comparing KcsA and NaK structures assert that while the structure of sites 3 and 4 appear the same between both channels, the access of water to the ion binding cages allows sodium to more easily permeate NaK (65). As the permeant ion is increasing coordinated by water, selectivity is lost with the decreased ligand dipole strength.

Other studies highlighted the preferred coordination number of the alkali ions in water (66). Calculating the preferred number of carbonyl or water molecules in the first hydration shell of each ion by molecular dynamics simulation, there is a direct correlation with atomic number where sodium is optimally coordinated by 6 ligands and potassium by 7. Further, for each hydration number there is a preferred geometry to the coordinating ligands, where the 8 coordinate state of potassium matches the carbonyl square anti-prism coordinated potassium ion within the selectivity filter KcsA.

Further studies on potassium channels have illustrated that, in addition to conducting sodium in the absence of potassium, sodium on the cytoplasmic side of the membrane acts as a voltage dependent channel blocker of potassium currents (67). Structurally, when crystallized in lithium KcsA no longer undergoes filter collapse as it did in sodium (68). The authors assert that a lithium ion binds in plane with the carbonyl moieties of between sites 3 and 4, though direct observation of the ion is not possible. Building off this uncollapsed KcsA structure, and evidence that both sodium and lithium act as fast blockers of KcsA, it was proposed that while the lowest energy state of potassium is the octadentate binding in the center of the ion binding site, sodium can be coordinated equatorially by the carbonyl ligands within the same protein structure and ionic interactions by ions bound at two sites give rise to potassium selectivity. This proposal partially matches with the NaK and MthK sodium structures, where sodium is seen to bind preferentially in plane with the carbonyl and hydroxyl groups of the filter. (Fig 2.8B & 2.10)

With the initial structure of an Na_V channel, the mechanisms of sodium selectivity can be addressed (56). The structure agrees well with an electrostatic model of selectivity. The narrowest point in the selectivity filter is defined by a ring of Glu side chains, presenting a high electric field site where a partially dehydrated Na^+ ion can preferentially bind over K^+.

As the filter structure and chemistry are clearly distinct from K^+ channels, and the NaK channel, sodium channels clearly use a distinct means of ion selectivity.

Folding of the Selectivity Filter

Despite the central role of the selectivity filter to potassium versus sodium discrimination, only limited studies have been carried out into how this structure is formed and stabilized by the protein which surrounds the filter. The initial low resolution KcsA structure described a cuff of aromatic amino-acids, from the pore helix and selectivity filter, which pack around the filter (47). With the high resolution structure of KcsA, the selectivity filter was seen to be directly stabilized by a network of hydrogen bonds between the filter and the pore helix (48). (Fig 2.11) The aromatic packing interactions noted in the low resolution structure are also a part of this hydrogen bond network between a glutamate on the pore helix, aspartate following the signature sequence, a buried water molecule and backbone amides the selectivity filter. Though un-noted in the high-resolution structure paper (48), a tryptophan on the pore helix is also involved in this network, hydrogen bonding to the aspartate. Later structures of other potassium selective channels had similar networks noted, though an acidic amino acid at the position equivalent to glutamate in KcsA is only seen in the KirBac and K_{ir} families of channels (51, 52, 69).

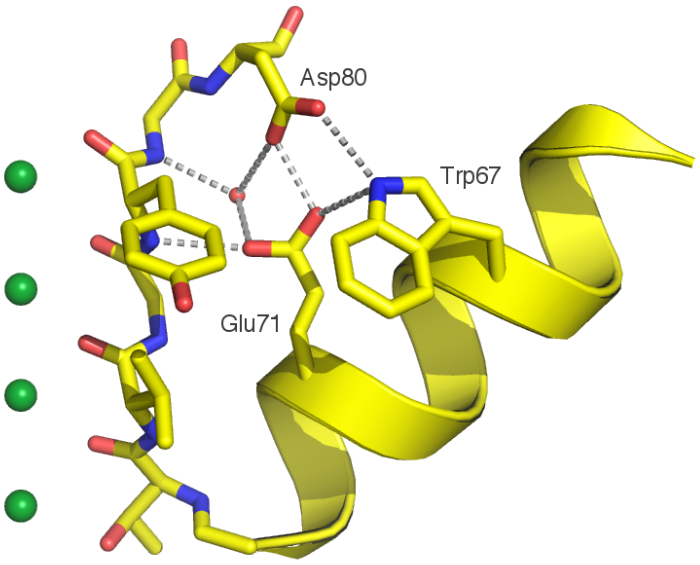

Figure 2.11. Extensive intermolecular bonds within the KcsA pore stabilize the selectivity filter (48). The pore helix and filter of KcsA is stabilized by a hydrogen bond network involving the side chains of Trp67, Glu71, Asp80 and the main chain amides of Tyr66 and Gly67. Water molecules and K^+ ions are drawn as red and green spheres, respectively.

The Inwardly Rectifying Potassium (K_{ir}) channels are known to have packing around the filter distinct from the previously crystallized channels as they had a distinct set of conserved residues in the P-loop. Rather than the hydrogen bond network seen in KcsA and the KirBac channels, the K_{ir} channels have a conserved pair of acidic and basic amino acids which functionally are required for selectivity and permeation (69). These conserved pairs were proposed to be structurally linked by a salt bridge. With the solution of the eukaryotic K_{ir} channel, $K_{ir}2.2$ from *Gallus gallus,* the salt bridge was confirmed and appears to structurally link the filter and pore helix in an analogous way to that seen in KcsA and KirBac (51). (Fig 2.12)

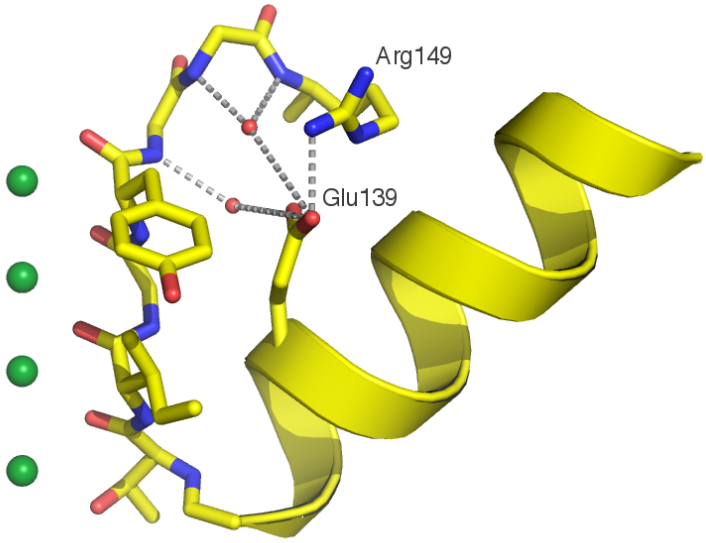

Figure 2.12. A salt bridge stabilizes the filter within the pore of $K_{ir}2.2$ from *Gallus gallus* (51). The pore helix and filter of $K_{ir}2.2$ is stabilized by a salt bridge between Glu139 and Arg149 and hydrogen bond network involving the side chains of Glu139 and the main chain amides of Gly147, Phe148 and Arg149. Water molecules and K^+ ions are shown as red and green spheres, respectively.

In the non-selective NaK channel, the two cytoplasmic binding sites are formed by the $_{63}$TVG residues as might be expected given their identity to the equivalent sequence within the filter of K^+ channels. However, the external binding site and vestibule appear to be stabilized by the orientation of Asp66, which points toward the external face of the protein and makes a hydrogen bond with the backbone amide group of Asn68 (53, 54). (Fig 2.13A) Later work showed that neutralization of the hydrogen bond acceptor at position 66 changed the filter stability around the vestibule and external binding site (70). Intermolecularly, there are three buried water molecules which link the backbone between subunits in an extensive hydrogen bond network.

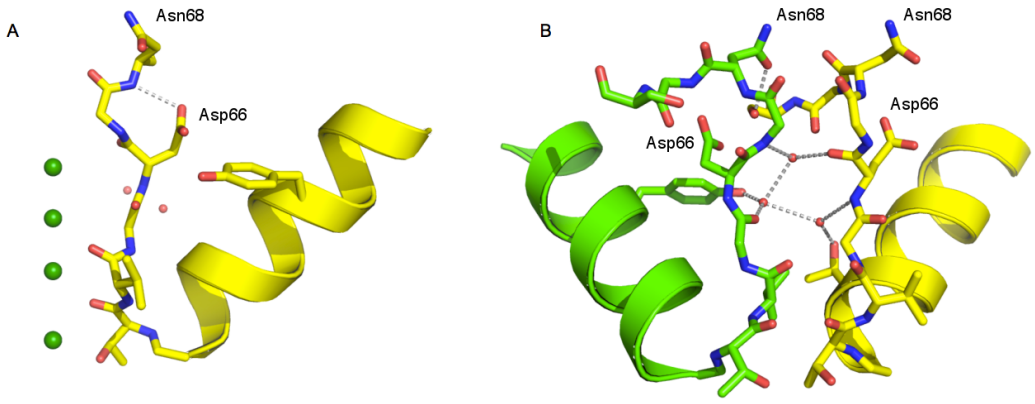

Figure 2.13. Intra- and intermolecular bonds within the NaK channel act to stabilize the filter (53). (A) The intramolecular hydrogen bond between Asp66 and the amide nitrogen of Asn68. (B) The inter-subunit bonds between two adjacent NaK filters, colored green and yellow for clarity. Inter-subunits bonds are mediated by Asn68 and Ser70 directly and in a a hydrogen bond network involving Tyr55, Thr60, amide nitrogen of Gly67, the backbone carbonyls of Gly65, both backbone carbonyl and amid nitrogen of Asp66. Water molecules and K^+ ions are shown as red and green spheres, respectively.

Further mutations were made on the NaK channel, engineering it to better resemble the CNG channel filter sequence and therefore study the ion conduction properties of this non-selective tertrameric cation channel family (71). The NaK filter sequence $_{63}$TVGDGNFSP was replaced with TVGETPP (NaK2CNG-E), TVGDTPP (NaK2CNG-D) and TVGNTPP (NaK2CNG-N). While the original wild-type NaK channel filter structure was proposed as a model of the CNG channel pore, these mutations illustrated that minor differences in sequence can give rise to major structural and biophysical effects. In the NaK2CNG mutants the filter now has three ion binding sites, structurally and chemically equivalent to sites 2-4 of KcsA. (Fig 2.14) The peptide backbone that formed external ion binding site and vestibule in NaK has rearranged into an ion binding site analogous to site 2 in KcsA. While the filter architecture is similar between the three NaK2CNG mutants, the packing of the side chains around this

structure are involved in distinct intra- and inter-subunit hydrogen bonding networks between the pore helix, selectivity filter and buried water molecules. (Fig 2.15)

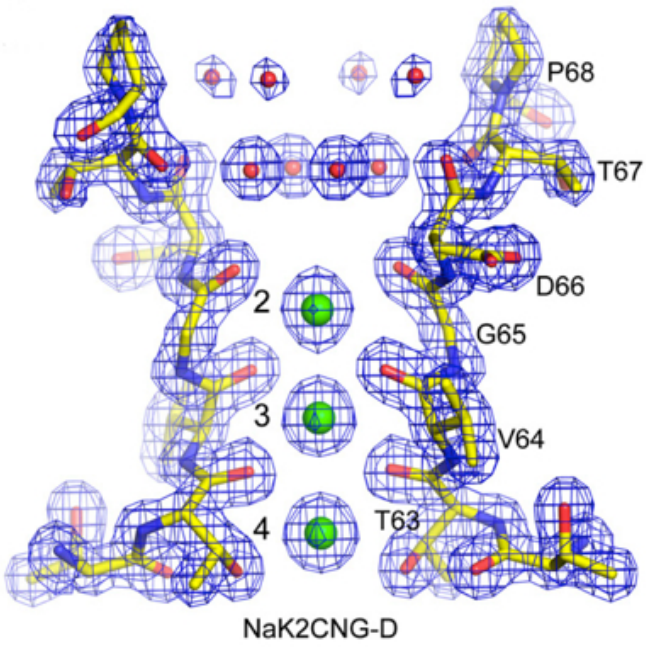

Figure 2.14. The NaK2CNG-D channel has a filter with three discrete potassium binding sites (71). Structure of the NaK2CNG-D selectivity filter with 2Fo-Fc electron density map contoured at 2σ. Binding sites are labeled 2-4, corresponding to equivalent sites in KcsA. Potassium ion and water molecules are colored green and red, respectively.

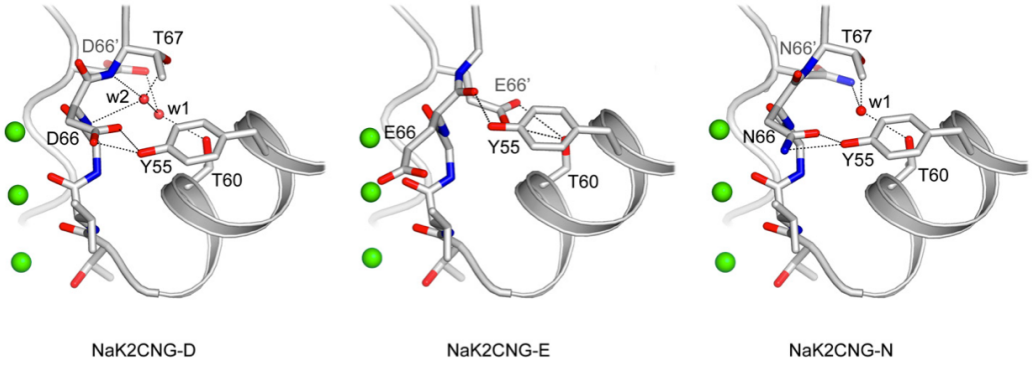

Figure 2.15. Intra and inter subunit hydrogen bonding differences in the NaK2CNG mutants are apparent despite similar selectivity filter structures and subtle differences of filter sequence (71). Despite similarities in sequence the packing around the filter varies between NaK2CNG-D, NaK2CNG-E and NaK2CNG-N. Side chains and water molecules involved in stabilizing the filter are shown as sticks and red spheres, respectively. Potassium ions within the filter are shown as green spheres.

Channel Inactivation

In addition to selectivity, the regulated opening and closing of the channel termed gating, plays an important role in the physiological function of many channels (3). The gating process of a channel regulates the duration and timing of ion flux through the pore and is in turn regulated both by external stimuli and the primary sequence of the protein. Beyond the stimuli induced channel opening some channels have the additional property of inactivation, a mechanism by which an open channel becomes non-conductive despite the continued presence of a channel opening signal. (Fig 2.16)

Within the potassium channels there are two types of inactivation, N- and C-type, named for the region of the protein which is responsible for the activity. In N-type inactivation, the so-called ball-and-chain mechanism, the amino-terminus of a protein directly interacts with the pore of the open channel to block the flow of permeant ions. (Fig 2.16C) This amino-terminal inactivation domain can be provided by either the channel itself or an associated regulatory protein. Alternatively, C-type inactivation occurs by changes within the selectivity filter itself, though the mechanism itself is not fully understood. It is believed during C-type inactivation the selectivity filter structure changes to a non-conductive state, though distant portions of the protein may regulate this process. (Fig 2.16D)

As KcsA is the only inactivating potassium channel for which high resolution structures are available it has become the structural model for the inactivation process. Without an extended N-terminal sequence, the inactivation observed for KcsA cannot be N-type. The bonds which appear to stabilize the selectivity filter also appear to play a role in the inactivation process (72). Mutations of the glutamate on the pore helix have been studied in particular for their role in changing the C-type inactivation

kinetics of KcsA (73). Structural differences in the filter between mutants, both the protein structure and buried water molecules, have been noted; as have differences in protein dynamics by B-factors and molecular dynamics simulations. These results suggest that destabilization of the filter, through the residues surrounding the signature sequence, underlies the C-type inactivation process.

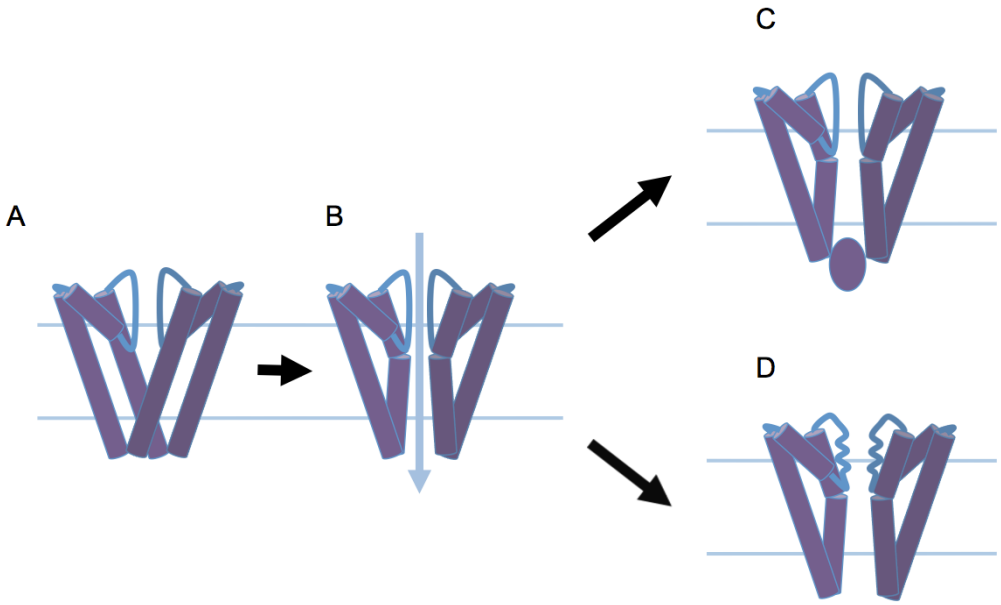

Figure 2.16. Channels block ion conduction after opening (inactivate) by a pair of distinct mechanisms. (A) A channel in the closed state. Upon some stimulus the channel activates (B) opening the cytoplasmic gate by bending at the glycine hinge on the inner transmembrane helix. The channel can then undergo inactivation by either N-type inactivation (C) where a peptide occludes the ion conduction pathway or C-type inactivation (D) where the structure of the filter changes to some non- or less conductive state.

Chapter 3. Methodology

Potassium Channel Studies

The aim of this work is to understand potassium channel selectivity, both the direct mechanisms of ion selectivity and the corresponding constraints on protein sequence, structure, and electrostatics that govern this selectivity. While much has been done previously to explain K^+ channel selectivity, most work is based around theoretical studies (59, 62), simulations (61), or mutational work of structurally uncharacterized channels (74). What structural information that is available focuses on the high resolution KcsA structure which has the added complexity of undergoing filter collapse structurally and inactivation functionally (72).

As the NaK channel represents a homolog of the potassium channel family it provides a useful tool for understanding potassium selectivity and its relation to the amino acid sequence which forms and surrounds the selectivity filter. (Fig 1.5) The selectivity filter of NaK has only a single difference from the canonical signature sequence and the overall fold of the pore domain is the same as the known potassium channels (53). (Fig 1.6) However, despite these similarities, the filter structure of NaK is markedly different from the K^+ selective channels. NaK has only two of the four contiguous ion binding sites characteristic of potassium channels, equivalent to sites 3 and 4. While the binding mode of potassium within those sites is similar to KcsA, binding in the center of square anti-prisms made by backbone carbonyls and threonine hydroxyls, NaK is clearly functionally non-selective between sodium and potassium.

The ability to routinely get high resolution structures of the NaKNΔ19 channel construct in a variety of ionic conditions serves as a good platform for the structural study of filter packing and ion selectivity (75). In addition, the ability to get clear single channel electrophysiological data on purified and reconstituted channels carrying the additional F92A mutation, distant from the selectivity filter, allowed for unambiguous

functional characterization and direct comparison of structure and function. Further, NaK has also proven robust to protein engineering, where channels extensive mutations been both crystallized and functionally characterized.

The close homology between NaK and the K^+ channel family's filter and its placement in the K^+ channel clade of the tetrameric cation channel superfamily suggested that NaK would serve as a good model system for understand how sequence could drive the structure of the filter and function within the potassium channel family. Mutants of NaK generated can be both structurally and functionally tested, with further validation by bioinformatics and testing of analogous mutations in canonical potassium selective channels. The results demonstrate a correlation between filter architecture and selectivity and allow for a description of the packing necessary for forming a potassium selective channel.

Bioinformatic Coupling Analysis

The ion_trans and ion_trans2 channel families were downloaded from Pfam (76) and aligned using the Promals3D server (77). Sequences containing the TVGYG within the filter region were retained and histograms of the position dependent amino-acid distribution were calculated as previously described (78).

Phylogenetic Tree Construction

The phylogenetic tree was generated as described previously (79). Briefly, protein sequences for the human Na_v, Ca_v, K_v, K_{Ca}, K_{Ir}, K_{2P}, HCN, and CNG channel families and structurally characterized bacterial channels were downloaded and aligned using the Promals3D server (77). The alignment was truncated to the pore domain based on the KcsA (1K4C), NaK2K (3OUF), K_v1.2/2.1 chimera (2R9R), and Na_vAb (3RVY). The tree was calculated in ClustalW (80) using the Blossum62 matrix.

All sequence alignments shownwere generated in Promals3D (77) and presented using Jalview (81) or Weblogo (82, 83).

Filter-like Structure Search

The whole of the Protein Data Bank (84) was searched using a custom made BioJava (85) script (courtesy Matthew Guttag) against the average sequence of Ramachandran torsion angles for the backbone of the K^+ selective channels KcsA (1K4C), K_vAP (1ORQ), K_v1.2/2.1 chimera (2R9R), NaK2K (3OUF), MlotiK1 (3BEH), KirBac3.1 (2WLJ), and Kir2.2 (3JYC). Those sequences within a defined tolerance of the reference angles were retained.

Protein Expression and Purification

Mutations were made using the Quickchange II mutagenesis kit corresponding residues of the K_v-K_{Ca} and K_{ir} channel families' conserved residues on the NaKNΔ19 gene cloned into the pQE-60 plasmid. The *E. coli* expression vector also included a C-terminal thrombin cleavage site and hexa-histidine tag. The NaK channel mutants were expressed as previously described for other mutants (71, 75, 86) and behaved similarly, with few exceptions. Briefly, protein was expressed in the *Escherichia coli* strain SG13009 transformed with the pQE-60 expression vector including the NaK channel or mutant. Protein expression was induced (at OD_{600} ~0.8) with 0.4mM IPTG at 25°C for 18 hours in the presence of 5mM $BaCl_2$. Cells were harvested and lysed in a solution of 100mM KCl, 50mM Tris-HCl pH 8.0, DNAseI and the protease inhibitors leupeptin, pepstatin, apropeptin, and PMSF. The channel was extracted by the addition of 40mM n-decyl-β- D-maltoside (DM) for 3 hours at room temperature and purified over a Talon Co^{+2} column (Clontech). The hexa-histidine tag was removed by digesting with 1 unit thrombin per 2mg protein and further purified by size exclusion chromatography on a Superdex 200 (10/30)

column (GE) in a solution of 100mM KCl, 20mM Tris-HCl 8.0 and 4mM DM. Notably, the NaK mutations corresponding to the K_{ir} channel family had low protein expression and multiple peaks on size exclusion chromatography. The peak corresponding to the typical NaK channel tetramer was used for functional characterization and crystallization trials.

Crystallization

All NaK channel mutants were concentrated to 12-24mg ml^{-1} using an Amicon Ultra centrifugal device (50 kDa MWCO) and crystallized at 25°C using the sitting drop vapor diffusion method. Equal volumes protein solution and well solution of 60-77.5% (v/v) (±)-2-methyl-2,4-pentanediol (MPD) and 100 mM of various buffers (MES for pH 6.0, Tris-HCl for pH 7.0–8.5, or Glycine for pH 9.0–9.5) were mixed. Crystal quality could sometimes be improved with the addition of 100mM KCl to the well solution. Crystals appeared within approximately 16 hours and grew to maximum size in 3 days. Crystals were flash frozen in liquid nitrogen using the crystallization solution as cryoprotectant.

Data Collection

Data was collected at the Advanced Photon Source (APS) beamlines 19-BM/ID, 23-ID-B/D and the Advanced Photon Source (ALS) beamlines 8.2.1 and 8.2.2. Diffraction data was processed and scaled using HKL2000 (87). All crystals used for structure refinement were of the I4 space group with unit cell dimensions of around α=β=68Å, γ=89Å and contained two molecules in the asymmetric unit. Structures were determined by molecular replacement using the starting models of NaKNΔ19 or NaK2K with the residues 65-69 removed, followed by cycles of model building in Coot (88) and refinement in Phenix (89). All structure figures were generated in PyMol (90). Ramachandran plots were made in Chimera (91).

Proteoliposome Preparation

Protein was reconstituted in proteoliposome of 1- palmitoyl-2-oleoyl-phosphatidylethanolamine (POPE) and 1-palmitoyl-2-oleoyl-phosphatidylglycerol (POPG) (Avanti Polar Lipids). Lipids dissolved in chloroform were mixed at 3:1 molar ratio, choloroform evaporated under argon and held under vacuum for one hour. The dried lipids were resuspended in 100mM KCl, 10mM HEPES-KOH pH 7.4. The lipid suspension was sonicated to clarity and 10mM DM added and vortexed for 3 hours. Purified protein was added and dialyzed against a buffer of 100mM KCl, 10mM HEPES pH 7.4 for 3 days with buffer changed every 24 hours. Proteoliposomes were alloquoted and stored at -80°C.

NaK Channel Electrophysiology

Currents of the NaK channel were measured by giant liposome patch clamp. Typically, single channel currents were measured at a protein to lipid ratio of 1:5000 (w:w). Giant liposomes were formed by drying proteoliposomes on clean glass coverslips overnight at 4°C followed by rehydration at room temperature. The bath solution contained 150mM KCl, 0.5mM EGTA, and 10mM HEPES-KOH pH 7.4. Pipettes were pull from borosilicate glass (Harvard Apparatus) to a resistance of 8-12MΩ. The pipette was filled with 150mM NaCl, 0.5mM EGTA, and 10mM HEPES-NaOH pH 7.4. The gigaseal (>10GΩ) was formed by gentle suction with the patch pipette attached to the giant liposome. To get a single layer of membrane patched, the pipette was pulled away from the giant liposome and the tip exposed to air for 1-2 seconds. Membrane voltage was controlled and data acquired using an AxoPatch 200B amplifier (Molecular Devices) and a low-pass analogue filter set to 1 kHz. The current signal was sampled at a rate of 20 kHz using a Digidata 1322A digitizer (Molecular Devices) and further analyzed with pClamp 9 software (Molecular Devices).

Eukaryotic Channel Functional Studies

The role of some interactions seen structurally and functionally in the NaK mutants were also functionally tested in the $K_v1.6$ voltage gated potassium channel. The $K_v1.6$ gene from *Rattus norvegicus* was cloned in the pEGFP-C1 mammalian expression plasmid. Included in the plasmid is a C-terminal GFP expression tag and mutations in the gene were made with the Quickchange II mutagenesis kit. Recordings were made in the standard patch clamp whole cell configuration using HEK 293 cells within 24-48 hours of transiently transfected. The pipette contained 140mM KCl, 4mM MgCl2, 5mM EGTA, 10mM HEPES pH 7.4. The bath solution contained 140mM NaCl, 4mM KCl, 2mM $CaCl_2$, 1mM $MgCl_2$, and 10mM HEPES pH 7.4. The holding potential was set to -80mV. To measure voltage activation, the membrane was stepped from the holding potential ot various testing potentials and then returned to the holding potential. Peak currents were measured 10ms after activation. Selectivity was measured by activating the channels at 60mV, followed by stepping the membrane to various testing potentials. Tail currents were recorded to generate the I-V curves used for determination of the reversal potential. The mean ± s.e.m. (n = 3-5) was used as data points to plot all I-V and G/G_{max}-V curves.

Chapter 4. Binding Site Studies

Introduction

Though the overall fold of the NaK channel is similar to previously described potassium channels there are clear differences within filter corresponding to the distinct signature sequence (53). (Fig 2.3) With no difference in the first three positions of the filter sequence between NaK and canonical K^+ channels, the NaK channel protein forms two binding sites structurally and chemically identical to sites 3 and 4 of KcsA. However, the structure at the extracellular side of the filter is clearly distinct, what would be sites 1 and 2 in the K^+ channels, with significant differences of both side chains and the peptide backbone. (Fig 2.8) The carbonyls of Gly65 and Asp66 are tangential to the four-fold axis of the ion conduction pathway, forming a large internal volume termed the vestibule. At the external face of the protein there is an external binding site formed by the backbone carbonyls of Gly67 and Asn68. Linking these two structures, the side chain of Asp66 points toward the extracellular face and makes a hydrogen bond with the backbone of Gly68. (Fig 2.13A) This is in contrast to the potassium channels where the equivalent position to Asp66, the tyrosine of the signature sequence, packs into a hydrophobic cleft between the two subunits and nominally toward the cytoplasmic face of the protein. (Fig 2.11)

Despite having two ion binding sites chemically and structurally identical to sites 3 and 4 of described potassium channels NaK was non-selective between sodium and potassium using a $^{86}Rb^+$ flux assay. (Fig 2.9) This result was later confirmed by giant liposome patch clamp with bi-ionic conditions (86). (Fig 4.5) The initial NaK structures soaked in sodium and potassium showed distinct ion density differences within the filter without an appreciable change in the filter architecture. However, the differences in ion binding between individual ions was compounded by high concentrations of calcium within the crystallization condition.

Further information on ion binding within the filter was gleaned when the high resolution structure of NaK was solved. Using a new NaK (NaKNΔ19) channel construct with the M0 interfacial helix removed and a new crystallization condition, calcium free high resolution crystals could be obtained (54). The overall fold of the protein remained the same, including the selectivity filter, thought the second transmembrane helix is now bent at Gly67 and consequently the intracellular gate is open. Within the NaK filter potassium ions were observed to bind as expected to sites 3 and 4 of the NaK channel, comparable to that of the equivalent sites in potassium channels. (Fig 2.8A) Additionally, a potassium ion binds both within the vestibule and at the external binding site where each ion is coordinated by ordered water molecules and the backbone carbonyls of Val65 and Gly67, respectively. Each potassium ion is coordinated in a square anti-prism configuration analogous to both that of the potassium channel filter and the first hydration shell of a solvated potassium ion.

Crystallizing NaKNΔ19 in sodium chloride, the sodium ions bind with distinct modes within the an identical filter structure to the potassium bound structure. (Fig 2.8B) While analysis of ion binding is made difficult by a contaminant ion bound at site 3, most likely barium, sodium is proposed to bind in plane with the oxygen atoms which form the potassium binding sites 3 and 4. The difference in ion binding mode is most clear at the cytoplasmic side of site 4, where no contamination is present. In all cases, the coordinating backbone carbonyls and side chains hydroxyls bind equatorially with the sodium ion; though an additional water molecule coordinates the Na^+ ion on the cytoplasmic side of site 4.

Previous studies on selectivity had primarily focused on the role of the individual binding sites to selectivity (64, 66) and separately ascribed the observation of four contiguous ion binding sites to the high conductance of the potassium channels (44). The structure of NaK, with two sites equivalent to potassium channels, clearly contradicts the notion that individual binding sites are the sole determiners of cation selectivity. In

addition, structure of the MthK pore in sodium also clearly demonstrated that a structural change is not required for sodium binding in a potassium selective channel (55). (Fig 2.10) Sodium ions can be seen bound in a similar mode to NaK within the filter of MthK, binding in plane with the carbonyls at the extracellular face of site 1 and agree with later work proposing lithium binding in plane with the carbonyls of KcsA (68). (Fig 4.1) In that study, KcsA crystals are soaked into LiCl solutions. The structure is seen uncollapsed, and while Li^+ density cannot be directly observed the ion is proposed to bind in plane with the carbonyls between sites 3 and 4 and further coordinated by water molecules.

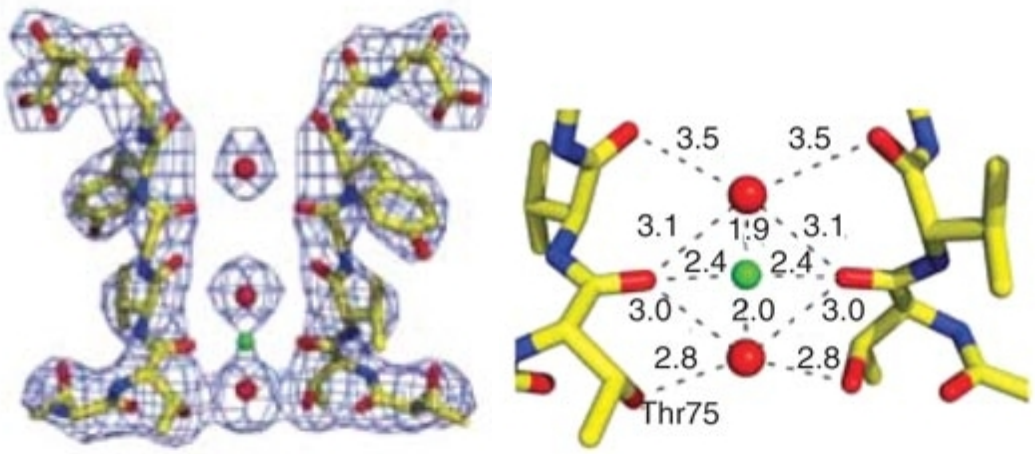

Figure 4.1. The structure of KcsA soaked into Li^+ and the ion's proposed binding site within the pore. KcsA soaked into 150mM Li^+, 0mM K^+ omit map contoured at 1.25σ and the proposed coordination of Li^+ between sites 3 and 4 by backbone carbonyls and water molecules. Figure reproduced from (68).

The further mutational work on NaK with the aim of modeling the CNG channel ion conduction pathway yielded more insights into selectivity (71). The modification the NaK selectivity pore sequence ($_{63}$TVGDGNFS) in NaK2CNG-D (TVGDTPP) results in a major reorganization of external portion of the filter domain, with loss of the external binding site and the formation of an additional potassium binding site. (Fig 4.2A) While the filter

amino acid composition is clearly divergent from the signature sequence of potassium channels, the peptide backbone itself adopts a conformation nearly identical to sites 2-4 of KcsA. (Fig 4.2B) This structural rearrangement is reflected in the backbone torsion angles of the filter where Gly65 has undergone a movement of approximately 120 degrees about Psi. (Fig 4.3) Strong density is clearly seen at sites 2-4 of NaK2KCNG-D when crystallized in the presence of potassium, corresponding to K^+ ions binding withthe same square anti-prism configuration as the equivalent sites in KcsA. When crystallized in sodium, the smaller ion bound in-plane with carbonyl ions at the same positions as previously seen in wild-type NaK. Tested functionally in giant liposomes patch clamp, this three-site structure was completely non-selective between sodium and potassium with a reversal potential of 0mV. (Fig 4.5B) Notably there is a distinct increase in the single channel potassium conductance to 110pS, corresponding perhaps to the loss of the constriction in the ion conduction pathway at the external binding site, a mechanism discussed further in the following chapter.

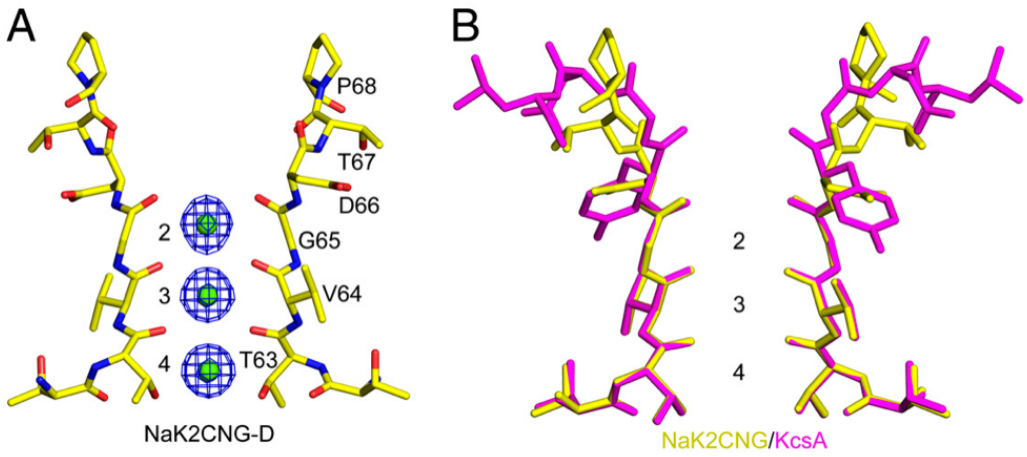

Figure 4.2. The NaK2CNG-D construct has three discrete ion binding sites and with similar chemistry and structure to equivalent sites in KcsA. (A) Selectivity filter structure and ion binding of NaK2CNG-D with K^+ ions bound at sites 2-4. Fo-Fc ion omit map contoured at 5σ. (B) Structural alignment of NaK2CNG-D (yellow) and KcsA (magenta). Figure reproduced from (86).

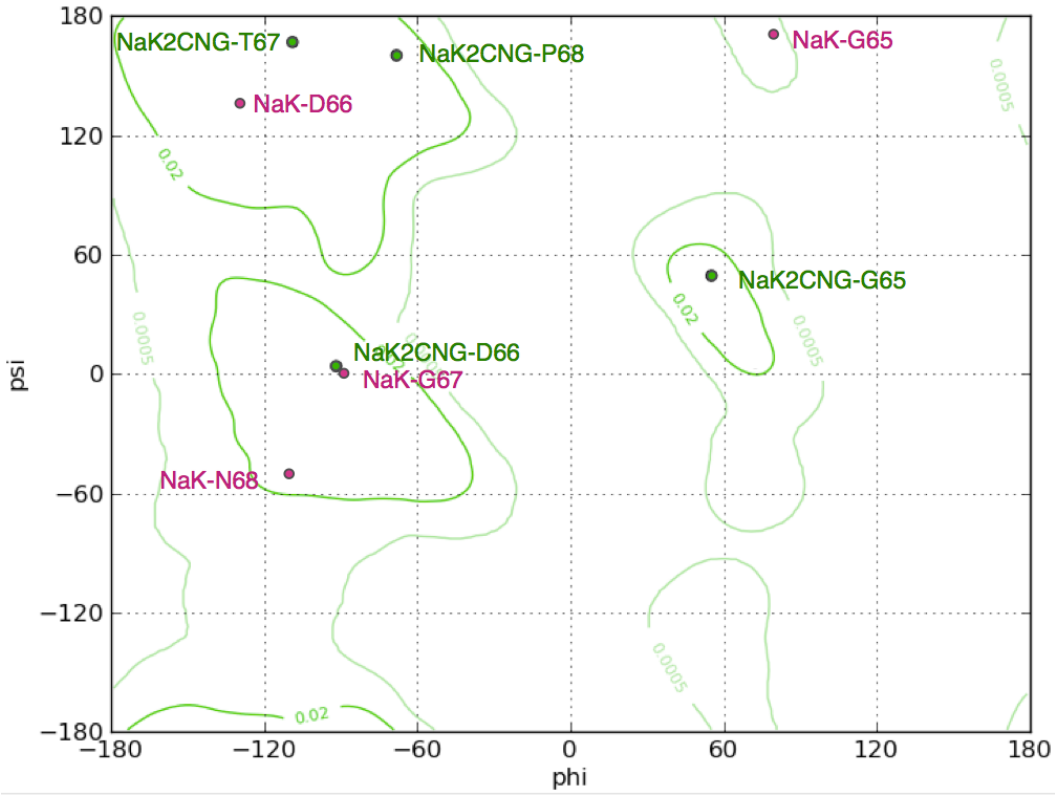

Figure 4.3. Ramachandran plot of the filter residues of NaK and NaK2CNG-D. The structural changes in the NaK2CNG-D (green) filter from NaK-WT (magenta) involve large changes in the protein back bone torsion angles within the filter. Figure reproduced from (86).

Results

Comparing the sequences of NaK to canonical potassium channels, notably the K_v and K_{Ca} family of potassium channels, there is a notable primary sequence difference outside the selectivity filter. Immediately following the signature sequence is a conserved aspartate residue in K^+ channels which is neutralized to asparagine in the NaK channels. The corresponding D66Y/N68D mutations were made in the NaK channel and the resulting channel named the NaK2K channel (86).

Figure 4.4. Alignment of the P-loop of NaK and mutants with representative potassium channels. The selectivity filter sequence is colored in green based upon identity to the potassium channel signature sequence.

When tested by electrophysiology, the NaK2K channel is potassium selective with a reversal potential of 80mV in giant liposome patch clamp under bi-ionic conditions with single channel conductance in symmetric potassium of 120pS. (Fig 4.5C) This reversal potential corresponds to a relative permeability (P_{Na}/P_K) of 0.04.

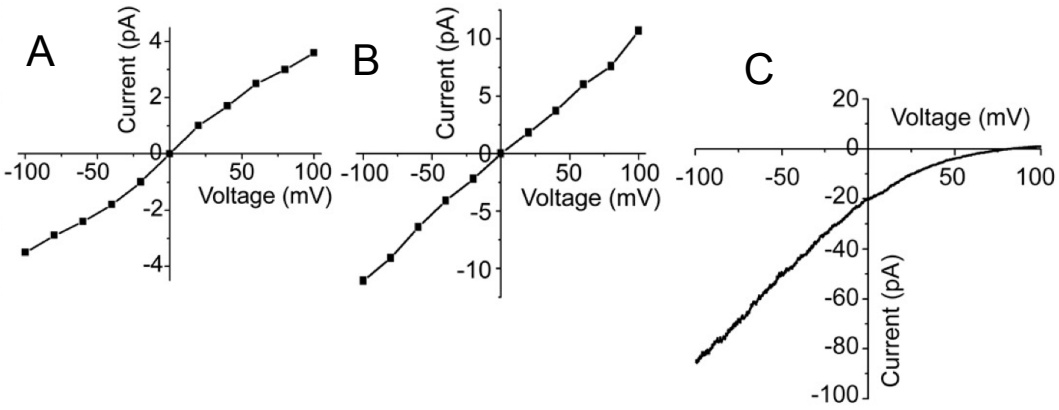

Figure 4.5. The NaK2K channel is K+ selective, while NaK and NaK2CNG-D are perfectly non-selective. Current voltage relationships under bi-ionic conditions of NaK (A), NaK2CNG-D (B) and NaK2K (C). Measured using giant liposome patch-clamp with 150mM NaCl inside the pipette, 150mM KCl in the bath solution. NaK and NaK2CNG were recorded as single channel currents at each test potential, NaK2K was measured by macroscopic current reversal potential. Figure adapted from (86).

This double mutation causes a significant structural rearrangement of the peptide backbone at positions 65 through 68, best illustrated by large changes in the torsion angles. (Fig 4.6) Both the backbone dihedral angles and the site chain orientations of NaK2K are very similar to those of canonical potassium channels. This movement of the backbone generates two new potassium binding sites that are equivalent in primary sequence, chemistry and structure to those of KcsA. (Fig 4.7B) Within the selectivity filter of the NaK2K channel are four well ordered potassium ions coordinated by backbone carbonyls and the hydroxyls of Thr63 in a mode identical to KcsA. (Fig 4.7A)

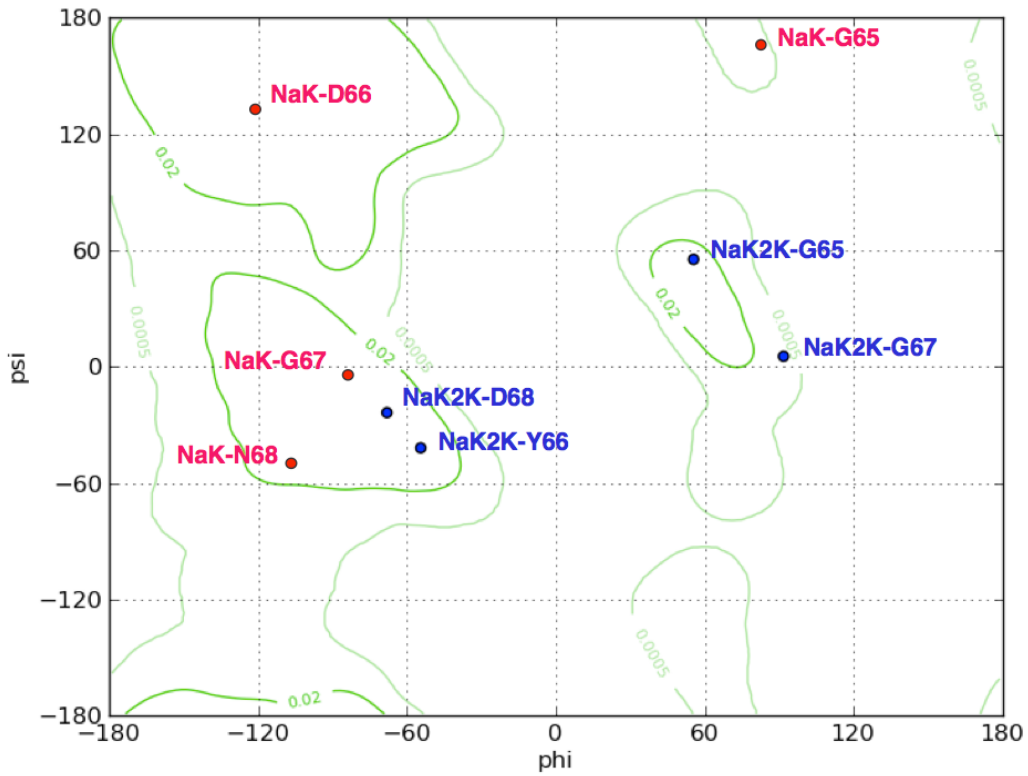

Fig 4.6. Ramachandran plot of the filter residues of NaK and NaK2K. The filter rearrangement of NaK (red) to NaK2K (blue) involves dramatic changes in the protein peptide torsion angles. Figure reproduced from (86).

Driving this rearrangement are two new packing interactions not present in the wild-type NaK pore. The position 66 Tyrosyl side chain now orients away from the extracellular face and inserts into a cleft at the interface between two subunits. (Fig 5.3) The Asp68 side chain points into the core of the protein, making a hydrogen bond with Tyr55 on the pore helix, in contrast to Asn68 in the wild-type protein which points out into bulk solution. Such interactions are similar to those present in many previously crystallized potassium channels and the nature and role of these interactions in potassium selectivity are the focus of the following chapter. Directly however, this increase in potassium selectivity with four sequential ion binding sites suggests that the number of binding sites plays a direct role in potassium selectivity.

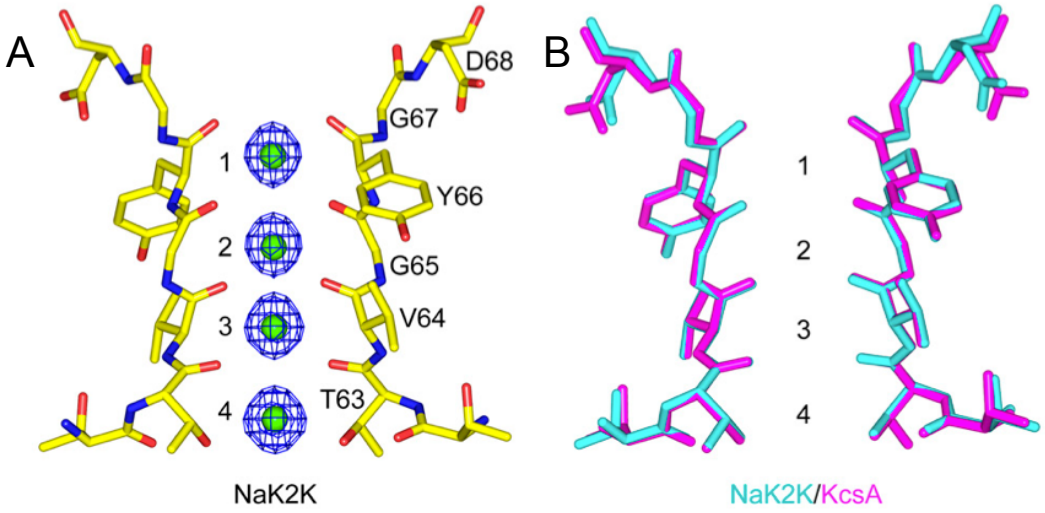

Figure 4.7. The NaK2K channel has 4 well ordered K+ ions bound within a filter structure superimposable with that of KcsA. (A) Selectivity filter structure of NaK2K and ion omit map of K^+ ions bound in the channel filter. Fo-Fc ion omit map contoured at 5σ. (B) Superimposition of the NaK2K (cyan) and KcsA (magenta) selectivity filter structures. Figure reproduced from (86).

As a means to further validate the importance of these four sites to potassium selectivity a additional mutation on the selective NaK2K channel was generated. As site 4 is created by both the side-chain hydroxyls and backbone carbonyls of Thr63, the mutation T63A truncates

this side to a single methyl group. This mutation removes the coordinating hydroxyl of site 4, presumably without otherwise changing the selectivity filter structure. This threonine to alanine mutant channel, NaK2K_T63A, has a reversal potential of 0mV (Fig 4.8), corresponding to an inability to discriminate between sodium and potassium, without a notable change in potassium conductance. Unfortunately, crystals could not be grown for NaK2K_T63A for unknown reasons. However, as this threonine is absolutely conserved in the signature sequence of potassium channels the corresponding mutation could be made on another structurally and functionally characterized K^+ channel. The equivalent mutation threonine to alanine (T59A) was made on the pore filter of the calcium gated potassium channel from *Methanothermobacter thermautotrophicus* (MthK). The MthK channel's pore domain has already been solved to high resolution and is known to be highly potassium selective without any known propensity to collapse in sodium or inactivate. (Fig 4.9A)

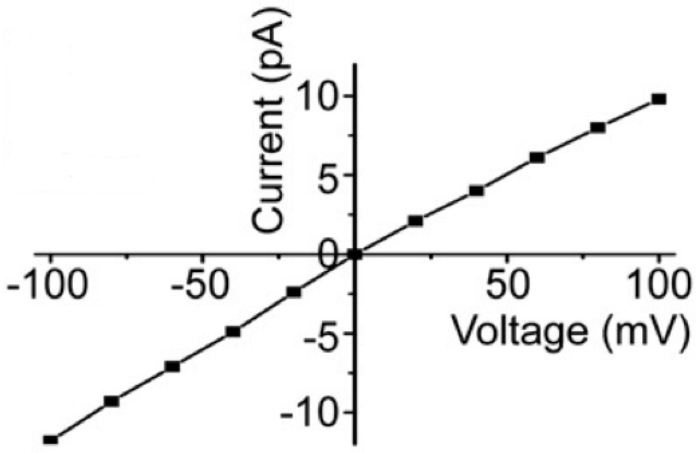

Figure 4.8. A single threonine to alanine mutation is sufficient to abolish sodium versus potassium selectivity in NaK2K_T63A. Single channel I-V curve of NaK2K_T63A measured under bi-ionic conditions with 150mM NaCl inside the pipette and 150mM KCl in the bath solution. Figure reproduced from (86).

The protein structure of the MthK_T59A pore domain is nearly identical to that of the wild type MthK pore, excepting the expected

absence of density beyond the beta carbon of the side chain at position 59. (Fig 4.9C) Within the filter, sites 1-3 show strong density corresponding to potassium ions, while site 4 has markedly reduced potassium binding as a consequence of the missing side-chain hydroxyl. Functionally the consequences of this mutation were tested, again using giant liposome patch-clamp under bi-ionic conditions. Though there is no change in potassium conductance, the T59A mutation causes a dramatic loss of selectivity with the reversal potential decreasing form 80mV to 10mV corresponding to a thirteen-fold loss in selectivity. (Fig 3.9B)

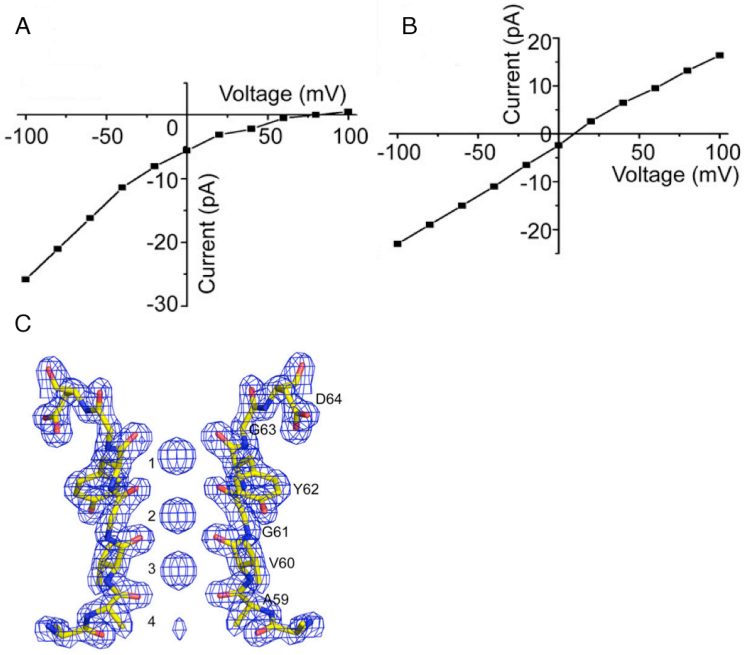

Figure 4.9. A single threonine to alanine mutation is sufficient to abolish ion binding at site 4 and selectivity in the mutant channel MthK_T59A. (A) Current-voltage relationship of wild type MthK under bi-ionic conditions. (B) Current-voltage relationship of MthK_T59A under bi-ionic conditions. Both wild-type MthK and MthK_T59A were measured as single channel currents at various testing potentials using planar lipid bilayers with 150mM NaCl and 150mM KCl on opposing sides of the membrane. (C) Filter structure of MthK_T59A with 2Fo-Fc ion omit map contoured at 5σ. Figure adapted from (86).

Discussion

Ultimately, these results demonstrate the necessity of at least four contiguous potassium binding cages for potassium selectivity. Notably, the selectivity in the NaK and its mutants is not graded with the number of binding sites but rather is apparent only in in the four-sited NaK2K channel. (Fig 4.5) This would be unexpected if the water access mechanism (65) or the compounded selectivity of multiple selective or partially selective binding sites were responsible for channel selectivity (64, 66). This result demonstrates that while other features of potassium channels may be necessary for selectivity, they are not sufficient, and at least 4 in-line binding sites are required for K^+ selectivity.

The requirement of four contiguous ion binding sites had been previously addressed for its proposed role in conductance and the energetic equivalence of the 1,3 and 2,4 states within the filter. However, these results demonstrate that selectivity, and not conductance, is governed by the number of ion binding sites. The conversion from three to four sites in the constructs NaK2CNG-D and NaK2K results in only a ~9% increase in K^+ conductance but a 20-fold change in selectivity. Similarly, reducing the number of binding sites from 4 to 3 in MthK-WT versus MthK_T59A or NaK2K versus NaK2K_T63A results in no significant change of conductance but 13- or 25-fold changes in selectivity, respectively. Differences in conductance between 2 and more sites is complicated by the structure of wild-type NaK. The dramatic shift in conductance that is seen in NaK mutants, their markedly higher K^+ conductance than wild type, may be attributable to the constriction between the external binding site and the vestibule in the wild type channel, absent in each mutant, and is discussed further in the subsequent chapter where mutations make this constriction is less rigid. (Fig 2.8)

Interestingly, some tetrameric cation channels closely related to potassium channels have clearly divergent sequences within the P-loop which may explain their differences in selectivity relative to canonical potassium channels. (Fig 2.2 & 2.3) The previously mentioned CNG channels clearly preserve in sequence the amino acids necessary for the first two ion binding sites (13) and perhaps also a third, based upon the NaK2CNG models. Conversely, the HCN channels preserve the C-terminal portion of the signature sequence but no longer have a hydroxyl available for the formation site 4 (14, 92). Corresponding to this partially similar filter sequence, these channel families are both non-selective between sodium and potassium. In addition, some channels described as potassium channels have markedly low P_{Na}/P_K. Within the small conductance calcium gated potassium channel ($K_{Ca}2.1$ or SK_{Ca}) the position of the highly conserved threonine of the signatures sequence is a serine and this channel has a permeability ratio (P_{Na}/P_K) of ~0.1 (93). (Fig 4.10) This lower K^+ selectivity may be the result of a less well ordered side chain hydroxyl forming site 4, a consequence of the smaller serine side-chain volume. The necessity of a rigidly ordered binding site in selectivity will be discussed in the next chapter, particularly with relation to the NaK2K_Y66F mutant.

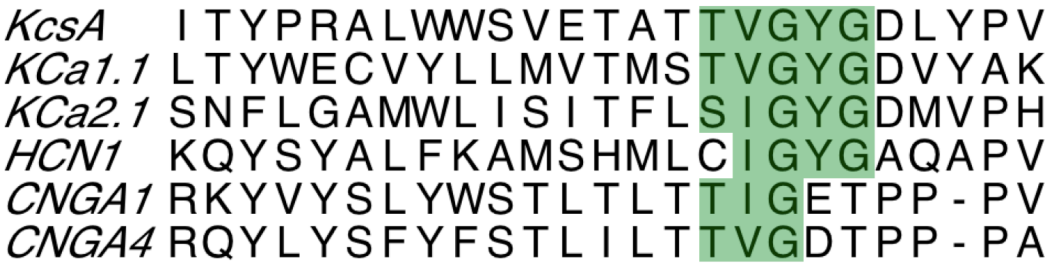

Figure 4.10. Alignment of the P-loops of KcsA and $K_{Ca}1.1$ with less and non-selective channels. The selectivity filter sequences are highlighted in green based upon similarity to the canonical K^+ channel signature sequence.

Comparison of the NaK, NaK2CNG and NaK2K structures suggests some possible geometric restrictions on forming an ion binding site. The NaK2CNG-D, NaK2CNG-N, NaK2CNG-E, and NaK2K channels each orient the position 66 side-chain into the same cleft between protein subunits, despite differences in coordination within that pocket and sequence of the filter (71). (Fig 2.15 & 4.11) Interactions within the cleft vary among the NaK2CNG and NaK2K mutants and clearly play a role in ion binding and selective permeation of each. Based on the NaK2CNG-E model, the calcium block of ionic currents is abrogated by swapping the threonine to glutamate hydrogen bonding positions in either bovine CNGA1 or NaK2CNG-E (E66T/T60E). If a similar bond is ablated in NaK2K there is a clear reduction in selectivity; as will be discussed in the following chapter. As a similar cleft is seen in the other potassium channel structures, it may serve to correctly orient the peptide backbone for the formation of site 2. Similarly, the side chain at position 64 in NaK also inserts into the cleft and is conserved as either a Val or Ile in both CNG and K^+ channels, perhaps playing a role in the forming of site 3. Interactions within this cleft may serve as a general mechanism to forming the selectivity filter within this clade of the tetrameric cation channel superfamily. Correspondingly, the equivalent position is threonine in the first pore domain of the $K_{2P}1$ channel and is suggested to underly the increased Na^+ permeability in conditions of low K^+ concentration (38).

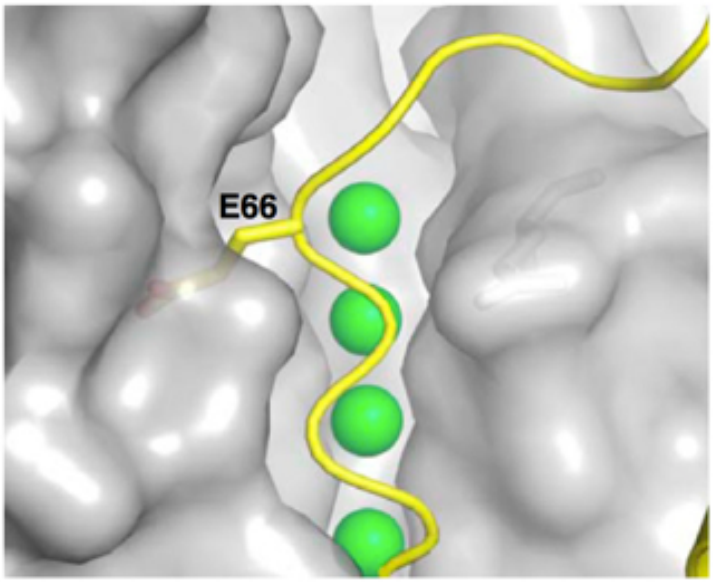

Figure 4.11. The glutamate of the NaK2CNG-E filter inserts into the adjacent cleft in a similar mode to that of the other NaK2CNG mutants and Tyr66 of NaK2K. Ribbon rendering of the proximal NaK2CNG-E monomer and surface rendering of the other monomers in the channel. Potassium ions within the pore are drawn as green spheres. Figure reproduced from (71).

Chapter 5. K^+ Channel Filter Packing

Introduction

The distinct conformational change of the filter seen in the NaK2K structure, relative to the wild-type NaK channel, appears to be a function of the changes in side-chain orientations and interactions as the peptide backbone length and chemistry is common to both. The mutations from NaK to NaK2K involve positions highly conserved within the K_v and K_{Ca} channel family (48, 94), and less so in the K_{2P} and K_{ir}, KirBac channel clades (52, 69). Earlier studies have attempted to address the functional consequences of many of these positions, but usually without insight into the structure of the filter itself (95-100). Alternatively, within the structure of previously solved potassium channels some analogous interactions have been observed, though their direct role in folding of the filter structure or selectivity were not directly interrogated (48).

These positions have been previously suggested to play roles in a number of potassium channel properties. The highly conserved aromatic positions within the pore domain had previously been noted (101) and in the absence of structural information it was proposed that these aromatic residues might be responsible for selectivity through cation-π interactions (102).

The acidic residue found to follow the signature sequence has previously been implicated to play a number of roles in various model potassium channels. As early studies had demonstrated mutation of the equivalent aspartate residue abolished currents in shaker channels later studies were carried out tandem hetrodimers where one subunit contains an aspartate to threonine mutation (103). These two-fold neutralize channels had a notable increase the permeability of all tested monovalent cations, though the channel still maintains the same ion selectivity sequence. Two later studies in the BK and Tok1p channels where the equivalent aspartate residue was neutralized to asparagine both noted

reduced currents in the mutant channel and suggested the charge of the acidic residue may serve to accumulate potassium ions at the external entrance to the filter (97-99).

With the structure of KcsA it became apparent that only the threonine of the signature sequence was the only side chain to directly interact with the permeating ion within the selectivity filter (47). (Fig 2.6) The low resolution structure suggested a network of aromatic residues which hold the filter at the proper diameter for potassium selectivity. In the later high resolution structure a hydrogen bond network between the pore helix, selectivity filter peptide backbone and buried water molecules was suggested to stabilize the filter structure (48). (Fig 2.11) This was further supported by the collapsed structure where this web of hydrogen bonds is significantly altered when the filter is occupied by sodium.

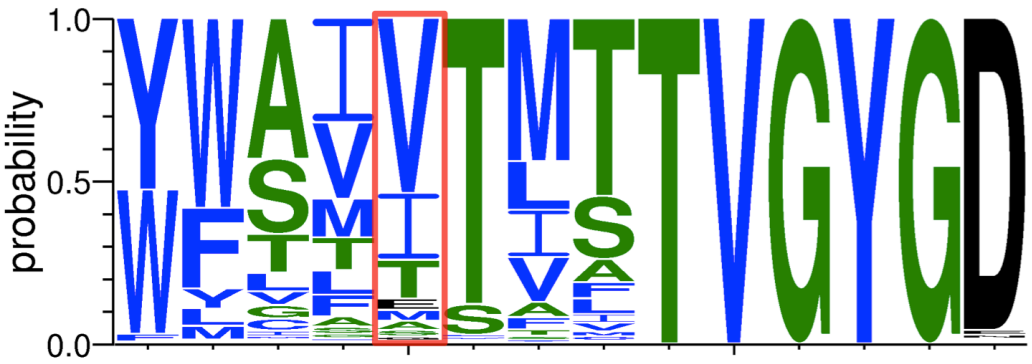

Figure 5.1. A small side chain is usually conserved at the equivalent position of Glu71 in KcsA. Multiple sequence alignment plotted as amino-acid probability by position of the Pfam ion_trans and ion_trans_2 family members containing the TVGYG signature sequence. The position equivalent to Glu71 of KcsA is boxed in red.

Interestingly, this glutamate on the pore helix of KcsA (Glu71) is not conserved in the K_v and K_{Ca} channel families, though it is in the K_{ir} family and KirBac orthologs. (Fig 5.1) In other potassium channel structures where the proteins are more similar to the K_v and K_{Ca} family, the equivalent position is a small hydrophobic residue. Notably, in those structures a second well ordered water molecule frequently occupies the

same location as the terminal carboxylate moiety of the pore helix glutamate on KcsA. (Fig 5.2)

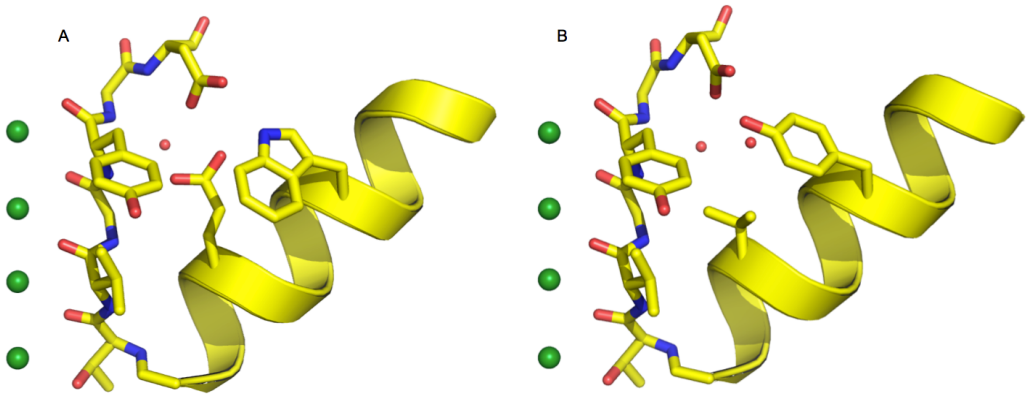

Figure 5.2. There are differences in the waters bound within the pore of KcsA and MthK (48, 55). Structures of the pore domain of (A) KcsA (1K4C, 2.0Å) and (B) MthK (3LDC, 1.45Å). Side chains involved in the packing of KcsA filter and equivalents in MthK are shown as sticks. Potassium ions and water molecules are shown as green and red spheres, respectively.

The later KirBac1.1, KirBac3.1, and *Mus musculus*-KirBac3.1 chimera structures have a similar network to that of KcsA involving glutamate to aspartate hydrogen bonds (52, 104, 105). However, the protein interaction network which stabilizes the eukaryotic K_{ir} family may not have been well represented by these structures. Prior sequence analysis and mutational work on IRK1 has shown that the K_{ir} family has a highly conserved and required basic residue which follows the signature sequence (69), rather than the acidic residue seen in the KirBac orthologs. (Fig 2.3) This residue, usually an arginine, was thought to be involved in an ion pair that is require required for forming a selective and functional channel. With the later structure of K_{ir}2.2, an inwardly rectifying channel from *Gallus gallus*, the direct salt bridge between the glutamate on the pore helix and the arginine on the pore helix was confirmed (51). (Fig 2.12)

Despite belonging to K^+ channel clade of tetrameric cation channels and having a pore sequence and overall fold largely similar to potassium

channels, the selectivity filter of NaK is clearly distinct from the canonical K^+ channel structure. (Fig 2.2 & 2.3) The two filter binding sites on the cytoplasmic side, equivalent to sites 3 and 4, are structurally superimposable with those of KcsA (53). (Fig 2.8) However, the extracellular portion of the filter adopts a distinct structure, forming a large open structure without direct ion coordination, termed the vestibule, and a external binding site formed by the backbone carbonyls of Gly67. These changes in the binding sites correspond to large changes in the peptide backbone structure of the filter region. In comparing the sequence of the wild-type NaK channel and canonical K_v and K_{Ca} potassium channel family members, there are two notables differences within the pore sequence. The first is Asp66 within the signature sequence and the second is the neutralization of the side chain immediately following the signature sequence. In the previously described NaK2K channel (NaK_D66Y/N68D) two new interaction give rise to a rearrangement of the extracellular side of the filter (86). (Fig 5.3) Within the NaK2K pore Asp68 make a hydrogen bond with Tyr55 on the pore helix. Additionally, the position 66 side-chain has reoriented relative to wild-type NaK and now points into a cleft between subunits, making a hydrogen bond with Thr60 on the adjacent subunit pore helix.

This NaK2K channel serves as a structural and functional scaffold to examine the protein interactions necessary for K^+ selectivity in both NaK2K and canonical potassium channels. Both the Tyr55 to Asp68 hydrogen bond and the insertion of Tyr66 into the adjacent cleft, with its associated hydrogen bond, the involvement of each interaction in selectivity can be tested individually by mutagenesis to study the consequences to channel selectivity and filter structure.

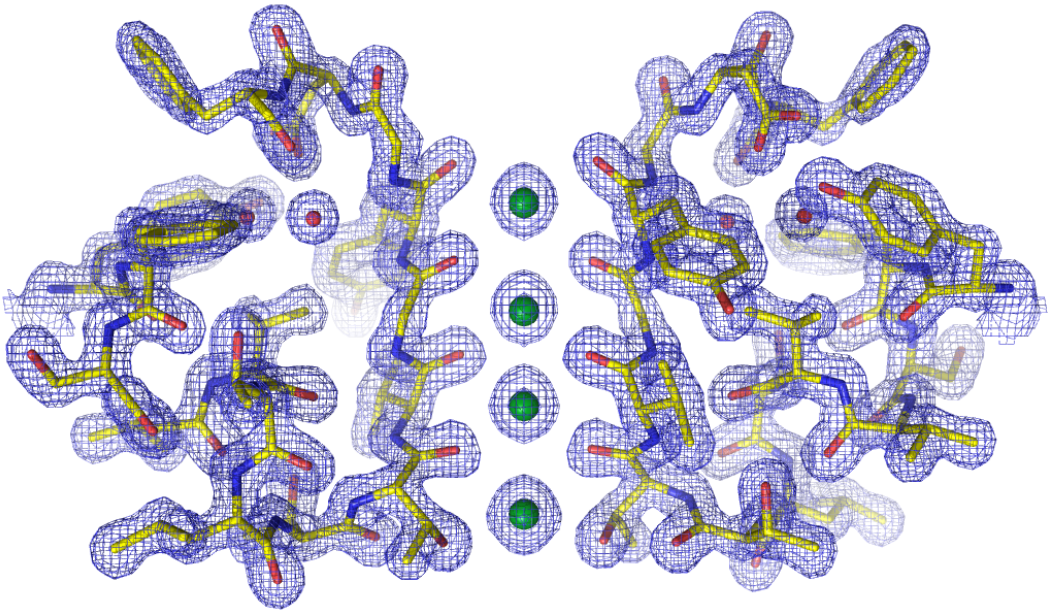

Figure 5.3. The filter of NaK2K is a well ordered structure with discretely bound ions resembling the pore domain of natively K^+ selective channels (86). (A) Structure of the NaK2K pore helix and filter (1.55Å) with 2Fo-Fc electron density map contoured at 2σ. Potassium ions and water molecules are drawn as green and red spheres, respectively.

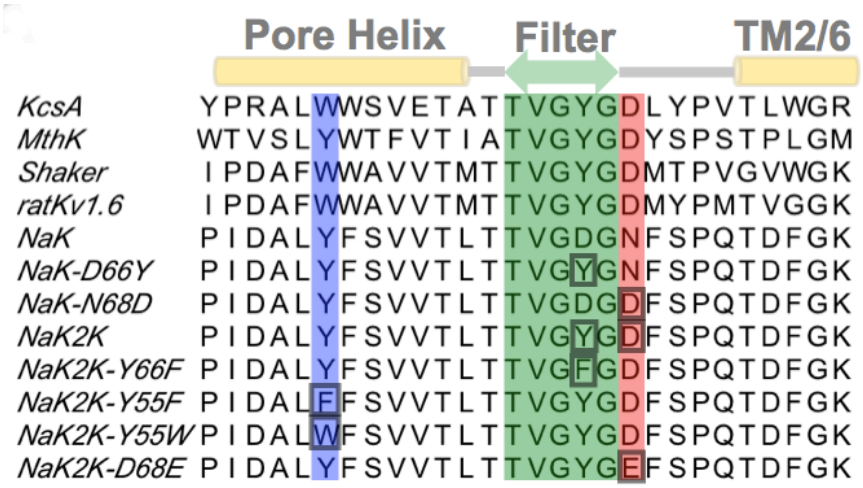

Figure 5.4. Mutants of the NaK2K channel with the NaK channel and representative K^+ channels. The position of mutations used in this study are boxed. Figure reproduced from (78).

Results

Building off of the wild type NaK channel, mutation of either Asp66 or Asn68 individually to the corresponding residues in K_v and K_{Ca} channels is insufficient to convert the NaK channel to a K^+ selective channel, as measured by reversal potential using giant liposome patch clamp of mutant protein reconstituted into proteoliposomes, though single channel currents are higher than wild type. (Fig 5.5B and 5.6B) Structurally, this lack of selectivity is expected as the filter of both NaK_D66Y or NaK_N68D resemble the wild-type filter structure. (Fig 5.5A and 5.6A) Interestingly, in both single mutants the vestibule and external binding site are much more disordered than in the wild-type channel, reflected by the weaker electron density near the external ion binding site.

In a comparison of canonical K_v and K_{Ca} channels, the position equivalent to Tyr55 in NaK2K is always an aromatic hydrogen bond donor, either tyrosine or tryptophan, and Asp68 is absolutely conserved. (Fig 2.3) Further analysis of the equivalent equivalent positions in a large set of K^+ channel like sequences, specifically excluding IRK channels, there is a clear evolutionary coupling between the two positions. (Fig 5.7) An aromatic hydrogen bond donor, either tyrosine or tryptophan, is highly conserved on the pore helix, equivalent to Tyr55 in NaK2K, when the signature sequence is followed by an aspartate or, more rarely, glutamate. However, if the signature sequence is followed by a neutral asparagine the distribution shifts and is predominated by phenylalanine. The functional consequences of neutralizing this acidic residue can be seen in NaK_D66Y, equivalent to NaK2K_D68N, where the channel is functionally non-selective and the channel resembles the non-selective wild type channel with Asn68 is orient away from the pore helix. (Fig 5.5)

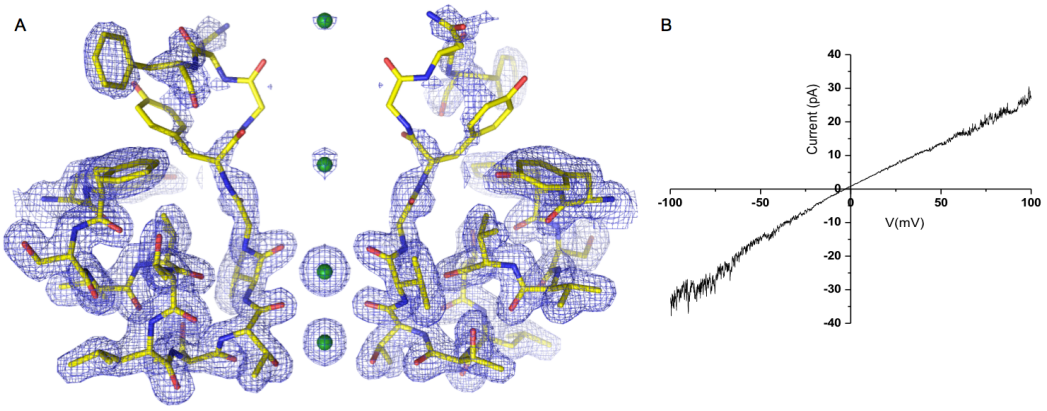

Figure 5.5. The filter structure clearly resembles wild type in the non-selective NaK_D66Y mutant. (A) Structure of the NaK_D66Y pore helix and filter (1.80Å) with 2Fo-Fc electron density map contoured at 1.5σ. Only two opposing subunits are shown for clarity. Potassium ions are drawn as green spheres. (B) Current-voltage curve of NaK_D66Y measured by giant liposome patch clamp I-V curve recorded from patch containing multiple channels, measured by voltage ramp from -100 to +100mV over 400ms. Figure reproduced from (78).

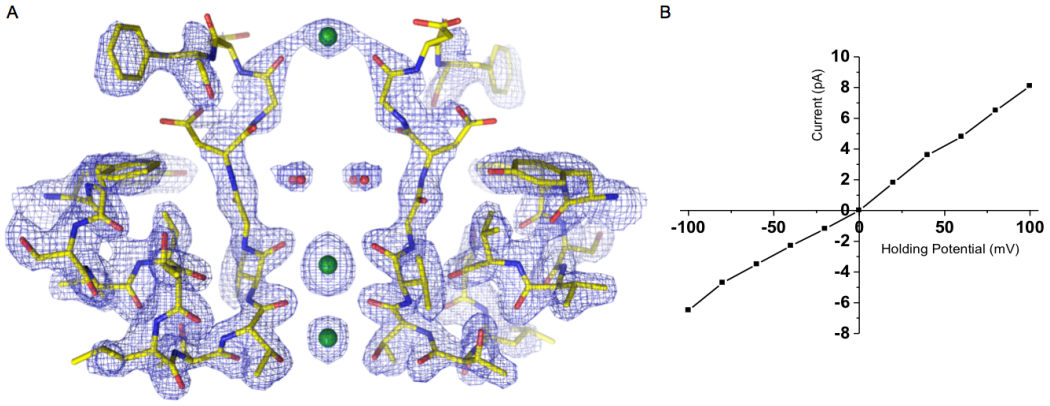

Figure 5.6. The filter structure clearly resembles wild type in the non-selective NaK_N68D channel. (A) Structure of the NaK_N68D pore helix and filter (1.95Å) with 2Fo-Fc electron density map contoured at 1.5σ. Potassium ions and water molecules are drawn as green and red spheres, respectively. (B) Current-voltage relationship for NaK_N68D measured by recording single channels at testing potentials. Figure reproduced from (78).

To address the role of this hydrogen bond donor in potassium channel filter folding and selectivity, mutations were made to the equivalent hydrogen bond donor position in NaK2K generating the mutant channels NaK_Y55W/D66Y/N68D (NaK2K_Y55W) and NaK_Y55F/D66Y/N68D (NaK2K_Y55F). Mutation of the hydrogen bond donor, Tyr55 in NaK2K to the other hydrogen bond donor aromatic tryptophan, results in the same filter architecture as NaK2K. (Fig 5.8A) The Asp68 side-chain continues to point toward the pore helix, making a hydrogen bond with Trp55. Functionally, under bi-ionic conditions NaK2K_Y55W has a reversal potential of 80mV, corresponding to strong potassium selectivity ($P_{Na}/P_K \sim 0.053$). (Fig 5.8B)

The mutation of Tyr55 to phenylalanine (NaK2K_Y55F) results in a channel that cannot discriminate between sodium and potassium under bi-ionic conditions with a reversal potential of 0mV. (Fig 5.8B) However, the filter structure itself is unchanged with four binding sites, each occupied by a potassium ion. (Fig 5.8A) Distinct from NaK2K and NaK2K_Y55W, the side chain of Asp68 is exposed to the external solution, away from the pore helix and unavailable for any interaction to the pore helix.

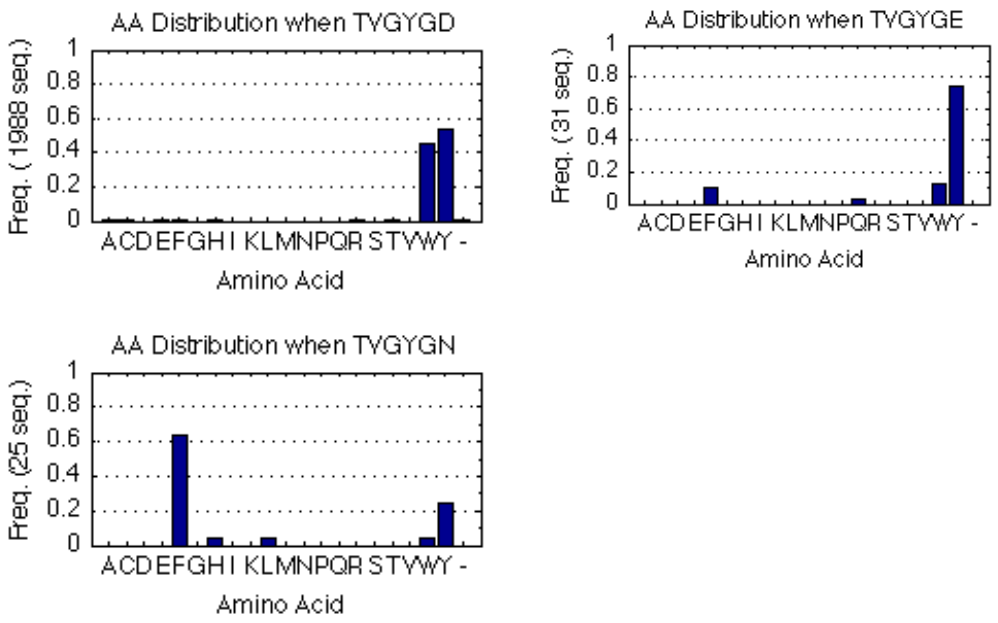

Figure 5.7. There is evolutionary coupling between the pore helix and H-bond acceptor position of potassium like channel. Amino acid distributions at the aromatic hydrogen bond donor position (Tyr55 in NaK2K) as it depends on the residue following the signature sequence (Asp68 in NaK2K). Figure reproduced from (78).

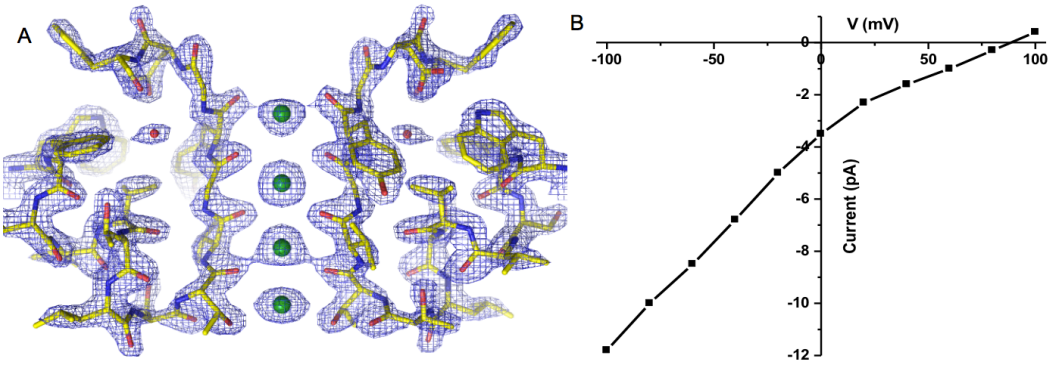

Figure 5.8. The well ordered filter structure resembles that of K+ channels in the selective NaK2K_Y55W mutant. (A) Structure of the NaK2K_Y55W pore helix and filter (1.90Å) with 2Fo-Fc electron density map contoured at 2σ. Potassium ions and water molecules are drawn as green and red spheres, respectively. (B) Current-voltage relationship for NaK2K_Y55W measured by recording single channels. Figure adapted from (78).

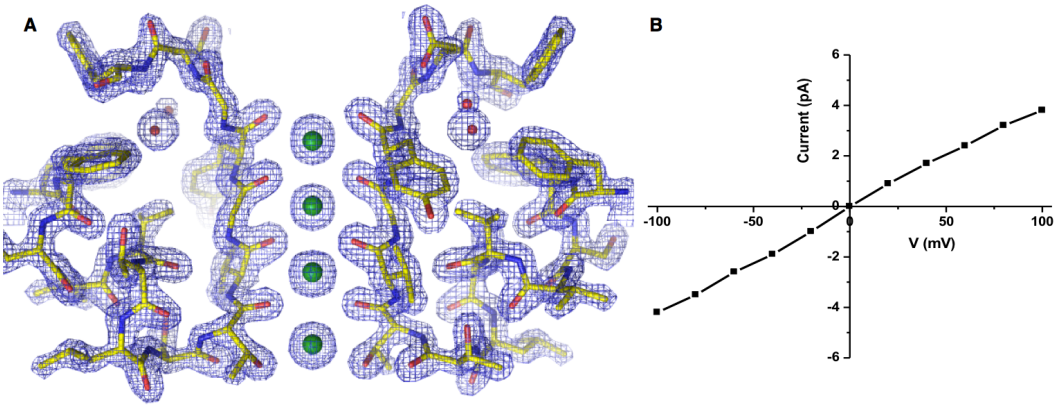

Figure 5.9. The filter is well ordered, though the Aromatic-Aspartate hydrogen bond is absent in the non-selective NaK2K_Y55F channel. (A) Structure of the NaK2K_Y55F pore helix and filter (1.70Å) with 2Fo-Fc electron density map contoured at 2σ. Potassium ions and water molecules are drawn as green and red spheres, respectively. (B) Current-voltage relationship for NaK2K_Y55F measured by recording single channels. Figure adapted from (78).

The signature sequence of K_v and K_{Ca} channels are usually followed by a aspartate, with glutamate rarely seen. (Fig 2.3 & 5.7) Mutation of the aspartate that follows the signature sequence of NaK2K to glutamate, NaK_D66Y/N68E (NaK2K_D68E), results in a non-selective channel with a reversal potential of 0mV under bi-ionic conditions. (Fig 5.10B) Structurally, while the filter architecture is similar to that of NaK2K, the external portions of the filter are clearly more mobile. (Fig 5.10A) The electron density at the external face of the protein and a continuous and broad density of partially occupied ions is seen at the interface between site 1 and the external solution. Additionally, Glu68 is oriented out into solution and does not make a hydrogen bond with Tyr55 on the pore helix. This indicates that in addition to the conserved acidic residue necessary for the hydrogen bond pair there are precise distance or stearic constraints on the packing at the top of the K^+ channel filter.

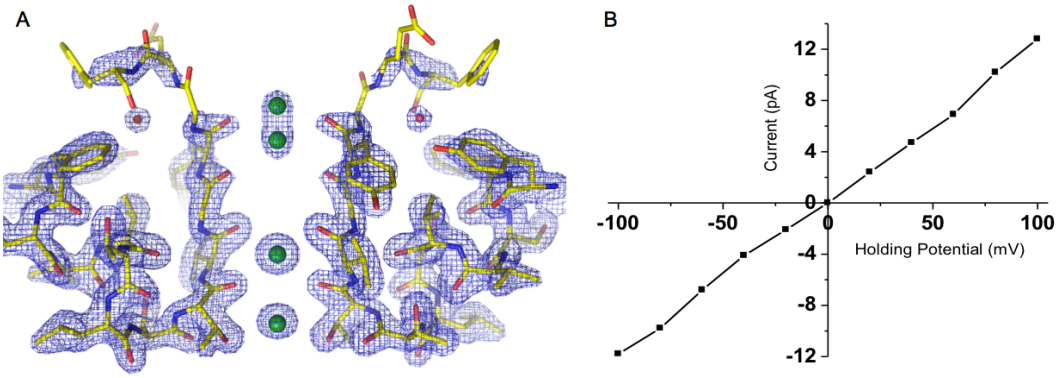

Figure 5.10. The addition of a single carbon is sufficient to destabilize the filter and render the NaK2K_D68E channel non-selective. (A) Structure of NaK2K_D68E (1.75Å) with 2Fo-Fc electron density map contoured at 1.5σ. Potassium ions and water molecules are drawn as green and red spheres, respectively. (B) Current-voltage relationship for NaK2K_D68E measured by recording single channels at testing potentials. Figure adapted from (78).

The role of this aromatic to aspartate hydrogen bond was confirmed in equivalent mutations on the rat $K_v1.6$ potassium channel expressed as a GFP fusion in HEK293 cells. The wild type channel had robust

potassium selectivity, P_{Na}/P_K <0.001, as measured by tail currents in bi-ionic conditions after activation of the channel. (Fig 5.11B) The mutation of the aromatic hydrogen bond donor (Trp415) to the other aromatic donor, tyrosine, results in a channel that is still potassium selective with a reversal potential of -90mV, corresponding to a P_{Na}/P_K ~ 0.008. (Fig 5.11C) However, ablation of the hydrogen bond donor in K_v1.6_W415F, neutralization of the hydrogen bond acceptor in K_v1.6_D428N, or replacing the hydrogen bond acceptor side chain with the larger acidic residue in K_v1.6_D428E, all result in notable reductions of potassium selectivity with P_{Na}/P_K ~ 0.130. (Fig 5.11D-F)

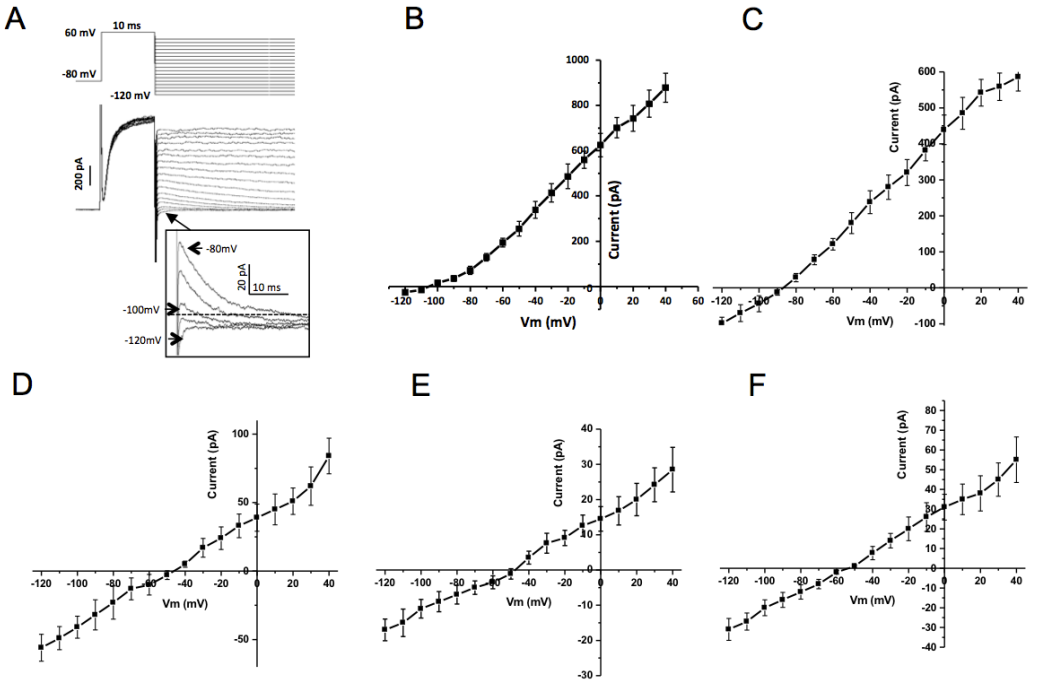

Figure 5.11. The aromatic to aspartate hydrogen bond (Trp415-Asp428) similarly plays a role in the selectivity of K_v1.6. (A) Currents were measured from K_v1.6, wild-type or mutant, expressed as GFP fusions in HEK293 cells. The channels were activated for 10ms and stepping to various testing potentials. Tail currents were recorded to measure reversal potential and generate I-V curves. Insert shows the tail currents near the reversal potential. (B-F) I-V curves of K_v1.6 (B) wild type and mutants (C) W415Y, (D) W415F, (E) D428E and (F) D428N. Figure adapted from (78).

In an effort to confirm the necessity of stabilizing the signature sequence in a selective conformation with interactions between positions on the pore helix and C-terminal of the selectivity filter, mutations were made on the NaK channel to recapitulate the salt bridge which stabilizes the pore of K_{ir} channels. Mutations were made on NaK and tested by bi-ionic giant liposome patch clamp. The NaK mutant introducing both residues necessary for this salt bridge and the K^+ channel signature sequence, NaK_V59E/D66Y/F69R, was still non-selective with a reversal potential of 0mV. (Fig 5.13A) However, sequence and structural comparison of NaK2K to canonical K_{ir} channels highlights an additional packing requirement of K_{ir} channels. (Fig 5.12) At the position equivalent to Tyr55 in NaK, K_{ir} channels usually a conserved leucine. Structurally, the Tyr55 present in NaK2K is in an orientation such that it would sterically clash with the salt bridge. Introducing the additional mutation Tyr55Leu (NaK_Y55L/V59E/D66Y/F69R, or NaK2Kir) yields a potassium selective channel with a P_{Na}/P_K of 0.331. (Fig 5.13B) Despite repeated attempts, crystals could not be obtained of NaK_V59E/D66Y/F69R or NaK2Kir, possibly due to markedly weak protein expression. As NaK2Kir does not recapitulate completely the robust potassium selectivity of the K_{ir} channel family, it suggests that other protein packing differences may further stabilize the filter for selective potassium conduction.

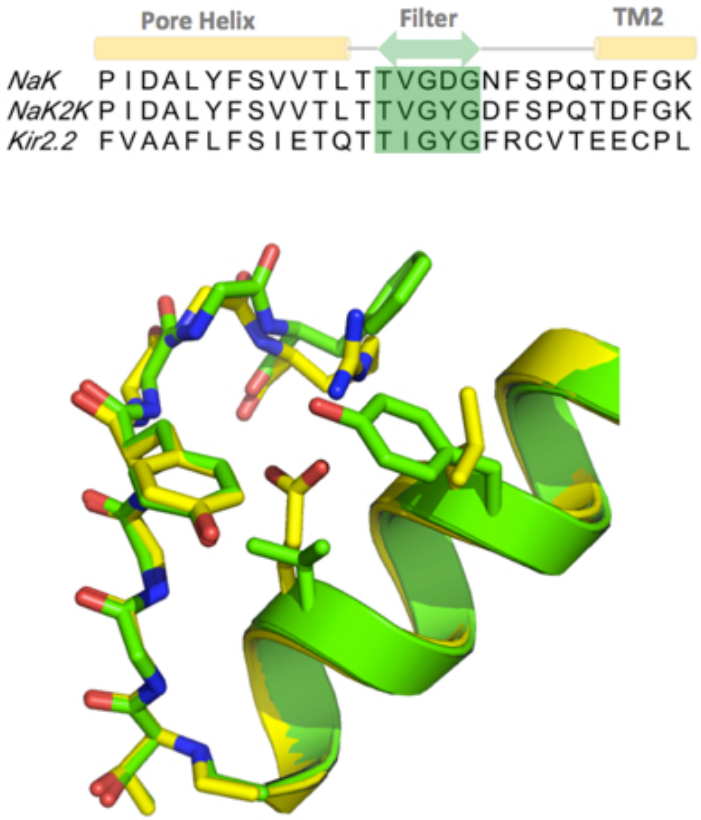

Figure 5.12. NaK2K and K_{ir} channels have similar folds within the filter though the interactions pinning the filter are distinct. Sequence alignment of NaK, NaK2K, and K_{ir}2.2 with structural elements noted. Structural alignment of NaK2K (green) and K_{ir}2.2 (yellow). Only the side chains of residues involved in K_{ir} packing, and equivalents in NaK2K, are shown. Figure reproduced from (78).

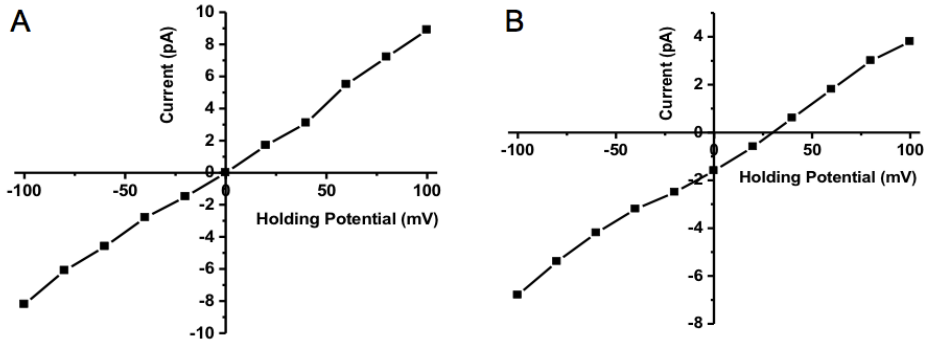

Figure 5.13. Creating a selective, K_{ir}-like filter requires additional packing differences (NaK2Kir) not simply the introduction of the salt bridge (NaK_V59E/D66Y/F69R). Current-voltage relationship under bi-ionic conditions of (A) NaK_V59E/D66Y/F69R and (B) NaK2Kir measured by single channel recordings. Figure adapted from (78).

Also present in the NaK2K and previous K^+ channel structures, and noted in the low resolution KcsA structure, are the interactions of the tyrosine within the signature sequence (Tyr66 in NaK2K) with a threonine on the adjacent pore helix. (Fig 5.15C) The equivalent of this threonine is highly conserved among K_v and K_{Ca} potassium-like channels with the signature sequence TVGYG. Those channels where the signature sequence is TVGFG have significantly reduced conservation of threonine at the equivalent position on the pore helix, suggesting evolutionary coupling between these two animo acids. (Fig 5.14) A similar coupling is seen on the pore domains of K_{2P} channels, where the first pore domain contains a tyrosine within the signature sequence while the second domain is most commonly phenylalanine or, more rarely, leucine.

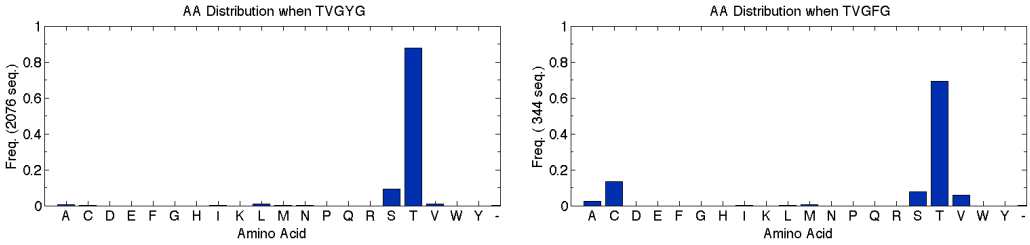

Figure 5.14. There is only weak evolutionary coupling of the signature sequence aromatic to the pore helix in K^+ like channels. Amino acid distributions on the pore helix (Thr60 in NaK2K) as it depends on the aromatic within the signature sequence (Tyr66 in NaK2K).

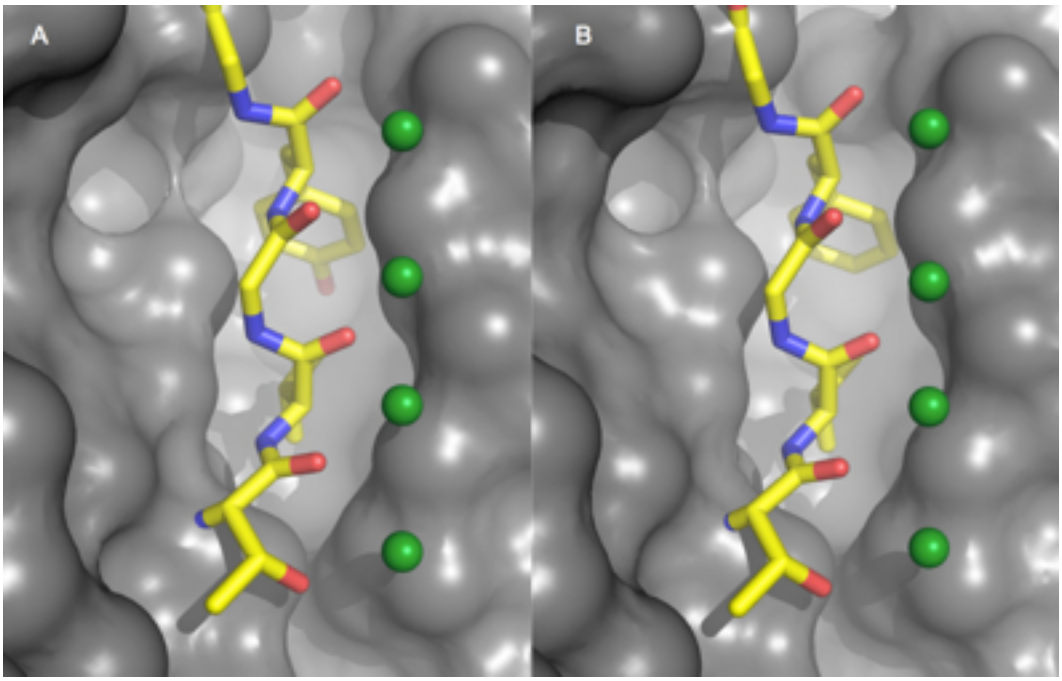
A
B

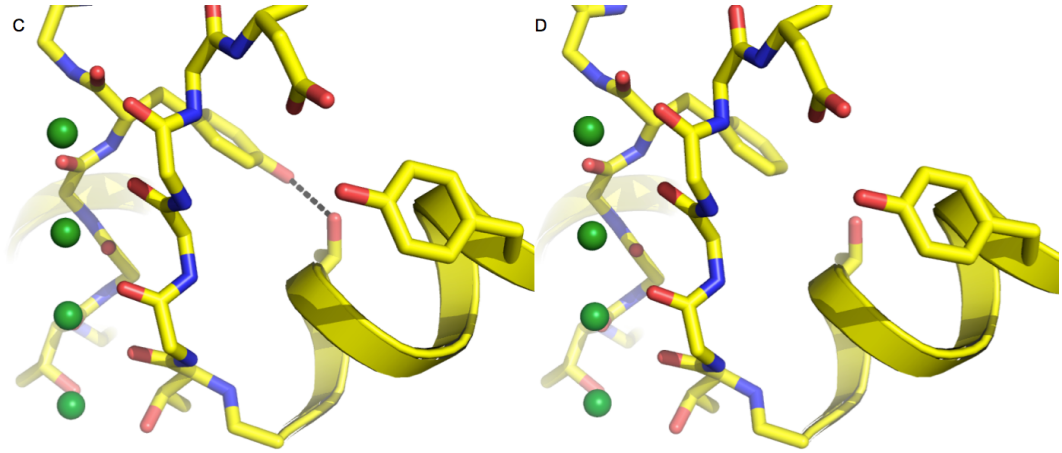
C
D

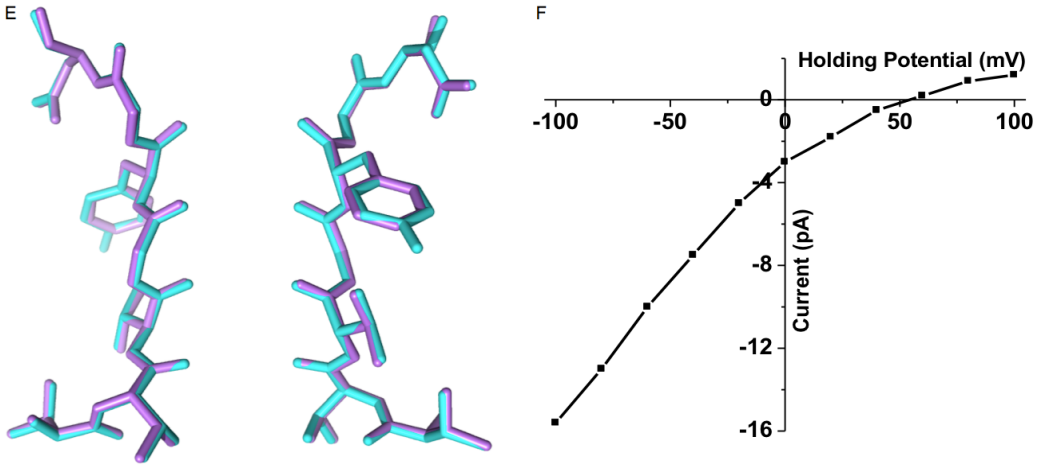

Figure 5.15. Ablating a single hydrogen bond between the filter and adjacent pore helix does not change the crystallized protein structure but weakens selectivity. Insertion of the (A) NaK2K and (B) NaK2K_Y66F filter side-chains into the cleft formed between adjacent subunits. (C) Tyr66 form a hydrogen bond to the adjacent subunit Thr60 in NaK2K. (D) The equivalent bond is absent in NaK2K_Y66F, despite the same side chain orientations, in the absence of an available hydroxyl group. Potassium ions within the selectivity filter are depicted as green spheres. (E) Structural superimposition of the NaK2K (cyan) and NaK2K_Y66F (purple) selectivity filters. (F) Current voltage relationship of NaK2K_Y66F as measured by giant liposome patch clamp. Figure adapted from (78).

The role of this interaction was interrogated using the mutation NaK2K_Y66F built on the K^+ selective NaK2K channel, removing the hydroxyl but maintaining the bulky aromatic phenyl ring within the signature sequence. Functionally, this mutation results in a reversal potential of 50mV under bi-ionic conditions, the 30mV shift reflecting about a 3-fold loss in potassium versus sodium selectivity (P_{Na}/P_K of 0.158). (Fig 5.15F) Structurally, the NaK2K_Y66F mutant had no gross change in filter structure. (Fig 5.15E) The phenyl ring continues to insert in the same orientation into the hydrophobic cleft formed between the two adjacent subunits, though notably NaK2K_Y66F is unable to the same threonine to tyrosine hydrogen bond seen in NaK2K. (Fig 5.15A-D) The comparable mutant of $K_v1.6$ similarly has a reduced potassium selectivity relative to wild type. Without the hydrogen bonding group on the phenyl ring of $K_v1.6$_Y426F the reversal potential shifts to -60mV, reflective of a P_{Na}/P_K ~0.08 and an eighty fold increase in the permeability of sodium.

Interestingly, a search of the PDB databank structures for similar secondary structures to the K^+ filter reinforced both the necessity of pinning the peptide in place and consequence if such interactions are absent. The PDB was searched using the sequence of torsion angles found in the potassium channel selectivity filter. There were two major hits, the Jumonji domain of the PHF2 protein from *Homo sapiens* (106) and the Ferredoxin I proteins of multiple bacterial species (107, 108). Despite both containing a polypeptide backbone similar to the selectivity filter of K^+ channels, these proteins belong to distinct protein families and have very distinct folds and functions, both from each other and potassium channels. (Fig 5.16A-B) Furthermore, the protein sequence over this region, KCKYT of Ferredoxin I from *Azotobacter vinelandii* and KLGSL of PHF2, bears little similarity to the potassium channel signature sequence of TVGYG. Notably, while the PHF2 K^+ filter like structure is mobile, resembling the K^+ channel filter only in a single of five crystal conditions. This mobility is possibly reflective this sequence being a part of a loop exposed to solution

and only a single hydrogen bond between the KLGSL sequence and the adjacent protein. In contrast, the K^+ filter like sequence makes five hydrogen bonds with the adjacent protein, in addition to the amide nitrogens of the polypeptide directly abutting an iron-sulfur cluster. These interactions may serve to stabilize the motif in Ferredoxin I proteins, as indicated by the filter like structure being seen in a number of species.

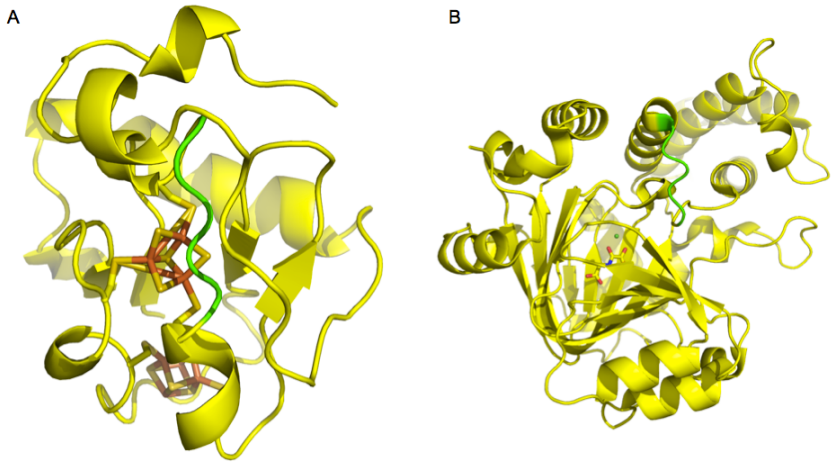

Figure 5.16. K^+ filter like structures are found in few other proteins, both stably and dynamically. Overall structure of (A) Ferredoxin I from *Azotobacter vinelandii* (6FDR, 1.40Å) (107) and (B) the Jumonji domain of PHF2 protein from Homo sapiens (3PUA, 1.89Å) (106). Colored in green is the K^+ filter like domain. Ligands within the structure are drawn as sticks.

Discussion

These results illustrate that there are two packing interactions critical for forming a potassium selective channel. Both the aromatic to aspartate hydrogen bond and the insertion of the signature sequence aromatic into the inter-subunit cleft appear to be necessary for the proper formation of sites 1 and 2 of the selectivity filter. Mutations of either position change channel selectivity, though the aspartate hydrogen bond acceptor appears to be the position most sensitive to mutation. Interestingly, while the Thr60-Tyr66 hydrogen bond appears to play a role

in the selectivity of NaK2K, as evidenced by the NaK2K_Y66F construct, some canonical potassium selective channels do not have this hydrogen bonding hydroxyl, but rather conserve a phenylalanine within their signature sequence of TVGFG. This may be a result of alternate interactions which stabilize the filter or represents a mechanism to tune individual channel selectivity to fit physiological function.

The ability to ablate selectivity by signature sequence mutation has already been noted functionally in studies on the Shaker potassium channel. In identifying the functional role of the signature sequence, systematic studies comparing selectivity to sequence were carried out (30). While the selectivity (P_{Na}/P_K) was defined by an upper bound rather than an average, notably mutation of the signature sequence from TVGYG to TVGFG to TVGVG results in a progressively higher maximum bound. While only defining the maximum permeability ratio, this trend agrees well with the NaK2K_Y66F results and the proposed necessity for structural rigidity within the filter for selectivity.

The differences in selectivity and sequence between these engineered potassium selective channels, NaK2K and NaK2Kir, and canonical potassium channel families shows that still other the means are seen to structurally restrain the selectivity filter. Particularly, in eukaryotic K_{ir} channels there is a conserved disulfide bond which further restricts movement of the selectivity filter relative to the pore helix (51).

Also of note are non-selective, or less selective K^+ channels, which have a K^+ channel signature sequence. Notable is the drosophila *ether-a-go-go* channel (*eag*) which has the signature sequences of SVGFG, very similar to the canonical K^+ channel signature sequence (43, 109-111) and yet is only weakly potassium selective. (Fig 5.17) However, the closely related mammalian K_v10 and K_v11 channel families, including the hERG channel, are known to be robustly potassium selective. In *eag* and the related mammalian channels the residue immediately following the signature sequence is an asparagine. In the case of *eag*, mutation of the

same position to aspartate (eag_N458D) still results in a non-selective channel (data not shown). However, this result could be partially or totally the result of packing difference in the pore domain of this distinct channel sub-family.

The sensitivity of selectivity to protein packing within the pore domain is further highlighted by natural occurring mutations. Disease causing missense mutations within the signature sequence and on the second transmembrane helix of $K_{ir}3.4$ cause a change in size and charge of these side chains, likely altering the packing of the selectivity filter (15). Correspondingly, these mutations result in non-selective channels under heterologous expression and *in vivo* likely initiate the signaling cascade which causes unrestrained cell proliferation.

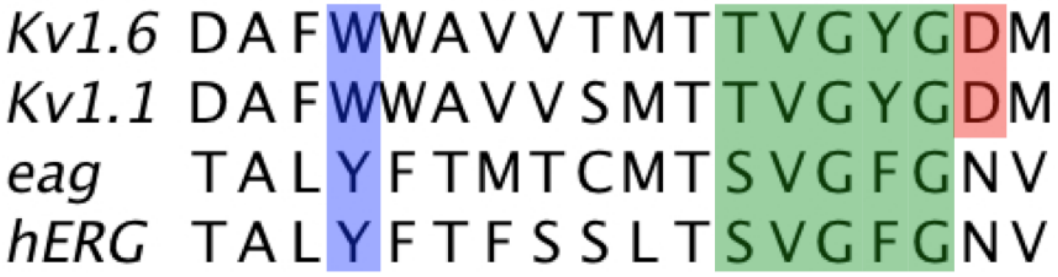

Figure. 5.17. There are K_v family potassium channels which clearly do not conserve the pinning aromatic to aspartate hydrogen bond. Partial alignment of the pore helix and filters of $K_v1.1$, $K_v1.6$, *eag* and hERG. The aromatic hydrogen bond donor, selectivity filter and acidic hydrogen bond acceptor positions are highlighted in blue, green and red, respectively.

The results of the torsion angle search demonstrate that while the selectivity filter structure may be energetically strained, with a significant portion of the sequence in the less favorable positive Phi region, such structures are not unique to K^+ channels. Notably, within in the K^+ channels two of these residues are glycine for which the allowable regions are much broader at positive and negative Phi angles. In this respect it is all the more remarkable to find a number Ferredoxin I proteins with this structure despite the absence of glycine in this sequence (107, 108).

Chapter 6. K^+ Channel Inactivation

Introduction

As the total ionic flux through the channel is a function of both unitary channel conductance and the time spent in the conductive state, regulation of time spent in the conductive state plays a significant role in channel physiology (3). Regulation of entry into non-conductive states, by both intrinsic properties of the channel and external factors, is central to the regulation of channel signaling. In potassium channels, a single channel may have a number non-conductive states with greatly disparate kinetics. (112-114). Broadly, the process of entering a long lived (seconds) non-conductive state is referred to as inactivation, while the appearance of a very transient (ms) non-conductive states is referred to as channel flicker.

The functional mechanisms and consequences of inactivation have been extensively studied in a number of channels, most classically in the voltage-gated sodium channels and its role in ending the depolarization step of the action potential (3). Within the potassium channels, inactivation is best studied in the voltage-gated potassium channels. There are two primary mechanisms of inactivation in tetrameric cation channels, named for the regions of the protein which govern the process. (Fig 2.16) N-type inactivation occurs when an amino-terminus from the channel or an associated protein inserts into the open channel and directly blocks ion flux. This “ball and chain” mechanism of inactivation can be alleviated by removal, enzymatically or genetically, of the amino-terminal residues. Differences in N-type inactivation among channels endogenous arise from differences in primary sequence or hetro-oligomerization with other subunits which provide the N-terminal inactivation peptide exogenously.

C-type inactivation is governed within the pore domain itself and typically has slower kinetics than N-type. It is believed to be the rearrangement of the selectivity filter into a non- or less conductive state,

based on its dependence on K^+ concentration or pore blockers. The kinetics of this filter rearrangement can also be altered by accessory proteins or pore domain interactions with the N-type inactivation ball, though such an indirect mechanisms remain poorly understood (115, 116). Interestingly, with C-type inactivation the selectivity of some potassium channels has been noted to change, further reflecting that structural changes in the selectivity filter are associated with the inactivation process (117, 118).

The C-type inactivation of potassium channels has been structurally studied primarily in the prokaryotic KcsA channel. As KcsA undergoes C-type inactivation after activation by pH jump, structural studies can be correlated to functional results in an effort to understand the selectivity filter structural changes that underly this inactivation. The side-chain most tightly correlated with inactivation kinetics is a glutamate on the pore helix (Glu71), the same side chain seen stabilizing the filter in the wild-type KcsA structure (72). (Fig 2.11) In association with the apparent differences in inactivation kinetics, the mutant channel KcsA_E71A crystallizes with two conformations, one similar to wild-type while the other has significant differences in the both the side chains packing around the filter and the selectivity filter structure itself. This rearranged filter, proposed as a non-conductive channel state and termed the “flipped” conformation, involves the rotation of the aspartate following the signature sequence toward the external solution and rotation of the carbonyls forming parts of sites 2-4 away from the ion conduction pathway. (Fig 6.1B) Interestingly, the kinetics of inactivation in KcsA seem to be tuned with the identity of this position on the pore helix. (Fig 6.3) Un-noted in the text of the same study, the same mutations which alter inactivation in KcsA also modulate potassium selectivity, and particularly KcsA_E71A has a notable increase in selectivity relative to the wild type channel.

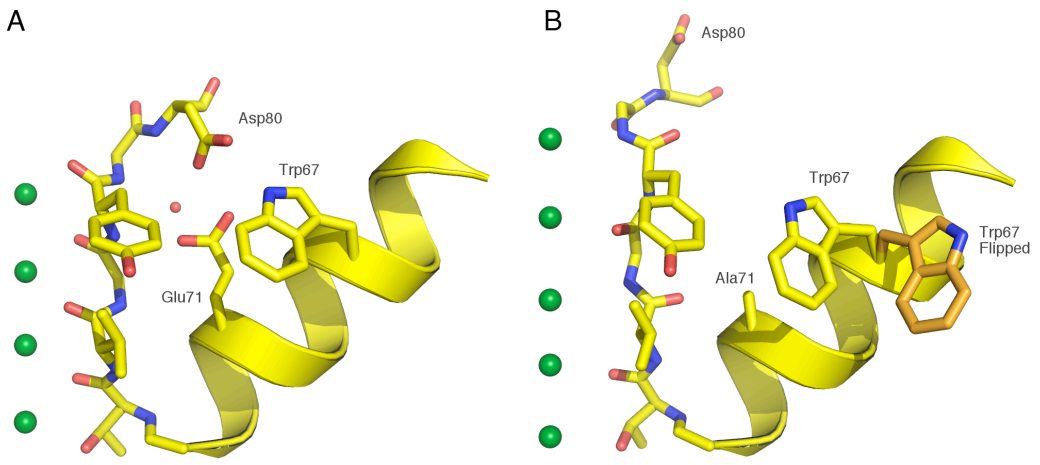

Figure 6.1. Structural changes with the P-loop proposed proposed during KcsA inactivation include structural changes in the filter and the aromatic to aspartate hydrogen bond (72). (A) Structure of the wild type KcsA (1K4C) pore helix and filter. (B) Structure of the KcsA E71A (2ATK, 2.5Å) highlighting the conformation changes in the flipped structure. Alternate conformations for Trp67 are shown in yellow and orange. Potassium ions and water molecules are shown as green and red spheres, respectively.

This result is contradicted by other studies on the KcsA_E71A mutation, using radioactive $^{22}Na^{+}$ flux assays, where sodium permeability is increased relative to the wild-type channel (119). In this study the KcsA_E71A filter is again observed in the flipped conformation when crystallized in sodium. Sodium ions are seen binding in plane with the carbonyls of the selectivity filter, in a mode similar to that seen in the high resolution NaK and MthK sodium structures (54, 55) and proposed in the KcsA lithium crystallized structure (68). These results suggest KcsA_E71A represents a less selective state and, more generally, a structural link link between selectivity and inactivation in potassium channel.

One additional later study demonstrated in KcsA the aromatic hydrogen bond donor on the pore helix of KcsA, equivalent to Tyr55 of NaK2K, also regulates the kinetics of inactivation, though without mention of selectivity (120). Mutation of the hydrogen bond donor tryptophan to

tyrosine yields a channel with slower inactivation, while the phenylalanine mutant has inactivation kinetics similar to KcsA_E71A.

Corresponding to the role of C-type inactivation as a mechanism which closes open channels, in KcsA the extent of filter rearrangement has been seen to correlate to the dilation of the cytoplasmic channel gate (121). Crystallization of KcsA with in a different detergent than typical can yields channels in a variety of open states despite a common crystallization condition. While the reason for the variety of crystallized channel states is unknown, there is a clear correlation between cytoplasmic gate diameter and structural change within the filter. Though resolution is limited, ion binding with the filter clearly changes, becoming inequivalent between the sites, and the filter peptide coordinating those ions appears to rearrange as the gate opens. (Fig 6.2) These structures provided the first direct evidence of coupling between cytoplasmic gate opening and structural rearrangements in the filter. This change is thought to be mediated by interactions between a bulky side-chain on transmembrane helix 2 of KcsA and the cytoplasmic ends of the selectivity filter and pore helix (122).

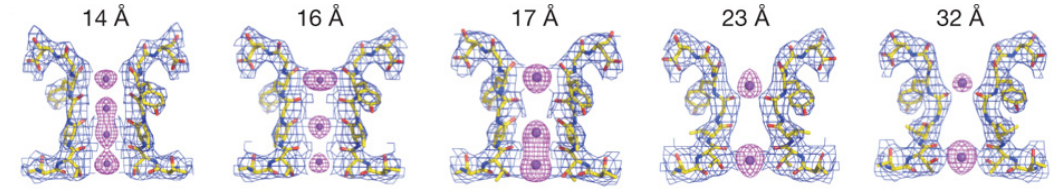

Figure 6.2. Changes in K^+ binding in the filter with cytoplasmic gate opening results in distinct changes in ion binding. Composite omit maps of the KcsA filter with various degrees of cytoplasmic gate dilation. Filter 2Fo-Fc density (blue) is shown at 2σ, while Fo-Fc ion omit maps are contoured at 4-6σ. Figure reproduced from (121).

Later work demonstrated that the side chain of this same glutatmate on the pore helix of KcsA, at position 71, also regulates short time scale gating in addition to modulating inactivation of the channel (123). (Fig 6.3) Differences in the millisecond timescale kinetics of the

channel, visualized as channel flicker in single channel traces, are apparent with mutation of this acidic group on the pore helix. This is also though to be due to differences in the hydrogen bond network between the pore helix and the selectivity filter.

However, while the amino-acid side chain identity at position 71 on the pore helix of KcsA is closely correlated inactivation and fast gating, this position is predominately a small, hydrophobic side-chain in other potassium channels; including those which natively undergo C-type inactivation. In addition, while the mutation of this pore helix glutamate in KcsA is more selective than wild-type (in one study) and does not inactivate the channel filter, a process believed to be related to rigidifying the filter, the structural study notes greater conformational flexibility (72). Thus KcsA may not serve as a general model for C-type inactivation.

Originally in an effort to confirm the role of this bridging hydrogen bond between the pore helix and selectivity filter, Tyr55 to Asp68 in NaK2K, mutations were made in the eukaryotic voltage gated channel K_v1.6 from rat (124). The comparable mutations were made to both the equivalent hydrogen bond donor, natively Trp416, and the hydrogen bond acceptor, Asp428. While the consequences to selectivity were discussed in the previous chapter, the mutation W415Y showed marked differences in inactivation and a time dependent correlation between both properties. In addition, mutations on NaK2K show difference in fast gating kinetics, perhaps suggesting a role for the effected bonds in regulating total channel conductance.

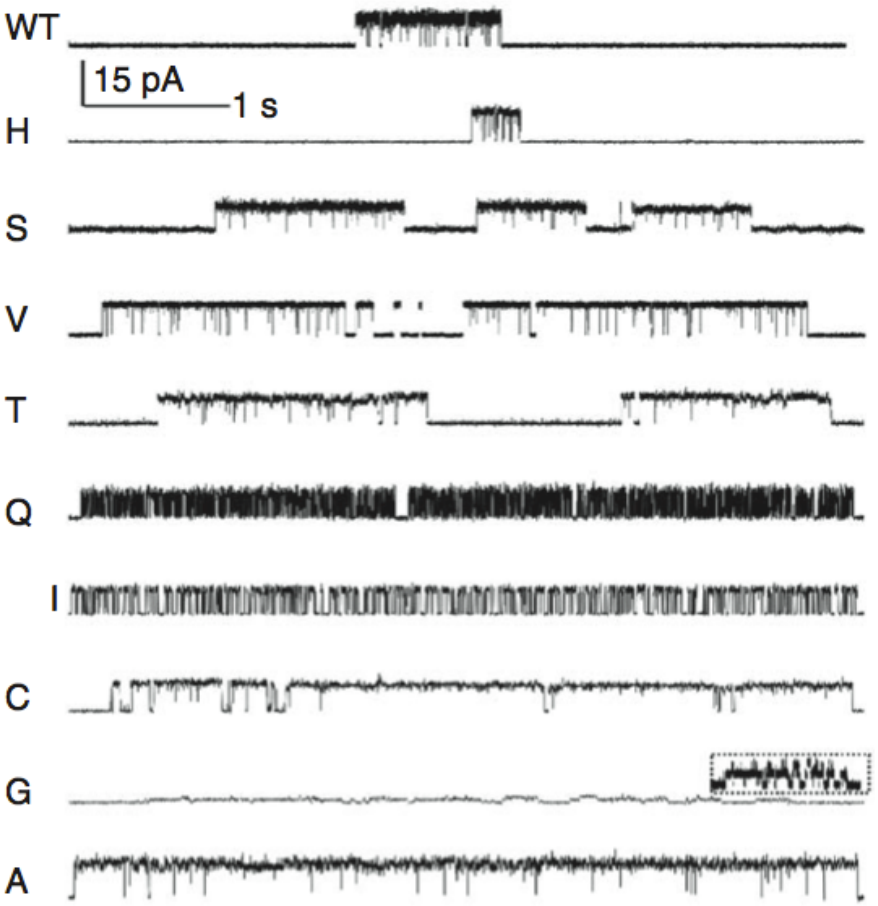

Figure 6.3. There are a variety of single channel KcsA behavior with changes in the interaction between the pore helix and the filter. Mutation of the KcsA channel pore domain Glu71 results in differences in differences in both short long gating kinetics after channel activation with pH jumps from 8.0 to 4.0. Figure reproduced from (123).

Results

The wild-type rat $K_v1.6$ channel and derived mutants were all expressed as GFP fusions in HEK293 cells and tested by bi-ionic whole cell patch clamp, with K^+ and Na^+ in the pipette and bath, respectively. The wild type channel is robustly potassium selectivity, as previously discussed, with a reversal potential of -105mV indicating a P_{Na}/P_K of less than 0.001. (Fig 5.10B) The channel is half maximally activated at -30mV and has a gating valence of 3.7, as calculated by fitting the voltage dependent activation to the Boltzmann equation. (Fig 6.4B) Notably, the channel does not appreciably inactivate after 200ms activation. (Fig 6.5)

The mutants $K_v1.6\_W415F$, $K_v1.6\_D428N$, and $K_v1.6\_D428E$ have markedly different voltage dependent activation relative to wild type, with a linear relationship between activation and voltage above 30mV. (Fig 6.4A) In each case these mutants are expected to break the bridging hydrogen bond between the pore helix and cytoplasmic end of the selectivity filter and the change in channel activation is perhaps due to voltage dependent changes in the filter or changes in coupling between the voltage sensor and channel filter. Given this anomalous behavior above 30mV descriptions of gating charge and voltage dependent activation will be based upon data recorded between -80 and 30mV. (Fig 6.4B)

Neutralization of the hydrogen bond acceptor, $K_v1.6\_D428N$, results in a channel requiring greater depolarization to open, with a $V_{1/2}$ of 0mV and the gating charge is reduced to 2.5. Similarly, replacing Asp428 with the other acidic residue, glutamate, yields the mutant $K_v1.6\_D428E$ which also causes the channel to open at more depolarizing voltages than wild-type, with a $V_{1/2}$ of -15mV and a gating charge of 2.6. The mutant $K_v1.6\_W416F$, which ablates the pore helix hydrogen bond donor, requires a positive voltage to open ($V_{1/2}$ of 20mV) and has a gating charge of 1.9. Each of these mutations the channel is non-selective and does not significantly inactivate over ≥200ms. (Fig 6.5)

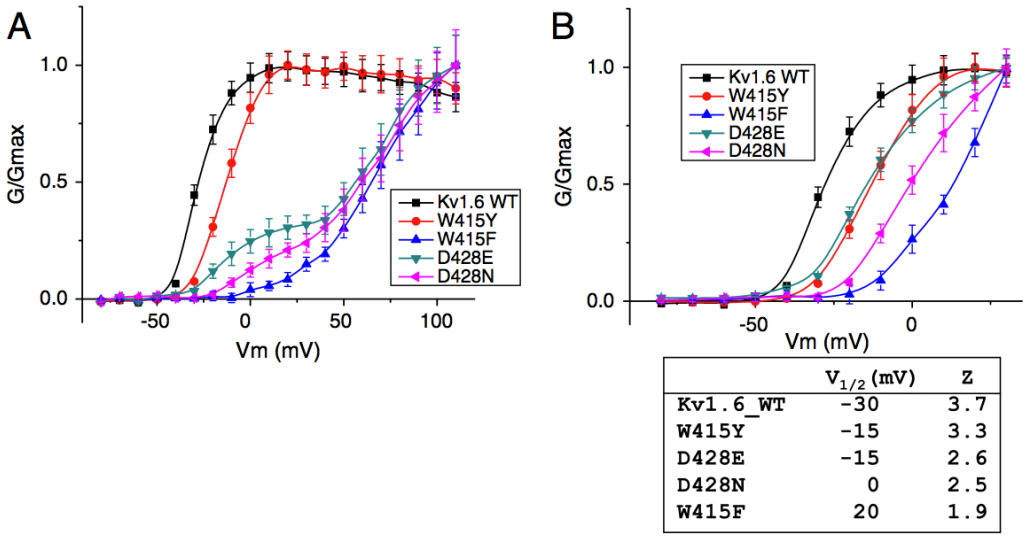

	$V_{1/2}$ (mV)	Z
Kv1.6_WT	-30	3.7
W415Y	-15	3.3
D428E	-15	2.6
D428N	0	2.5
W415F	20	1.9

Figure 6.4. Voltage dependent activation curves of K_v1.6 and derived mutants. (A) Plot of G/G_{max} from -80mV to +120mV. (B) Plot of G/G_{max} from -80mV to +30mV with $V_{1/2}$ and Z values calculated by fitting to the Boltzmann equation. Figure reproduced from (78).

The greatest differences in selectivity and gating appears in the K_v1.6 mutant K_v1.6_W415Y, where the aromatic hydrogen bond donor is maintained. Though the channel activates similarly to wild-type over the entire voltage range, with a $V_{1/2}$ of -15mV and gating charge of 3.3, there is a marked difference in channel inactivation and selectivity. (Fig 6.4) While the wild-type channel did not noticeably inactivate over experimental timescales of activation, the mutant K_v1.6_W415Y channel rapidly inactivates under the same conditions. (Fig 6.5) Interestingly, this inactivation correlates with selectivity. Measuring reversal potentials 10ms after activation K_v1.6_W415Y is still potassium selective with a P_{Na}/P_K of 0.007. (Fig 6.6) However, if held for 200ms at the activating potential and allowing the channel to apparently inactivate, the channel becomes markedly less selective with a reversal potential of -40mV indicating a P_{Na}/P_K of 0.20.

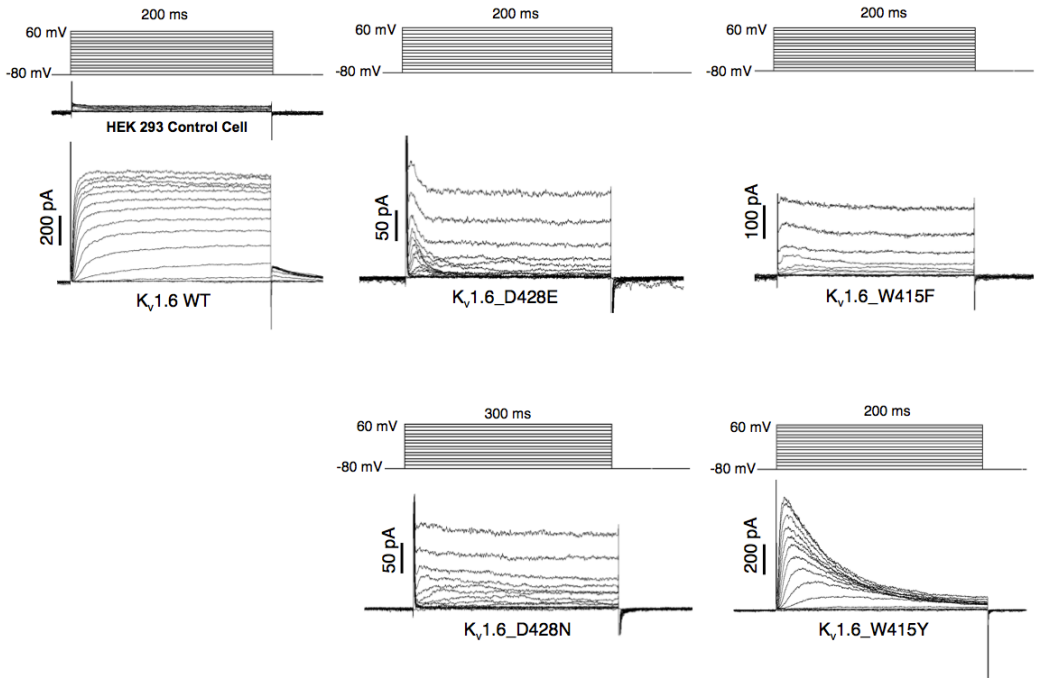

Figure 6.5. Mutation of the aromatic hydrogen bond donor is sufficient to cause Kv1.6 to inactivate after channel opening. C-type inactivation was not observed in wild-type K_v1.6, nor any of the mutants except W415Y where the channel significantly inactivated after membrane depolarization. Figure adapted from (78).

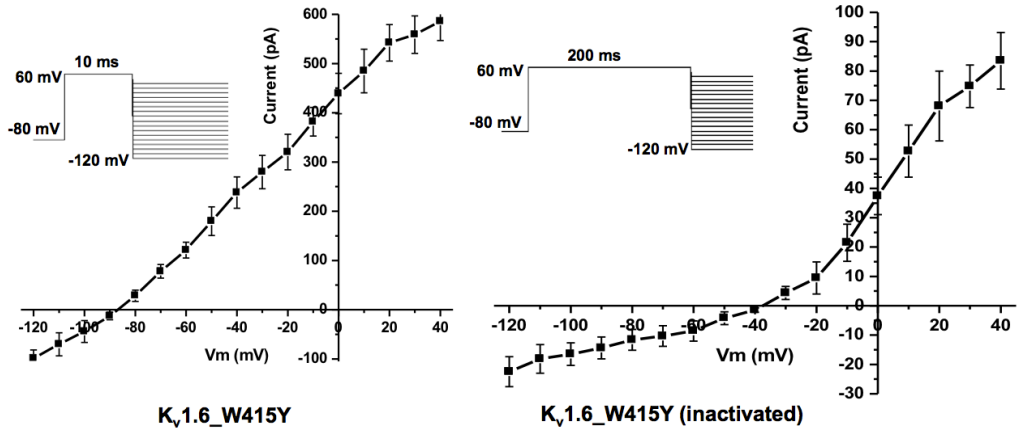

Figure 6.6. The selectivity of the K_v1.6_W415Y mutant is inactivation state dependent. I-V curves of K_v1.6_W415Y after 10ms (left) and 200ms (right) under bi-ionic conditions tail currents using whole-cell patch clamp of HEK293 cells. Figure adapted from (78).

Also of note are channel gating properties in the millisecond scale, also referred to as channel flicker. The NaK2K channel and derived mutants at either the aromatic hydrogen bond donor or aspartate acceptor positions (55 or 68) exhibit rapid opening and closing kinetics in single channel traces, irrespective of channel selectivity. (Fig 6.7) However, the mutant NaK2K_Y66F exhibits only rare and brief channel closing under the same conditions, in addition to the previously discussed three-fold loss in potassium selectivity. (Figs 5.14F & 6.7)

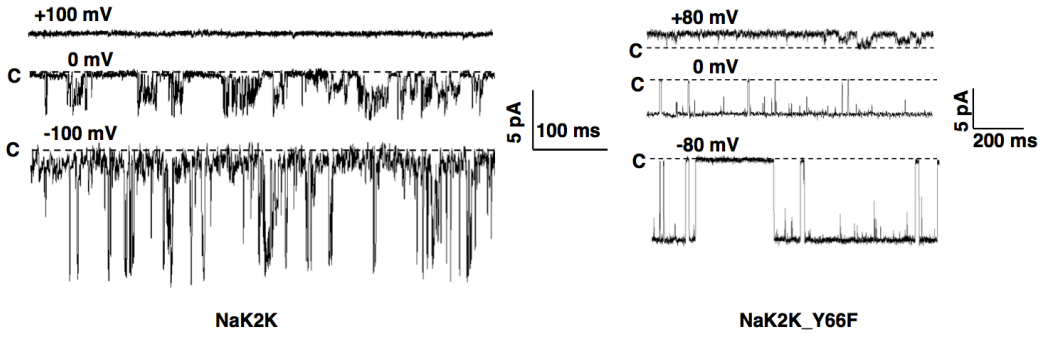

Figure 6.7. Loss of a single hydroxyl is sufficient to change the fast single channel gating behavior between NaK2K and NaK2K_Y66F. Single channel recording under bi-ionic conditions of NaK2K (left) and NaK2K_Y66F (right). Figure adapted from (78).

Structurally there is no discernible difference in the filter of NaK2K_Y66F relative to NaK2K. (Figs 5.14E) However, there is a ~1Å movement of the water hydrogen bonded to Asp68 and the B-factors of the buried water molecules within the pore domain are higher than NaK2K, perhaps reflecting a similar mechanism of modal gating seen in KcsA. (Fig 6.8)

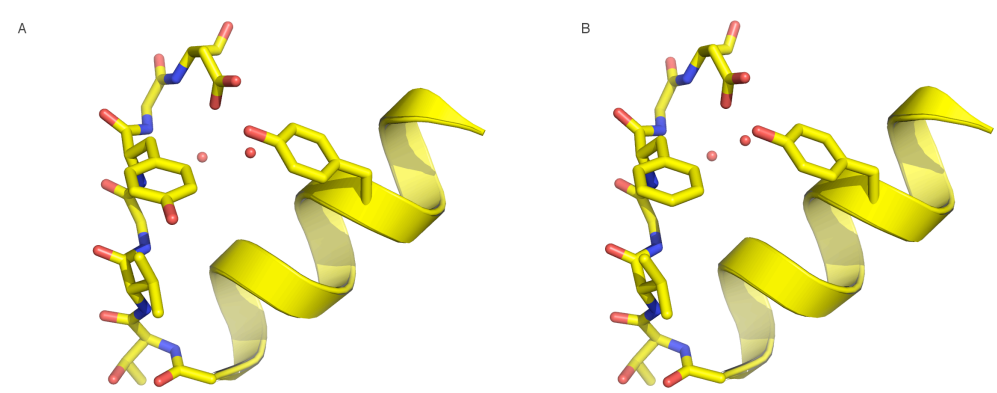

Figure 6.8. The tyrosine to phenylalanine mutation results in a shift in the location of a water between NaK2K and NaK2K_Y66F (78). Stick rendering of (A) NaK2K and (B) NaK2K_Y66F. Potassium ions and water molecules are drawn as green and red spheres, respectively.

Discussion

These results indicate that both fast and slow closing of the channel pore is governed by a number of interactions within the pore domain. While complicated by different model systems these results do appear to confirm the role of the aromatic hydrogen bond donor in regulating C-type inactivation at the channel filter, in agreement with previous studies on KcsA, $K_v1.1$ and $K_v1.2$ (72, 120, 125). However, the exact role of this aromatic group or mechanism of filter rearrangement with C-type inactivation remains unclear.

In the present studies of $K_v1.6$ only tyrosine causes inactivation, not phenylalanine or tryptophan. These inactivation results are also remarkable in terms of inactivation when taken together with the NaK2K mutations. The NaK2K mutants do not observably inactivate under any condition. When comparing the role these aromatic mutations in altering C-type inactivation kinetics, no consistent pattern is apparent, other than confirming the role of this particular position. In aggregate, these results suggest that other residues, both within and perhaps outside of the pore domain, must be involved in regulating inactivation. This is perhaps

expected as C-type inactivation is thought to be coupled to channel opening and therefore the movement protein domains distant in both primary sequence and ternary structure from the filter.

Channel	Rate of Inactivation by Pore Helix Aromatic
KcsA	W > Y >> F
K_v1.1	Y > W (F non-conductive)
K_v1.2	F >> Y > W
NaK2K	(never inactivates)
K_v1.6	Y >> W = F

Table 6.1. Rates of C-type inactivation depend on the pore helix aromatic differentially between a number of K^+ channels.

Notably, the flipped structure of KcsA_E71A mutant is similar in some respects to the non-selective NaK2K_Y55F, NaK2K_D68E, and NaK_D66Y (equivalent to NaK2K_D68N). In all cases the side chain following the signature sequence, at position 68 in NaK2K, is reoriented away from the core of the protein and within the NaK2K mutants there is a clear increase in the mobility of the filter backbone. However, as previously mentioned, none of the NaK2K mutants notably inactivate or undergo as extensive the structural rearrangements seen in KcsA_E71A, suggesting that more than the movement of the conserved Asp or general mobility of the filter is required for inactivation. Temptingly, in the flipped KcsA_E71A structure only the site 4 potassium binding site is retained (72), while in all the NaK2K mutants the original sites 3 and 4 of NaK are preserved. It is possible that differences in the binding site number or shape might be the basis of the differences in conductance.

While there are no consistent differences in pore sequence between K_v1 family members related to inactivation, there is clear functional coupling between the gating domain, cytoplasmic gate and filter which regulates C-type inactivation. Structurally the cytoplasmic gate and

filter have been shown to be linked by the dilation induced filter changes of KcsA (121, 122). Additionally, it is known that N and C-type inactivation are functionally coupled, where the presence or absence of the N-type inactivation peptide alters C-type inactivation kinetics, despite being distant in the primary sequence and site-of-action within the channel (115, 116). Collectively, these results suggest C-type inactivation in K_v channels may be regulated by parts of the protein, perhaps distant in primary sequence from the filter. Such a hypothesis is supported in part by the changes in voltage-dependent activation of rat K_v1.6, with mutations in the pore domain, distant from the voltage sensor, altering the voltage dependence of channel opening.

While differences in buried water molecules have been implicated in the modal gating of KcsA, such differences were thought to be dependent on the identity of the amino acids on the pore helix (73). A comparison of NaK2K and NaK2K_Y66F shows no corresponding change in the number of buried waters, though there is a notable difference in the position and mobility of the waters. However, as the filter backbone amide of Gly67 is involved in coordinating these water molecules, this difference may be the result of the absent hydrogen bond restraint on position 66 in NaK2K rather than direct interactions with the mutated tyrosyl side-chain.

Similar to this study of fast gating in NaK2K, the inwardly rectifying potassium channel K_{ir}6.2 normally has brief channel inactivation events by single channel electrophysiology with grossly similar characteristics to NaK2K (126). This is despite the absence of hydroxyls on the pore helix or selectivity filter positions equivalent to the Thr60 or Tyr66 of NaK2K, and rather are Val and Phe in K_{ir}6.2, respectively. The double mutation restoring the more typical threonine and tyrosine at each respective position of K_{ir}6.2 (V127T/F133Y) results in a channel with fewer fast kinetic events, though changes in selectivity are not discussed. While this mutation should result in a hydrogen bond similar to the Thr60-Tyr66

hydrogen bond seen in NaK2K it is notable that the changes in channel kinetics are opposite of what would be predicted by NaK2K.

Chapter 7. Heavy Ion Binding

Introduction

In the studies of potassium channel selectivity it has been noted that while K^+ channels can largely discriminate between the group 1 cations this selectivity appears to be discriminatory primarily against the smaller cations. (Table 2.1) The K^+ channels preferentially conduct potassium in the presence of either lithium and sodium despite sub-angstrom differences in radius (3). However, the selectivity is much weaker against the larger alkali metal rubidium despite the larger ionic radius. Further, the next group 1 cation, cesium, is still appreciably conducted despite a difference in radii larger than that between potassium and sodium.

In the initial structural studies of KcsA, Rb^+ and Cs^+ were used to determine the ion conduction pathway and ion binding sites, taking advantage of their significantly stronger diffraction relative to potassium (47). Rubidium and cesium binding sites were seen within the filter, demonstrating the direct carbonyl-ion coordination of conducting ions. With the availability of high resolution structures, comparisons were drawn between the differences in ion binding profiles of rubidium and potassium and correlated to the rates of ion conduction (44). The inequivalent ion binding of rubidium within the filter was thought to underly the saturating conductance rubidium, as compared to the increasing conductance of potassium with greater concentration which was thought to be related to the equivalent K^+ binding across all four sites.

With the availability of both structural and functional analysis, KcsA has been extensively used to study the structural and energetic consequences of ion binding in the potassium channel filter. In structural studies of ion binding it was noted that ions larger than potassium still bound the filter without a structural change of the coordinating protein (44, 127). The larger rubidium and cesium ions bind inequivalently at only

three sites within the filter. While the ion binding at sites 1 and 4 is similar among monovalent ions an additional Rb^+ and Cs^+ binds more broadly between sites 2 and 3, clearly not centered as is seen with K^+ within the square anti-prism structure of the filter. In all cases the occupancies of the ions total approximately 2 ions per filter, arguing for a specific charge requirements of ions within the filter to electrostatically balance the partial negative charge of the ion coordinating groups.

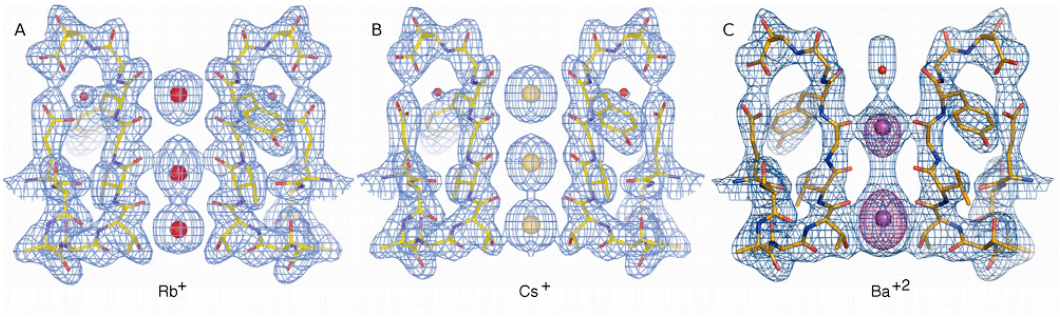

Figure 7.1. Rubidium, cesium and barium cations bind distinctly within the KcsA filter. (A) The KcsA filter structure in the presence of Rb^+ with 2Fo-Fc electron density map in blue. Rubidium ion are drawn as large red spheres. (B) The KcsA filter in the presence of Cs^+ with 2Fo-Fc electron density map in blue. Cesium ions are drawn as large gold spheres. (C) The KcsA filter in the presence of Ba^{+2}. The 2Fo-Fc electron density map and the anomalous difference density map are shown in blue and magenta, respectively. Barium ions are drawn as large magenta spheres. Water molecules are shown as small red spheres in all panels. Figure adapted from (127, 128).

Later work analyzing the thermodynamics of ion binding by ITC in KcsA provided further information about how the potassium channel selects ions. Heat was clearly liberated with the addition of potassium to the detergent solubilized channel in sodium. This heat appears to be a consequence of the filter transitioning out of a non-conductive state, as a constitutively non-conductive mutant has no heat associated with sodium to potassium titration. Rubidium and cesium both also liberate heat with ion binding. This result demonstrates that the free energy of binding is similar between potassium and cesium and even more energetically

favorable for rubidium. This energetic trend is in contrast to the permeability series for these ion, where potassium and rubidium are of similar permeability and cesium is significantly less conductive. However, this result represents the steady state binding of ion to the filter and not the dynamic permeation of ions through the filter. While the free energy of ion binding reflects the favorability of the binding reaction permeation is a kinetic process also dependent on the energy barriers between binding sites. Put another way, ion permeation may also be governed by the activation energy between ion translocation steps.

Ion	Radius (Å)	K_D (mM)	ΔG^o (kcal M^{-1})	ΔH^o (kcal M^{-1})	ΔS^o (kcal M^{-1} K^{-1})
Na^+	0.95	nhd			
K^+	1.33	0.43 ± 0.04	-4.54 ± 0.06	-1.24 ± 0.13	11.2 ± 0.48
Rb^+	1.48	0.12 ± 0.06	-5.29 ± 0.29	-1.93 ± 0.24	11.4 ± 1.27
Cs^+	1.69	0.44 ± 0.13	-4.53 ± 0.17	-1.81 ± 0.30	9.23 ± 1.18
Mg^{+2}	0.65	nhd			
Ca^{+2}	0.99	nhd			
Ba^{+2}	1.35	0.19 ± 0.06	-5.03 ± 0.15	-5.51 ± 0.68	35.7 ± 2.37

Table 7.1. The ion binding thermodynamics of KcsA vary with cation. These energetics have distinct entropic and enthaplic contributions despite similar free energies (128). Values measured from isothermal calioremetry of detergent solubilized KcsA. nhd = no heat detected.

The study is also difficult to interpret based on selectivity as some potassium selective channels conduct sodium in the absence of potassium, perhaps as a consequence of the filter not collapsing into a non-conductive state. Similar measurements in a non-collapsing channel may prove informative on the competition for ions within the filter of K^+ selective channels. This point is further confused when comparing the energetics of the ion titration from lithium. Though heat is liberated when

titrating potassium into lithium soaked KcsA, none is observed when titrating with sodium. While the authors argue that the heat measured comes from structural changes in the protein, this is contradictory to previous structural studies on KcsA in lithium which demonstrated that the filter adopts the conductive conformation even in the absence of potassium (68).

Interesting also to ion binding and selectivity is the classic K^+ channel blocker barium. The ion Ba^{+2} permeates through some portion of the pore to reach a low energy binding site and block current through the channel (129, 130). While the Ba^{+2} ion may also permeate the entire length of the channel, it must do so with such slow kinetics as to effectively block any apparent current. Structurally, Ba^{+2} appears to bind at sites 2 and 4 in the KcsA channel filter (128, 131). Corresponding to a very similar ionic radius to potassium, the barium bound structure largely does not change relative to the K^+ saturated KcsA structure. As expected for a blocker, the free energy of ion binding is the slightly lower for barium than potassium. However, the thermodynamics driving this binding are significantly different from the group 1 cations, as the enthalpic contribution is unfavorable but compensated for by a large entropic contribution.

A channel family where ionic blocking of channel current is of particular biological relevance are the CNG channels. Calcium in believed to act as a classical permeating blocker of CNG channels, where its slow conduction blocks the sodium and potassium currents. While the CNG channel family are non-selective they are phylogenetically related to K^+ channel and believed to have filters utilizing similar chemistry (13). In studies on the NaK2CNG model channels, calcium was observed to bind within the filter in modes similar to potassium (71). Further, calcium binding occurred without a structural change within the filter itself. The common binding site for potassium and calcium in NaK2CNG channel filters is interesting given the distinct differences in ion size and charge

and the fact that despite the individual binding sites being equivalent K^+ channels are not known to either conduct or be blocked by calcium.

While heavy ion binding within the filter of KcsA has previously been characterized, the differences in ion binding among the NaK2CNG channels suggest that ion binding can be regulated by the protein in ways outside of direct ion-ligand chemistry. Based on the hypothesis that the protein environment around the filter is distinct between KcsA and NaK2K, soaking experiments were carried out using rubidium, cesium and barium to examine differences in heavy ion binding between these potassium selective channels.

Results

To compare monovalent cation binding NaK2K crystals crystallized in a potassium containing buffer were soaked into a stabilization solutions where rubidium and cesium replaced the potassium of the mother liquor. For the barium soaked crystals, barium was added via barium chloride to the stabilization solution still containing potassium. Data sets of the soaked crystals were collected at a wavelength of ~1Å. Each structure was refined to 2Å or better and anomalous diffraction allowed for unambiguous identification of the Rb^+, Cs^+ and Ba^{+2} binding sites. While all heavy ions could be fit, in each case the native Fo-Fc maps near the ions clearly showed Fourier truncation ripples near the strong scatters as a result of insufficient resolution to fully describe the diffraction of these elements (132).

The overall structure and that of the selectivity filter does not significantly change in the rubidium soaked NaK2K channel structure relative to potassium, with an RMDS over the signature sequence of less than 0.2Å. (Fig 7.2A) Rubidium ions bind clearly at sites 1, 3 and 4 based on the strong diffraction at these sites. (Fig 7.2B) The identity of the ions at these sites were confirmed by the anomalous signal of the anomalous difference map. (Fig 7.2C)

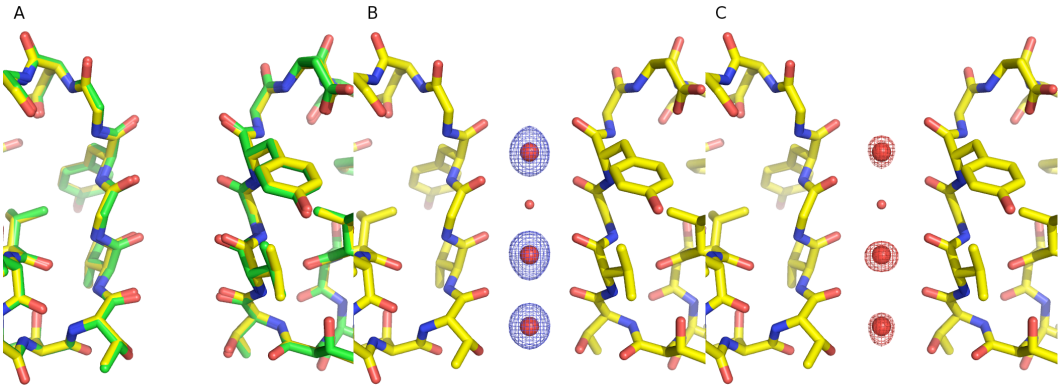

Figure 7.2. Rb^+ binding can clearly be seen with an unchanged NaK2K channel filter. (A) Structural overlay of NaK2K in K^+ (green) and Rb^+ (yellow) (B) Fo-Fc ion omit map of NaK2K soaked in Rb^+, contoured at 8σ. (C) Anomalous ion omit map of NaK2K soaked in Rb^+, contoured at 8σ. Rubidium ions and water molecules are show as large and small sphere, respectively. The structure is refined to 1.8Å.

The cesium soaked NaK2K structure also show strongest density at site 3 in the selectivity filter, with weaker density at sites 1 and 4. (Fig 7.3B) Sites 1 and 3 were confirmed as cesium by strong density in the anomalous map. (Fig 7.3C) However, site 4 has been built as a contaminating K^+ ion as no anomalous diffraction is seen at this site. As with the rubidium soaked NaK2K structure, only minor changes are seen in the structure, with an RMSD over the signature sequence of approximately 0.2Å. (Fig 7.3A) Interestingly, a cesium ion partially coordinated by the channel protein is seen at the external face of the filter, as had been previously seen in the high resolution K^+ crystallized KcsA structure, though in this case the partially dehydrated ion is clearly off the central axis of the ion conduction pathway.

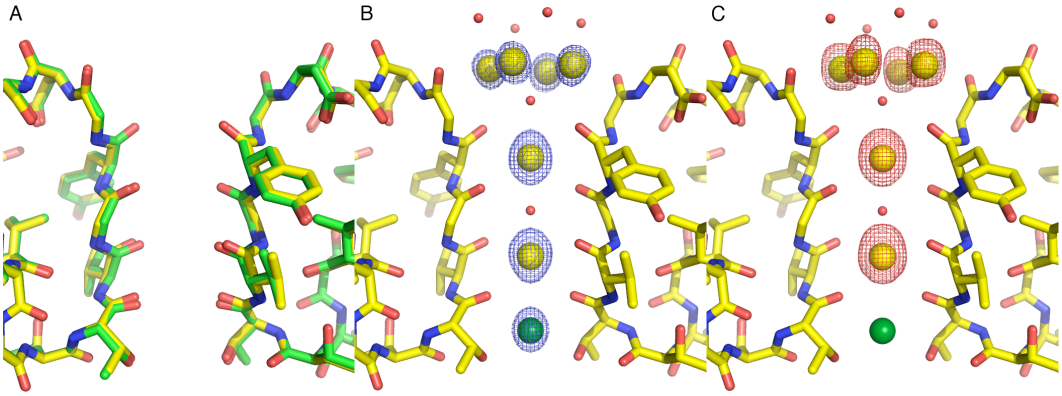

Figure 7.3. Cs^+ ions bind discretely at two sites within an unchanged NaK2K filter structure. (A) Structural overlay of NaK2K in K^+ (green) and Cs^+ (yellow) (B) Fo-Fc ion omit map of NaK2K soaked in Cs^+, contoured at 8σ. (C) Anomalous ion omit map of NaK2K soaked in Cs^+, contoured at 5σ. Cesium ions, potassium ions and water molecules are drawn as yellow, green and red spheres, respectively. The structure was refined to 1.83Å.

As with both rubidium and cesium, barium binding within the filter did not result in significant structural change (RMSD 0.1Å). (Fig 7.4A) The structure of the NaK2K channel soaked into a buffer containing both K^+ and Ba^{+2} has ion clearly bound at sites 1, 3 and 4 within the filter and with an additional ion at a site external to the filter (S0) coordinated by water molecules. (Fig 7.4B) The native map has strongest density at site 3, with density also seen in the anomalous difference map, corresponding to a bound Ba^{+2} ion. (Fig 7.4C) Potassium ions are seen bound at sites 1 and 4, in positions similar to the potassium co-crystallized NaK2K channel. Notably, the potassium ion at site 4 is clearly translated toward the cytoplasmic surface of the membrane relative to the K^+ only NaK2K and KcsA structures (Figs 7.4B and 5.3).

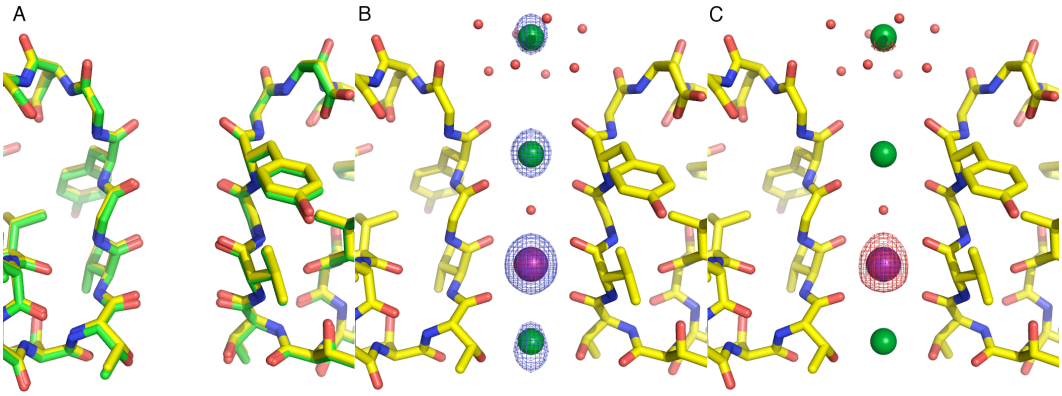

Figure 7.4. Ba^{+2} binds at a single site within the unchanged NaK2K selectivity filter. (A) Structural overlay of NaK2K in K^+ (green) and Ba^{+2} (yellow) (B) Fo-Fc ion omit map of NaK2K soaked in Ba^{+2}, contoured at 8σ. (C) Anomalous ion omit map of NaK2K soaked in Ba^{+2}, contoured at 8σ. Barium ions, potassium ions and water molecules are drawn as purple, green and red spheres, respectively. The structure is refined to 2.0Å.

Discussion

The differences in Ba^{+2} and Cs^+ binding sites between NaK2K and KcsA, despite identical chemistry and geometry of the coordinating ligands, is perhaps a consequence of the electrostatic environment surrounding the filter. The glutamate on the pore helix of KcsA introduces a negative charge adjacent to the selectivity filter absent in most K^+ channels, as discussed previously. This difference in local electrostatic environment may underly the two Ba^{+2} ions bound within the KcsA filter, distinct from the single ion bound within the NaK2K selectivity filter. This single barium bound within the filter of NaK2K fits well with the functional studies of barium-potassium competition in the BK channel (130), while modeling of barium block in KcsA requires a two ion block model (133). This, in addition to the greater similarity of protein packing interaction between NaK2K and the K_{Ca} family, compared to KcsA and K_{Ca}, suggest that NaK2K may serve as a better structural model for comparing previous functional studies of ion binding and block to K^+ channel structure in the K_v and K_{Ca} channel families.

The differences in ion binding between NaK2K in K^+ or a K^+/Ba^{+2} mixture are most intriguing as they suggests both a mechanism for the barium block of K^+ currents and also give a direct visualization of the electrostatic interactions between ions within the filter. Barium binding at site 3 causes a shift in the binding position at site 4, suggesting that the presence of an ion at site 3 alters the affinity and equilibrium ion binding position at adjacent sites. This change in affinity agrees well with previous functional studies of barium blocking of the BK channel, where K^+ affinity is particularly weak adjacent to the apparent Ba^{+2} site. This result is still more dramatic at site 2 of the NaK2K-K^+/Ba^{+2} structure, where the occupancy of K^+ is zero and a water appears to be bound between the ions at sites 1 and 3. While this repulsive interaction of ions within the filter is most likely exaggerated due to the more strongly charged Ba^{+2}, this structure can serve as a model for a channel trapped in the 1,3 state during K^+ conduction (44, 127). The reduction in electron density and shifted position of the K^+ at site 4 in NaK2K with barium bound suggests that ion-ion interactions alter K^+ occupancy within the filter, even in the absence of major structural changes of the filter polypeptide. Similar mutual destabilization of K^+ ions within the filter has previously been proposed for efficient K^+ conduction, though this structure allows for direct visualization of the effect.

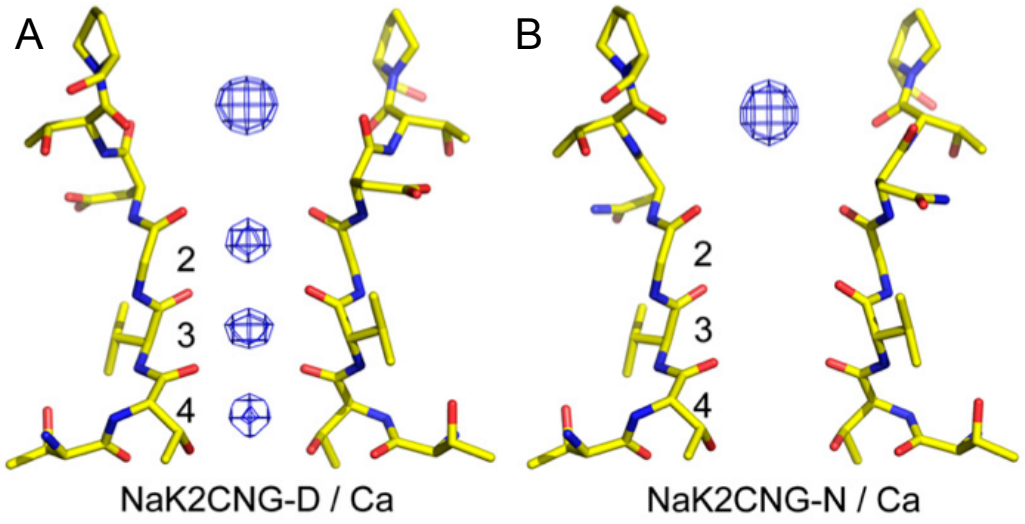

Figure 7.5. Calcium binds distinctly between NaK2CNG-D and NaK2CNG-N despite identical coordinating chemistry at sites 2-4. (A) Fourier difference map between NaK2CNG-D soaked in solutions containing 100mM NaCl/25mM CaCl2 and 100mM NaCl. (B) Fourier difference map using the same solutions for NaK2CNG-N. Maps are contoured at 8σ and at 1.8Å resolution for both. Figure adapted from (71).

Complementary to this study of K^+ channel heavy ion binding are an additional series of mutations on NaK modeling the CNG channel pore which generated two additional three-sited channels by replacement of the NaK2CNG-D Asp66 residue in the pore sequence with either glutamate (NaK2CNG-E) or asparagine (NaK2CNG-N) (71). These channels are also non-selective under bi-ionic conditions and had similar conductance of potassium alone. While the packing within the core of the protein varies between mutants, all maintain a three-site selectivity filter configuration similar to NaK2CNG-D. However, these mutants did not have equivalent ion binding despite the common structure, as each mutant had distinct ion binding differences are seen via calcium and sodium co-crystallization. Most illustrative is the affinity for calcium, a permeating blocker in both the NaK2CNG model channels and canonical CNG channels. When crystallized in the presence of calcium there are clear differences in

number and position ion calcium binding within the filter of these mutants,.This calcium binding corresponds to known differences calcium affinity in the equivalent CNG channels and agrees well with the effective calcium block of currents in the NaK2CNG channels. These differences indicate that indirect interactions can alter ion affinity within the pore and need not include structural changes within the filter.

Chapter 8. Discussion

Potassium channels are proteins which selectively conduct potassium ions to the exclusion of other monovalent cations, most notably sodium. Frequently opened by voltage or ligand dependent gating domains these channels are ubiquitously expressed in human tissues but most classically studied for their role in the action potential of excitable cells (3). In this role the ligand gated K^+ channels are involved in the cellular response to stimulation, inwardly rectifying potassium channels set the resting potential of the cell, and voltage gated potassium channels restore the resting membrane potential to terminate the action potential.

Given their central role in cell signaling, the importance of potassium channels to human physiology has been demonstrated in a number of processes, including a direct role in gustation (taste) (134, 135), glucose homeostasis (136), and renal function (137) and indirectly in the propagation of numerous sensory and locomotive signals. As a consequence of their ubiquitous role, mutations in these channel genes results in numerous diseases. While many of these mutations are nonsense or frame shift mutations, where the disease is simply the result of absent or non-functional protein (138); other missense mutations result in channels with altered behavior including adrenal adenomas, long-QT syndrome, and seizure (15, 16, 139).

In these studies of potassium channels, using NaK as a structural scaffold, the importance of protein packing to K^+ channel filter stability, selectivity, and gating was clearly illustrated. Channel selectivity, gating and ion binding depend on residues distant in both sequence and structure from those which directly coordinate the permeating ions. Ions are bound by and conduct through a structure primarily made up of the backbone carbonyls of the signature sequence, in addition to threonine hydroxyls. However, despite the coordinating ligands being the largely from the common polymer backbone, channel structure and selectivity can

be both subtly and grossly changed by the side chains which stabilize this structure.

These results contradict some, though not all, previously proposed mechanisms of potassium selectivity. Based upon the binding site number study, the chemistry of each individual site sequential ion is insufficient alone to determine selectivity. This suggests that previously proposed selectivity mechanisms based on ligand chemistry and individual binding site coordination number may represent necessary but insufficient features of K^+ selective channel pores. It is also notable that the sequential increase from 2-4 binding sites in the NaK mutants has a step function-like increase in selectivity at four sites, rather than a graded increase in selectivity. Such a graded response might be expected if hydration of ions within the filter were expected to play a role in selectivity, as water access to the permeation pathway should scale inversely with number of binding sties (65). A similar graded change in selectivity with number of binding sites would be expected if channel selectivity were the result of multiple partially selective sites. Further, the NaK2K and NaK2K_Y66F comparison highlights the fact channels can have appreciably different selectivity despite identical protein structures. However, these results are not in conflict with other proposals of selectivity, notably the hypothesis that sodium and potassium bind at distinct locations within the same binding site structure and interactions of competing ions within the filter underlies selectivity (54, 60, 71). Additionally, these results do not exclude the possibility of necessary features within each ion binding site, such as ligand-ion chemistry, geometry or coordination number.

This potassium selective filter structure requires at least two key interactions to stabilize the filter, highlighted in this study. These interactions, between the filter sequence and the pore helix, act to hold the filter in the proper structure for forming a four sited K^+ selective structure. Though the nature of these interactions appears to change between

families, some type of interaction appears conserved in each clade of potassium channels.

Common to all K^+ channel structures is the insertion of the conserved aromatic within the signature sequence, either phenylalanine or tyrosine, into a cleft formed at the interface to the adjacent subunit. In many cases the same position, when a tyrosine, is further restrained by a hydrogen bond to a conserved threonine on the pore helix. An additional bond between the C-terminal end of the filter and the pore helix is also required. In the K_v and K_{Ca} channel family this pinning interaction is an aromatic, tyrosine or tryptophan, to aspartate hydrogen bond while in the K_{ir} channel family a salt bridge is conserved. Mutations which interfere with these bonds often result in a ablated or lost potassium selectivity, as was functionally illustrated in the K_v1.6 and NaK2Kir channels and both structurally and functionally demonstrated in the NaK2K channel.

The sensitivity of selectivity to mutations within the pore domain has been demonstrated previously in a number of eukaryotic channels, in some cases correlated to disease. Mutations in the pore domain of K_{ir}3.4 cause a loss of selectivity which appear to be causative in the formation of adrenal adenomas (15). In addition, the naturally occurring differences in the P-loops of K_{Ca}2.1 (93), HCN (14, 92), and CNG (13) channels may underly the differences in their selectivity relative to canonical potassium channels and be relevant to their physiological function.

In some cases the differences in packing around the filter can also give rise to changes in both C-type inactivation and fast channel gating. In the rat K_v1.6 channel, mutations that alter selectivity can also change inactivation kinetics. Interestingly the inactivating K_v1.6 channel mutant (W415Y) also has state dependent differences in selectivity, as has been previously described (117, 118). However, the fact that equivalent mutations show no change in the inactivation of NaK2K indicate that other positions around the filter must also regulate inactivation. Differences in millisecond scale channel gating were also observed when the signature

sequence of the NaK2K channel was conservatively mutated from $_{63}$TVGYG to $_{63}$TVGFG. Both these results suggest subtle differences in the packing within the filter domain which may control the gating properties of each channel, and perhaps similar differences around the filter underly functional differences of physiological consequence in potassium channel genes.

Chapter 9. Future Directions

K^+ Channel Filter Packing and Ion Binding

With respect to protein packing around the selectivity filter of K^+ channels it might also be of interest to study the packing around those K^+ channel filters where the signature sequence is atypical. The most distinct are the K_{2P} channel family where two pore domains are encoded on a single polypeptide. These channels frequently have asymmetric filter sequences including larger departures from the highly conserved signature sequence of K^+ channels. (Fig 2.3) As the protein sequence has proven critical to the selectivity and gating of a number of model channels (30, 50, 86), examining the amino-acid conservation and co-evolution within this family may prove informative about the packing necessary for forming a potassium selective filter. While the overall K^+ channel fold is conserved, as expected, coupling between pore domains may be related to those residues that form the cavity where the bulky side chains of the selectivity filter insert, equivalent to the cleft which accommodates the valine and tyrosine of the canonical TVGYG sequence. It would be expected that in those cases where the filter sequence is atypical, such as TIGLG of the second domain of $K_{2P}1.1$ and $K_{2P}6.1$, that there are compensatory mutations on the first domain to account the loss of phenyl ring rigidity and side chain volume. Correspondingly, in the $K_{2P}1.1$ structure, the orientation of the leucine side chain of the TIGLG selectivity filter sequence is roughly parallel to the membrane plane, rather than pointed toward the cytoplasmic face as is seen in the aromatics at the equivalent position in other K^+ selective channels. However, the confidence in this side chain orientation is suspect given the limited diffraction resolution. Interestingly, the conserved hydrogen bond partner of the tyrosine within the signature sequence, Thr60 in NaK2K, is not conserved in the K2P first domain, but rather small hydrophobic side chains is mostly frequently found in this position. (Fig 9.1) This perhaps is

a consequence needing to accommodate the uniquely oriented leucine of the selectivity filter. Additionally, in the ion_trans_2 family of potassium-like channels, there are a number of genes with selectivity filter sequences distinct from both the wild type NaK channel, and the sodium and potassium channel families. Structural, functional and bioinformatics analysis may illustrate compensatory mutations which complement the packing of these atypical pore filters and any unique folds of the filter may prove informative a general understanding of ion coordination, conduction, and selectivity.

More broadly interesting to the folding of the potassium channels might be those channels that have filter sequences similar though not identical to the classical potassium channel signature sequence. This has already been addressed to some degree in the NaK and NaK2CNG studies. However, other channels are distinct from K^+ channels in unique ways. While the K^+ channel signature sequence can be generalized TTVGYG, where the first threonine is less well conserved, HCN channels have the signature sequence LCIGYG. Based on homology the filter of HCN channels may resemble that of K^+ channels, but with a thiol side chain forming what would be the cytoplasmic side of site 4 (92). A equivalent mutation has previously been made previously on KcsA, demonstrating reduced potassium binding at site 4 and consequently saturating potassium conduction, but without any mention of selectivity (140). The decreased electronegativity of the sulfur in the coordinating thiol may underly weaker coordination of the potassium ion. Mutations on NaK2K may allow for more thorough structural and functional characterization of the consequences of this thiol moiety to ion binding and selectivity. Alternatively the loss of the gamma carbon at this site 4 may result in a less well packed side chain, discussed further in the next section.

Relatedly, some less selective K^+ channels have the filter sequence SVGYG (110, 111). Mutating the highly conserved threonine to serine the

loss of a single methyl group may increase the mobility of the side chain, weaken potassium binding at site 4, and therefore increase P_{Na}/P_K despite the availability of an equivalent hydroxyl. An equivalent mutation in the Shaker K^+ channel noted continued potassium selectivity (30). However, the threonine to alanine mutation at the same position also was potassium selective, contradicting the MthK_T59A and NaK2K_T63A studies and perhaps reflecting more complex selectivity in the Shaker channel.A similar threonine to serine mutation has been done on the viral Kcv channel without a notable change in selectivity (74). However, these results are confounded by a discrepancy in the literature over the baseline selectivity in addition to the channel inactivating (141). As previously shown in comparing NaK2K and NaK2K_Y66F, simply creating a less restrained filter, without structural change, can alter potassium channel selectivity differences in selectivity with the loss of the beta carbon at site 4 are worthy of further pursuit.

Within the K_{2P} family the aromatic to aspartate hydrogen bond is frequently absent in the first pore domain but highly conserved in the second. A cursory analysis of the K_{2P} domain 1 sequences notes that neither characteristic set interactions from the K_v-K_{Ca} or K_{ir} families are conserved. It would be of particular interest to see if compensatory mutations, within or between pore domains, act to stabilize the filter structure of the first subunit. There is a conserved threonine on the pore helix and a conserved asparagine or histidine following the signature sequence within the first pore domain. (Fig 9.1) This threonine is in the equivalent position of the glutamate on the pore helix of KcsA and may be involved in a hydrogen bond network, through intervening water molecules, with the asparagine or histidine residue following the filter. This grossly appears to be the case of K_{2P}1.1 and K_{2P}4.1 structures, with a threonine on the pore helix and histidine or asparagine, respectively, following the signature sequence (37, 38). However, in both cases a water

molecule is not built in the published model, perhaps a consequence of the limited resolution of both crystals.

Figure 9.1. The P-loop of the first pore domain of K_{2P} channels contain hydrophilic groups around the signature sequence. Probability distribution by position of amino-acids in the first P-loop of K_{2P} channels based on an alignment of the Treefam KCNK family. Boxed in red are the Thr and Asn/His positions conserved in the first domain of K_{2P} channels.

In the study of NaK2K_Y55F it is noteworthy that despite being non-selective between sodium or potassium the filter structures is similar to those of NaK2K and KcsA. This is notable given other the NaK channel mutant studies with varying numbers of binding sites where the absence of selectivity was only seen in those with less than 4 ion binding sites or with significant filter mobility in the case of NaK2K_D68E. While the binding of sodium within a non-collapsing potassium channel may not be unexpected, as it had been seen previously in MthK, it leaves the mechanism of selectivity ambiguous. One hypothesized mechanism for the loss of selectivity is in the absence of a hydrogen bond between the pore helix and selectivity filter of NaK2K_Y55F the filter becomes more mobile, though too subtly to be discerned structurally, and therefore sites 3 and 4 are less well ordered. This is supported by the structure of NaK2K_Y66F, where in the absence of a hydrogen bond between the filter aromatic and the pore helix there is also a concurrent diminution in potassium selectivity without a structural change. However, this hypothesis implies a mechanism of selectivity, dynamics within the pore,

which are not observable by crystallography. Molecular dynamic simulations of NaK2K, NaK2K_Y55F and NaK2K_Y66F, specifically addressing mobility of the filter and relative affinities for Na^+ and K^+, may be able to illustrate dynamics which underly the differences in selectivity.

K^+ Channel Inactivation and Gating

In the study of inactivation there is clearly a disconnect between functional and structural studies. While evidence demonstrates that both eukaryotic and prokaryotic channels can inactivate, the current prokaryotic structural model of C-type inactivation, KcsA, does not appear to well match the mechanisms of eukaryotic channel inactivation. While KcsA does undergo C-type inactivation, it is dependent upon the identity of the amino acid which are not conserved in inactivating eukaryotic channels (72, 73, 120-122). In addition, while KcsA_E71A does not inactivate it has greater filter mobility by crystallography, contrary to the proposed mechanism of C-type inactivation. Clearly, while KcsA does inactivate, the proposed mechanisms may not be directly translatable to the eukaryotic channels it is intended to model. Relatedly, while mutations on KcsA, $K_v1.1$, $K_v1.2$ and $K_v1.6$ have been made and show changes in inactivation, any equivalent mutations on NaK2K do not inactivate. In aggregate, these results highlight that C-type inactivation is a complex process dependent on the protein environment which surrounds the filter, positions not yet identified or characterized.

To further investigate inactivation from both a structural and biophysical perspective, multiple avenues of study may prove illuminating. As a control study, the equivalents of those residues which modulate KcsA inactivation can be introduced in the NaK2K channel. This would allow direct testing of KcsA like inactivation in an orthologous system using the ease of single channel recording in NaK2K. NaK2K has the advantage of structural and functional studies being possible using the same protein construct and the ability to routinely get high-resolution

structures to examine changes in the filter with high precision. However, this study contains the caveat that the NaK2K channel construct used for electrophysiology is constitutively active and so may inactivate before experiments begin. Getting useful data from such a situation would highly depend upon the dwell time of the channel in the inactivated state.

Correlated to the structural changes with C-type inactivation is the fundamental biophysical question of how channels the channel inactivate only after the cytoplasmic gate opens. With N-type inactivation the inactivating ball is an open state blocker and so channel opening is required inactivation. However, the mechanism of state-dependent inactivation in C-type inactivation is less clear. In structural studies on KcsA filter rearrangement couples to the dilation of the cytoplasmic gate. However, as previously mentioned, in the K_v1 family the side chain identity at the equivalent position to that identified in KcsA does not vary with channel inactivation propensity. Further studies looking at statistical coupling between gating domains and the filter or comparing the coupling networks of inactivating and non-inactivating channels, may prove informative. As the NaK channel can be structurally characterized in both closed (NaK-full length) and open (NaKNΔ19) it may prove a useful scaffold for examining multiple states of the inactivation process, though the NaK2K mutations have never been tested on the full length construct.

The differences in millisecond scale gating between NaK2K and NaK2K_Y66F, are worthy of further examination as well. As total ion flux is a function of both channel current and open time, these short brief channel closings may serve to tune the conductance of some channels to suit their physiological role. Such single channel behavior has been observed previously in $K_{ir}6.2$ and other channels (112, 113, 126). However, differences in channel flicker are seen K^+ channels where the signature sequence is the canonical TVGYG, and the corresponding hydrogen bonding partner on the pore helix is present as well. Conversely, in $K_{ir}6.2$ where this bond is expected to be absent, mutations which would

introduce this bond actually increased fast channel closing kinetics, the opposite effect of that seen in NaK2K. Clearly there are other residues around the filter which alter this brief channel closing, outside of those highlighted in the NaK2K_Y66F work and previous studies. Systematic mutagenesis studies on the pore domain of NaK2K and other model K^+ channels, coupled with single-channel electrophysiology and bioinformatic studies, may illustrate packing differences which underly this process.

Heavy Ion Binding in the K+ Channel Filter

The specific binding of Ba^{+2} within the pore of model K^+ channels may provide a helpful experimental handle for studying ion binding within the filter and a means to study heterogeneous ion binding and competition within the K+ channel filter.

The anomalous diffraction data of barium soaked KcsA and NaK2K clearly shows differences in ion binding within similar selectivity filter structures. This is despite nearly identical ionic radii, suggesting that subtle electrostatic differences underly ion binding within the filter. While the chemistry of the peptide backbone and threonine side chains is identical for the coordinating residues, and the adjacent sequence is highly similar, the presence of a charged residue on the pore helix of KcsA may underly this difference. Mutating the equivalent position in NaK2K or the MthK pore to charged or neutral but polar side chains may provide structural information about how the electrostatic environment of the filter is shaped by the pore sequence and architecture. A similar effect has been seen in the NaK2CNG channel mutants, most notably in the structure and functional Ca^{+2} binding differences (71).

As barium binds at a single site within the filter, and clearly alters ion binding elsewhere in the filter, it could provide a way to compare ion-ion interactions within the filter to first principles of electrostatic interactions. Such experiments are difficult to address structurally in K^+-only conditions as the apparent equivalence between 1,3-2,4 states

equalizes the ion density across the sites. With barium binding specifically at site 3, the electron density at sites 2 and 4 clearly changes relative to the NaK2K channel with K^+ alone, suggesting that electrostatic interactions with the divalent ion reduces ion affinity distant to the Ba^{+2} binding site. A similar mechanism has been hypothesized in models of K^+ channels conducting potassium only but the novel NaK2K-K^+/Ba^{+2} structure provides the first opportunity for direct visualization of such an interaction. Using the anomalous signal of Ba^{+2} to precisely define the ion's location and occupancy it may be possible to study ion-ion interactions within the filter as the Ba^{+2} bound filter of NaK2K may represent similar case to the 1,3 configuration of K^+ ions during conduction. Further, the ability of K^+ ions to displace a bound Ba^{+2} ion within the filter has previously been used to describe the ion binding sites prior to any structural description. Using an analogous experiment, the ability of other permeant ions to displace barium bound at site 3 of the NaK2K channel may allow for functional interrogation of how ion-ion interactions with the filter may play a role in K^+ selectivity.

Appendix 1. P_iT Family Transporter Studies

Phosphate Physiology and Transport

Phosphate is a physiologically essential ion involved in numerous biologically relevant processes and its presence is required in all forms of life, with one possible exception where arsenate may be a tolerated replacement in the nucleic acids (142). In addition to being central to the action of kinase and GTPase signaling and the energetic currency of the cell, the triphosphate bond, it also is the structural scaffold of both DNA and bone.

Inorganic phosphate (P_i) is the most minimal form of phosphate available for uptake by living organisms. While phosphate is available to organisms in a number of forms for accumulation P_i in aqueous solution has the added complication of four possible protonation states, the result of three titratable groups with different pKa's. Additionally, this inorganic phosphate must be scavenged from an external milieu including numerous other oxyanions, most notably sulfate which has a very similar structure. Selective acquisition of phosphate from the external environment is a basic biological process required for cell growth and proliferation. Given its central in a number of biological process it is not surprising there are a number of mechanisms which have evolved for organisms to acquire P_i.

In the average human 0.5% of body weight is phosphorus, in the form of phosphate, but this is largely found mineralized in bones and to a lesser extent within the cell volume, with less than 0.1% found extracellularly (143, 144). However, the phosphate stores of the body are constantly in flux; with large amounts absorbed, exchanged and excreted daily. Bone is continually being remodeled, built by osteoblasts and broken down by osteoclasts, and acts as a buffer of total phosphate by dissolving and depositing 500 milligrams of phosphorus per day on average. The phosphate present in circulation is continuously filtered through the kidney

where it is actively reabsorbed, with nearly 10 grams filtered per day and 9.85 grams recovered, relative to the average of 1 gram typically consumed. While this homeostasis is regulated by Vitamin D and other hormones, generally the regulation of phosphate is best characterized by its closely coupling to that of calcium; as the liberation of phosphate from bone necessarily frees calcium as well.

Given this actively regulation of phosphate homeostasis there are necessarily a number of mechanisms for its uptake and retention. In humans there are four major families of described inorganic phosphate transporters, those on the plasma membrane are labeled sodium-phosphate transporters one through three (NaPi-I, NaPi,-II, and NaPi-III); while the mitochondrial transporter is labeled (PiC) (145). Apparent based on the names, the plasma membrane transporters couple the import of phosphate to the established sodium gradient in a symport fashion. In a similar manner PiC couples phosphate import to the proton gradient of inner mitochondrial membrane.

NaPi-I was the first identified as a phosphate transporter. However this assignment has generally been found to be incorrect and the family is now described as glutamate transporters (146). NaPi-II is the major phosphate recovery mechanism in the kidney (144, 147). With a high (1mM) concentration of free phosphate in the blood, recovery is necessary to avoid excess loss in the urine. PiC is the mitochondrial phosphate transporter, providing inorganic phosphate for the synthesis of ATP from ADP (148). Belonging to the mitochondrial transporter family it correspondingly uses the available proton gradient to import inorganic phosphate, has high sequence similarity to other mitochondrial transporters (148, 149) and presumably has the same fold previously illustrated by the ATP-ADP antiporter structure (150).

NaPi-III is a ubiquitously expressed protein in humans responsible for basal phosphate uptake in most tissues, as required for basic growth and metabolism (147). It is highly conserved in all kingdoms of life, reflecting both the gene's ancient origin and the fundamental requirement of phosphate for life (145). In addition to this native function, NaPi-III acts as a viral receptor for retrovirus in some mammalian species (151). In addition, a recently identified ortholog in *Plasmodium falciparum*, a causative agent in malaria, allows the parasite to acquire necessary phosphate from the host erythrocyte cytoplasm (152).

In addition to the human mechanisms of phosphate accumulation bacteria, lower eukaryotes and plants have unique mechanisms of their own phosphate acquisition. In bacteria there are at least two major phosphate absorption pathways, PstSCAB ABC transporter system with its associated periplasmic binding protein and the PitA proton coupled symporter which belongs to the same protein family as NaPi-III (153). In yeast and plants there is an additional transporter family, based in the major facilitator superfamily, that is also responsible for accumulation of inorganic phosphate necessary for growth (154, 155). This acquisition of phosphate in plants is central to their symbiotic relationships with fungi, exchanging phosphate liberated from the soil by the fungi for sugars synthesized by the plant (156, 157).

While there are obviously numerous means for phosphate accumulation the physical mechanisms by which each system works is largely unknown. Given the fundamental role phosphate plays in numerous biological processes investigation of these transporters might provide basic insight into their selectivity and activity. The challenge of selecting phosphate against the mixture of ions in solution is the impetus for this study, to understand selectivity in a membrane anion transporter. In particular, as NaPi-III has the most precisely described function, both in its native function and role as a viral receptor, it serves as an interesting

biological target for both basic transporter biophysics and virology/cancer biology.

Selectivity of Small Molecules

This issue of how proteins select particular substrates has been extensively addressed previously in the cases of soluble proteins, where the ability to discriminate between similar ligands is also frequently important to biological function. A classical example of the diversity of ligand specificity mechanisms are the periplasmic binding proteins of bacteria (158). This family of proteins bind their substrates in the periplasm with high specificity and then deliver them to the appropriate ABC transporter on the plasma membrane for import. These protein achieve specificity by creating specific binding pockets within the scaffold of a common ternary structure. Differences in shape, charge, van der Waals contacts and hydrogen bonds result in the ability to selectively bind ligands in the periplasmic milieu.

An excellent example of such specificity is the ability of bacterial Phosphate Binding Protein and Sulfate Binding Protein to specifically select either phosphate or sulfate despite a similar size and oxyanion structure of both ligands (159). Both phosphate and sulfate are bound completely dehydrated within the cleft of the binding proteins, coordinated largely by hydrogen bonds. (Fig A1.1) The most notable difference is within the phosphate binding protein where a negatively charged side chain in the pocket serving as a hydrogen bond acceptor from the protonated phosphate ion. (Fig A1.1B) The sulfate binding protein does not have any comparable side chains in the binding pocket, solely coordinating the fully deprotonated sulfate ion by hydrogen bonds, as any negative charge would repel the anion. (Fig A1.1A) Further engineered mutations on the phosphate binding protein can make the receptor selective for the monovalent form of phosphate by the introduction of an additional acidic side chain in the binding pocket, though this may not be

of biological advantage to the organism and so such specificity is not see in the wild-type gene (160). (Fig A1.1C)

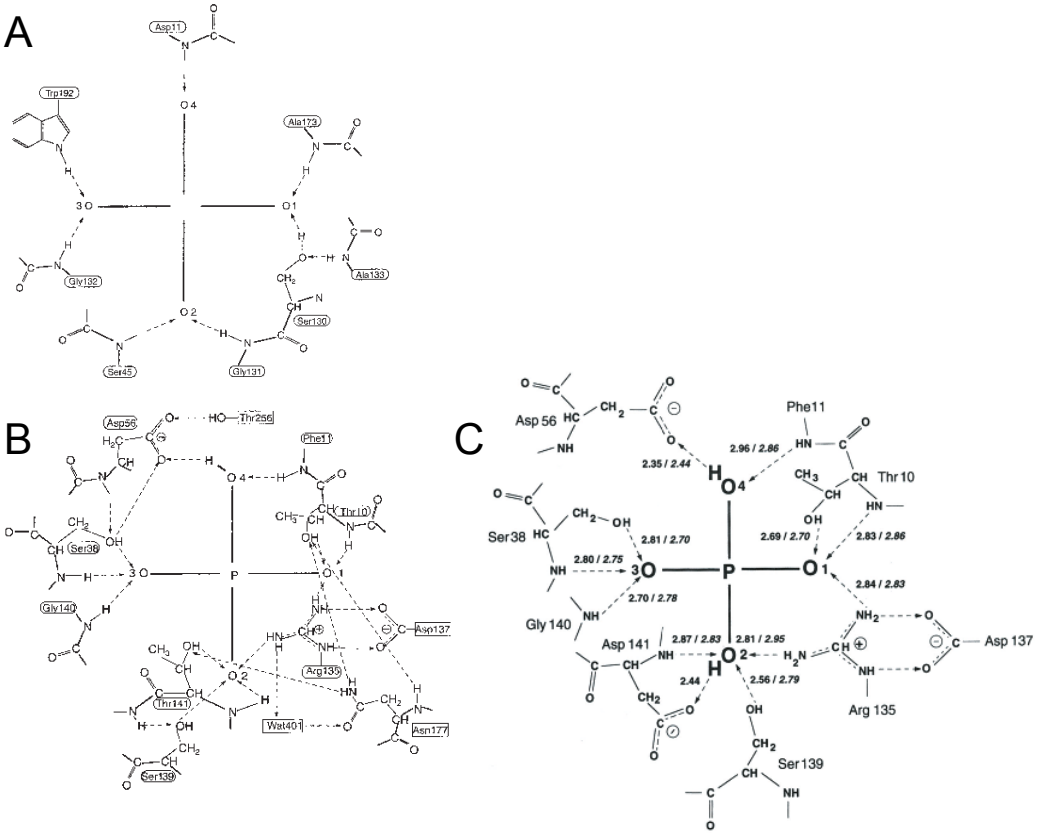

Figure A1.1. There are clear differences in oxyanion binding among natural and engineered periplasmic binding proteins. (A) Schematic diagram of the sulfate in the sulfate binding protein of *Salmonella typhimurium*. The sulfate binding pocket is completely dehydrated and has only uncharged hydrogen bond donors coordinating the anion. (B) Phosphate anion binding in the phosphate binding protein of *Escherichia coli*. A negatively charged Asp acts as a hydrogen bond acceptor from the protonated phosphate ion. Phosphate is coordinated primarily by hydrogen bonds, though charged salt bridge contributes as well. (C) A mutation on the phosphate binding protein introduces an additional charged hydrogen bond acceptor, making the mutant binding protein selective for doubly protonated phosphate. Figure adapted from (159, 160).

Among membrane proteins the mechanisms of selectivity are less well elucidated due to the limited availability of structural information. While biochemical and biophysical studies have noted sequences and regions of the protein important to function, without ternary structure the precise mechanism are not frequently known. Bioinformatic studies among characterized proteins can note primary sequence differences that correlate with changes in protein specificity or function. In addition, homology modeling based on proteins related by evolution or function has provided insights into the mechanisms of selectivity. Structures that have been solved can be used to validate previously known primary sequence motifs and explain their physical role in selectivity (47). As expected, given that the binding sites of both membrane and soluble proteins are formed out of the same library of amino-acids, similar chemistry is often employed in the binding sites of proteins with similar function. This is true in the cases of the betaine transporter and SERCA calcium pump (161, 162). In the case of the betaine transporter, a further study comparing sequences of the betaine and choline transporter families allowed the authors to engineer a sodium coupled betaine transporter to a proton coupled transporter selective for choline by changing the chemistry of the ligand binding site (163). Similar comparative studies have been done among the related P-type ATPases, where despite a common ternary architecture there are a great diversity of substrates, governed by the chemistry of the ligand coordination site (164).

The NaPi-III/P_iT Transporter Family

In mammals, absorption of phosphate for most cell types from the external milieu is primarily the responsibility of the type 3 sodium coupled phosphate transporter (NaPi-III), also described as the solute carrier 20 family (151). Ubiquitously expressed, the NaPi-III gene encodes a ~600 amino acid membrane protein which couples the influx of phosphate to the established sodium gradient. (Table 1.1) While studied *in vivo*, especially

in the context of its transcriptional level regulation and role as a viral receptor, basic biophysical knowledge about the mechanics ion binding and transport of this protein is largely lacking. This research aimed at addressing these gaps through a systematic and detailed biochemical and structural characterization of NaPi-III. Beyond characterizing this protein, this data would expand our limited knowledge of mechanisms of specificity and substrate flux by membrane transporters.

Previous work on the mammalian protein via electrophysiology and other methods characterized the function and some of the structural characteristics of the NaPi-III transporter. In humans there are two known paralogs, Inorganic Phosphate Transporter 1 and 2 or SLC20A1 and SLC20A2. Via electrophysiology and $^{32}P_i$ flux assays the gene family has been characterized as a symporters, using a sodium or proton gradient to accumulate monovalent phosphate ($H_2PO_4^-$) with the co-transport of two sodium ions (152, 165). By sequence analysis and epitope accessibility experiments both human proteins appeared to have twelve transmembrane helices formed via a gene duplication event where the N- and C-terminal halves of the protein sequence are related by an evolutionary gene duplication event (166). (Fig A1.2) Additionally, there is a large regulatory loop between the two 'halves' of the protein in humans and other mammals, important for physiological regulation of the protein. Much of the study of this protein has been based around, or used as an experimental tool, the fact that this family of proteins acts as a receptor for transforming viruses (165). Virus transformation is used to demonstrate correct targeting and folding of the protein and conversely mutant proteins can characterize the requirements for viral binding and entry. Clearly demonstrated is the fact that viral transformation is independent of phosphate transport activity (167).

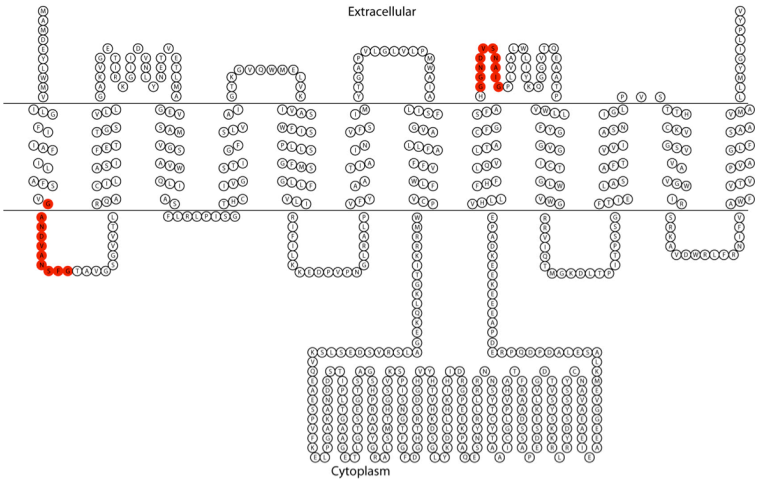

Figure A1.2. The transmembrane topology of SLC20A1. The NaPi-III family transporter is predicted to consist of twelve transmembrane with the two motifs on opposing sides of the membrane, in red.

For the aims of this research the focus is not on the mammalian proteins directly but rather on their bacterial and archaeal homologs. This is due to the fact that their shorter, less complex, sequences makes them far more amenable for expression and experimentation. These genes will allow for a general description of the overall transporter fold and a mechanistic understanding of P_i transport, though the viral transformation activity of the SLC20 genes may not be recapitulated in these genes.

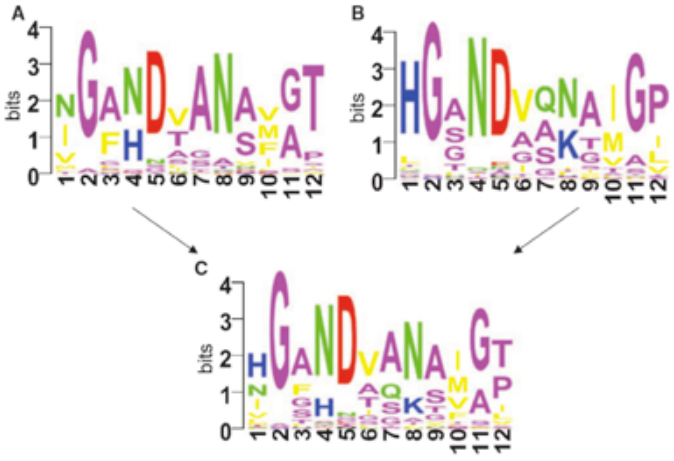

Figure A1.3. There is a twice repeated sequence motif within the PiT family of transporters. The (A) N-terminal and (B) C-terminal and (C) consensus motifs of the PiT family. Figure reproduced from (168).

There are two previous publications of particular note to this study. In one, a repeated motif contained within the primary sequence of the PiT transporter is noted to be conserved within the larger transporter family (168). (Fig A1.3) Mutations of this sequence abolish phosphate transport. This motif, with the consensus sequence GANDVANA, is contained within both domains of the protein and conserved in all branches of the evolutionary tree. A second study characterized the previously unknown function of the gene, ylnA, within a cysteine biosynthesis operon of *Bacillus subtilis* (169). The gene is functionally identified as a membrane sulfate transporter, and the corresponding gene product is named CysP. Of particular interest is the note that this protein actually belongs to the PiT transporter family, yet has altered its selectivity to favor sulfate. While a common gene origin is not unexpected given the common oxyanion shape, size and structure of phosphate and sulfate, the characterized P_i transporters are generally known to discriminate between sulfate and phosphate. Therefore, the differences in primary sequence between CysP and the phosphate selective transporters may prove informative about the mechanisms of anion selectivity in PiT the family.

One additional fact of note are the periplasmic binding proteins, part of the previously mentioned ABC transporter operons. This family has been extensively studied both in terms of its mechanism of activity and selectivity. Of importance to this study, both phosphate and sulfate binding proteins structures are available and mutations which create valence selective phosphate binding proteins have been described. (Fig A1.1) While related only by ligand selectivity and not sequence or structure to the membrane phosphate transporters, these periplasmic binding proteins provides an intellectual handle on how phosphate can be bound selectively within a protein.

Methods

Gene Search and Cloning

Using the PiT gene from *Methanococcus jannaschii* as a search model, 21 genes were initially identified by BLAST search, cloned by PCR and ligated into pQE-60 or pQE-70 expression vectors.

Protein Expression

Plasmids for the PiT genes were transformed into chemically competent *Escherica coli* strains. Initially a number of strains were tested for optimal expression, including XL1-Blue, SG13009, M-15, BL21, C41 and C43. The transformed cell were grown on LB-Agar plates with Ampicillin selection overnight, then those colonies were scraped into LB broth liquid culture with Ampicillin selection. The liquid culture was grown at 37°C with 250rpm. Cells were induced at OD_{600} ~0.8 with 0.4mM IPTG and the culture was transitioned to 17°C overnight.

Protein Purification

The cell culture was harvested by centrifugation at 5000g for 30 minutes at 4°C. The cell pellet resuspended in lysis buffer of 400mM NaCl, 100mM HEPES pH 7.5. Cell were broken first by sonication and then homogenized, keeping the instruments and samples ice cold. Protein was

extracted for 3 hours at room temperature with 40mM dodecylmaltoside (DDM) with gentle shaking then purified by gravity flow over a Talon Co^{+2} column pre-equilibrated with a column buffer of 100mM NaCl, 20mM HEPES pH 7.5, 3mM DDM. The IMAC column was washed with column buffer containing 15mM Imidazol and protein eluted in column buffer with 300mM Imidazol. The protein tag was removed by thrombin digestion overnight at room temperature and the protein further purified on a Sephadex 200 (10/30) column. Column buffer varied by experiment but was based around 100mM NaCl and 20mM HEPES pH 7.5. Detergent exchange experiments were carried out by the addition of highly concentrated detergent, equilibration overnight, and then size exclusion chromatography.

Bioinformatics

Sequences of the NaPi-III homologs were collected using repetitive BLAST searches using the PiT gene from *Methanococcus jannaschii* as a search model. Sequences were aligned using ClustalW (80) and Promals3D (77) and analyzed in either Jalview (81) or Weblogo (82, 83). Membrane topology was rendered in TOPO2 (170)

Functional Study

The *Escherichia coli* phosphate transporter deficient strain strain CE1491, with the genotype *pitA pitB pitS*, and pJF118EH plasmids were kindly provided by Jan Tommassen (171). Chemically competent CE1491 cells were transformed with the pJF118EH plasmid containing either PiTA, PiTB, CysP, CysP with mutations of interest or no gene as control and grown in liquid LB culture. The cultures were then put on ice, diluted in ice cold LB broth to a defined OD_{600} and subsequently serial diluted stepwise by orders of magnitude. Each concentration was then pipetted onto LB plates or LB plates with 10mM Na_2HAsO_4. The plates were stored in an incubator overnight prior to imaging.

Results

Of these 14 genes cloned (Table A1.1) 10 showed expression in LB broth by western blot analysis for the fused carboxy-terminal hexa-Histidine tag. However, most of this was only trace levels of expression, unsuitable for structural study. Most orthologs showed slow cell growth after transformation with pQE based expression plasmid, particularly after induction of expression, implying that gene toxicity coupled to the leaky expression vector played a role in low protein yields. Only one gene, from *Bacillus halodurans*, showed significant and pursuit-worthy expression, further confirmed by SDS-PAGE and Coomassie Brilliant Blue staining. (Fig A1.4)

	Species	MW (kDa)	Expression
2	*A. fulgidus*	33272.92	
3	*M. mazei*	35565.37	pQE/SG/TB
4	*T. maritima*	32201.42	pQE/SG/TB
5	*P. horikoshii*	33348.88	pQE/SG/TB
6	*D. radiodurans*	35149.93	pQE/SG/TB
9	*E. coli* (PiTA)	53392.33	
10	*M. magnetotacticum*	34658.04	pQE/SG/TB
11	*S. typhimurium*	53492.5	pQE/SG/LB
12	*T. fusca*	34525.74	
14	*C. psychrerythraea*	44798.64	
15	*B. halodurans* (BH_CysP)	37429.38	pQE/XL/LB
17	*B. subtilis* (CysP)	36838.31	pQE/XL/LB
18	*P. horikoshii 2*	42931.01	pQE/SG/TB
19	*T. maritima 2*	42696.57	pQE/SG/TB

Table A1.1. Fourteen PiT homologs were successfully cloned and expression tested. Table of genes cloned, size and optimized expression conditions for NaPi-III homologs cloned. Optimal expression is listed by vector, compotent cell strain and growth media. XL = XL1-Blue, SG = SG13009, LB = LB-Miller Broth, TB = Teriffic Broth

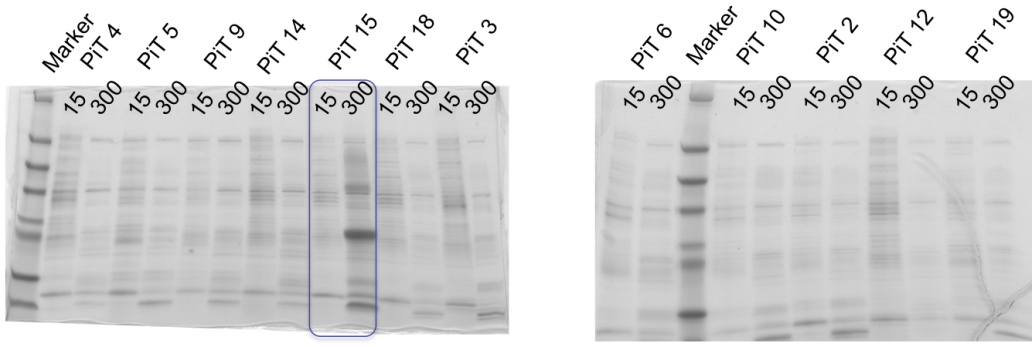

Figure A1.4. Representative coomassie gel of PiT homolog expression trials. The PiT_15 ortholog from *Bacillus halodurans* boxed. Expression trials of PiT homologs expressed in XL1B, purified on Co^{+2} columns, and visualized by SDS-PAGE with Coomassiee staining.

Based on further sequence examination of the PiT ortholog from *Bacillus halodurans*, the gene appears to be a close ortholog of the *Bacillus subtilus* sulfate transporter CysP (55% identity, 73% similarity) and was therefore named BH_CysP. These transporters are believed to be closely related to the phosphate transporters, yet transporter sulfate. Despite being highly expressed, BH_CysP protein was largely aggregated when expressed at 37°C, based upon much of the protein being detergent insoluble. Reducing the protein expression temperature to 18°C and expressing the protein overnight improved detergent solubility, presumably by reducing the expression rate and allowing for the proper protein folding and targeting. However, solubilized BH_CysP proved largely unstable in detergent solutions, corresponding to multiple broad peaks during size-exclusion purification. In many cases, the protein purified as a large molecular weight aggregate in the void peak. (Fig A1.5)

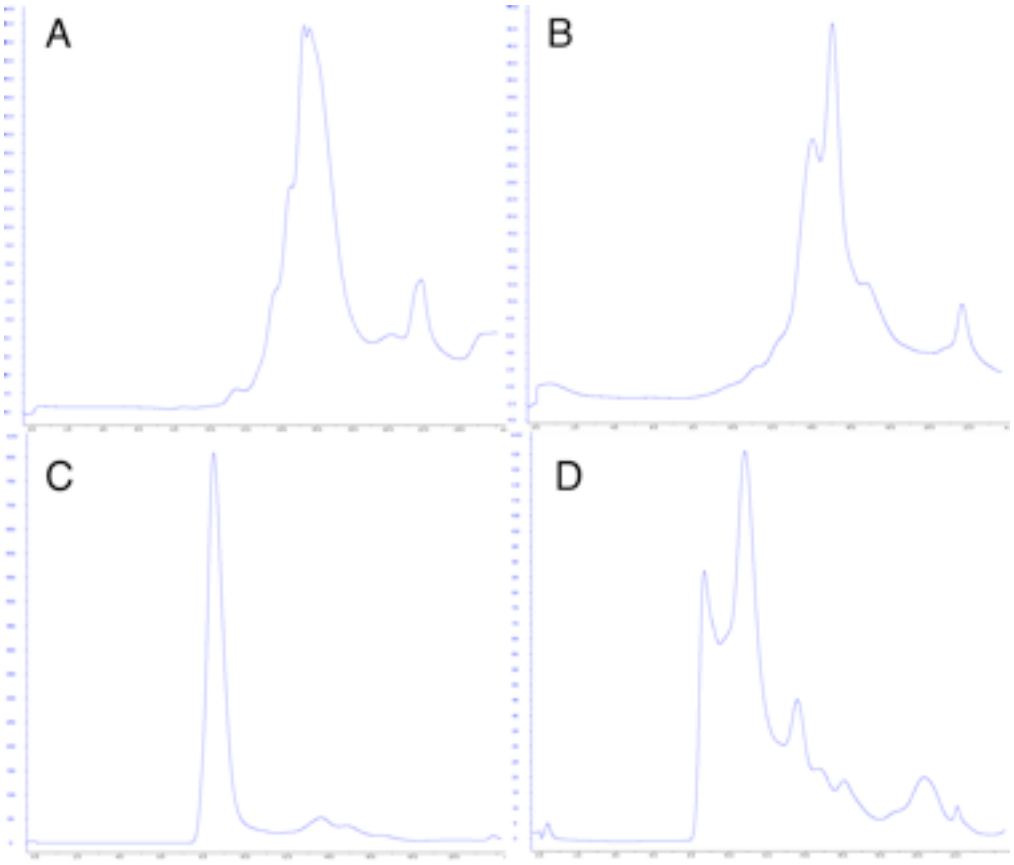

Figure A1.5. Representative traces of BH_CysP purification. Protein was purified on Superdex 200 size exclusion chromatography with varying detergents showing largely aggregate (C,D) or heterogeneous behavior (A,B,D). Profile of BH_CysP on gel filtration in (A) beta-octylglucoside (B) Lauryldimethylamine-oxide (C) Dodecylmaltopyranoside or (D) Decylmaltopyranoside.

Sequence analysis for the PiT transporter family gave a few hints into the possible mechanisms of selectivity for the PiT family. Of particular use was the previously characterized CysP, a family member with the ability to transport sulfate rather than selectively phosphate. While the GANDVANA motif is highly conserved in the PiT, as previously reported, there are clear changes in the equivalent CysP and BH_CysP motifs. (Fig A1.6) These differences neutralize the acidic residue, usually aspartate, to either glycine or asparagine. Additionally, while not noted in the paper that identified the GANDVANA motif there is a conserved histidine that typically precedes only the second motif, which is an alanine in CysP and BH_CysP.

Figure A1.6. The acidic residues typically conserved with the PiT family motifs are absent in CysP. Alignment of PiT motifs of SLC20A1, PitA and BH_CysP from *Homo sapiens*, *E. coli* and *B. halodurans*, respectively. The highly conserved aspartate (red) and histidine (blue) residues are colored.

These conserved charged residues may act as hydrogen bond acceptors and bond with the phosphate substrate. Given that these hydrogens are not present on the sulfate anion, such charged side chains at the ion binding site would repel sulfate, providing a means of phosphate versus sulfate selectivity and explaining the neutralization of equivalent positions in CysP. (Fig A1.7)

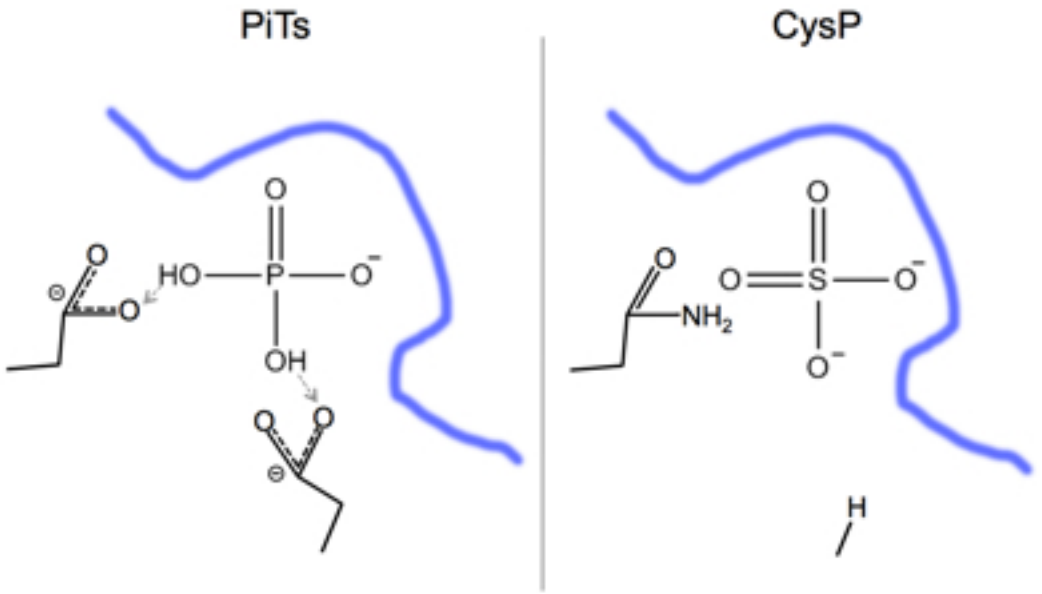

Figure A1.7. A proposed mechanism of coordination and selectivity in the phosphate and sulfate selective transporters. Phosphate transporters conserved Asp side chains act as two hydrogen bond acceptors coordinating the monovalent phosphate ion. Sulfate is coordinated without these acidic residues as the charge repulsion would make binding of the fully deprotonated anion unfavorable.

Based on this hypothesis functional studies were carried out on the BH_CysP and *E. coli* PitA genes in an attempt verify the importance of these locations. The assay depends upon the toxicity of arsenate to cells. Arsenate is also an oxyanion with structure, size and pKa's similar to phosphate and can act as an analog of phosphate, being transported by the phosphate transporter systems and replacing phosphate in a number of cellular reactions. However, this replacement is deleterious to the cell as the arsenate based di-ester bond is unstable and spontaneously hydrolyzes (172).

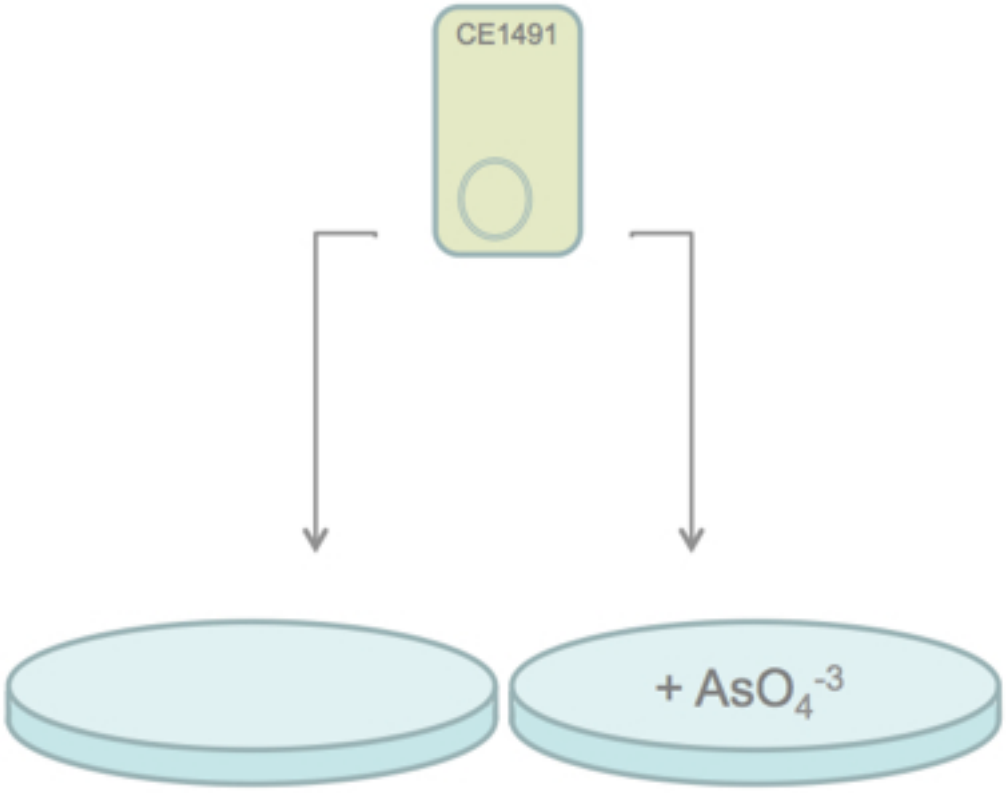

Figure A1.8. Schematic of the arsenate sensitivity assay to select for arsenate transport deficient mutants. The phosphate transporter deficient strain CE1491 is transformed with CysP mutants, or control plasmids, and grown briefly in liquid culture. Cells are then spun down and plated on LB plates supplemented with arsenate. Arsenate acts as a toxic inorganic phosphate analog in those cells expressing a functional phosphate transporter.

The CE1491 phosphate transporter knockout strain of *E. coli* was transformed with a constitutive low expression plasmid containing either PitA, PitB, or no gene as controls. Experimental plasmids attempting to change BH_CysP selectivity contained either wild-type BH_CysP as a control or derived mutants. Cells were grown briefly in LB liquid culture, diluted into sterile LB to fixed OD_{600} and plated on control or arsenate plates. After overnight growth it was noted that CysP could not restore arsenate sensitivity to the CE1491 strain. (Fig A1.9) The additional mutations on CysP (G20D, N184D, G20D/N184D and G20D/A180H/ N184D) which convert introduce acidic hydrogen bond acceptor side chains the to motifs of CysP, making those motifs more like the canonical PiT family, were also insufficient to render transformed cells sensitive to arsenate.

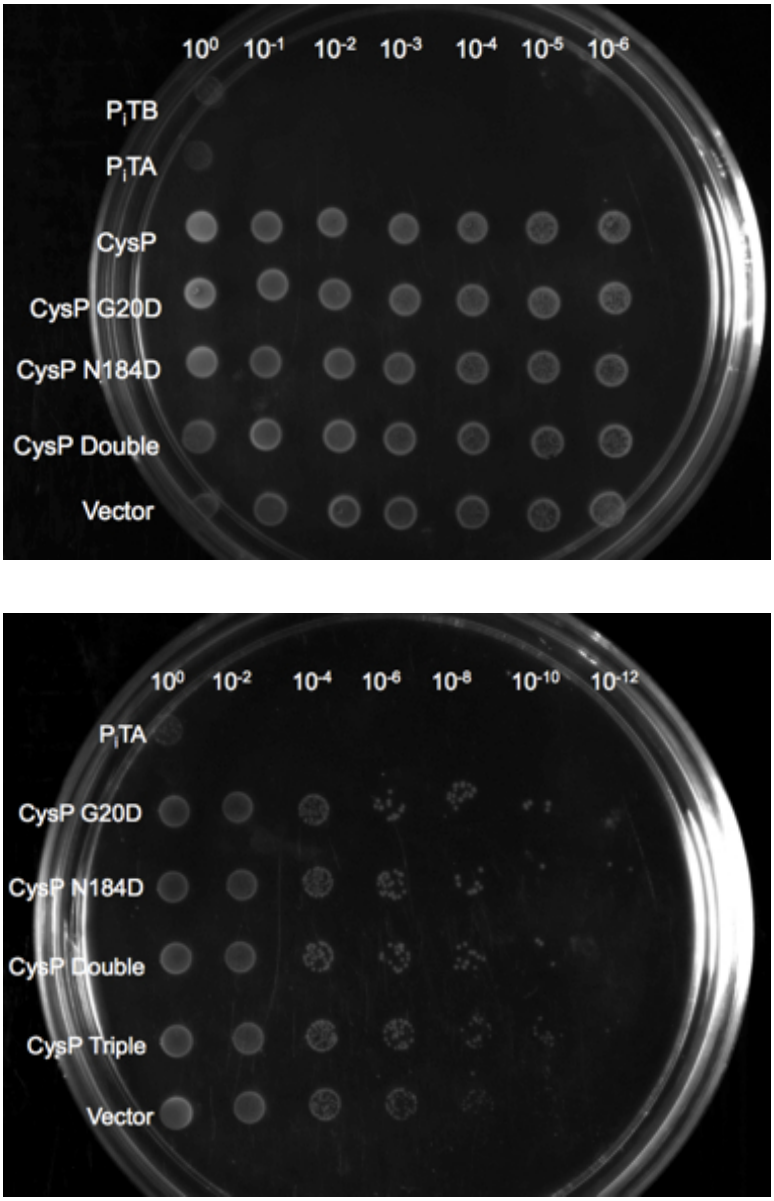

Figure A1.9. The engineered CysP constructs do not introduce arsenate sensitivity and therefore presumably do not transport phosphate. Serial dilution of the phosphate transporter deficient E. coli strain CE1491 transformed with PiTA, PiTB, CysP, single mutants G20D or N184D, double mutant G20D/N184D and triple mutant G20D/A180H/ N184D.

Discussion

While one homolog gave reasonable expression its instability a number of detergents made it intractable for further study. To be worthy of pursuit for crystallographic study the protein would need to be highly expressed, stable and preferably mono-disperse in at least one and ideally a number of detergents. Notably, the one homolog of the PiT family that did give reasonable expression, from *Bacillus halodurans,* is most likely a sulfate transporter. This coupled with the slow growth of other homologs under similar conditions may reflect inherent toxicity of the PiT family during overexpression.

With respect to these limitations of the current PiT genes to structural study, a number of strategies can be attempted. Given the noted toxicity of PiT orthologs and the notable expression of a sulfate transporter, the sulfate transporters of the PiT family may have fewer issues with toxicity and prove more amenable to over-expression. Among the CysP orthologs genes from thermophiles and hyperthermophiles may prove more stable in detergent. These genes may have the added benefit of being most active at higher temperature and therefore activity-dependent toxicity may be lessened in the mesophilic *E. coli* expression system. In a similar effort, 46 genes of this PiT family have been selected for testing by a number of structural genomics groups, with 5 under active development though only 2 are confirmed as expressed. A more guided approach, based on these observations of PiT over-expression and toxicity issues, may make the selection and expression of orthologs more successful.

Functionally, it is noteworthy that CysP did not restore arsenate sensitivity to the CE1491 strain, clearly indicating that the transporter cannot transport arsenate. However, none of the tested mutations on CysP were able to restore sensitivity to arsenate, a result that is not directly informative. It is possible that the introduced aspartate side chains

of the CysP mutants are necessary but insufficient for phosphate selectivity in the PiT family. Alternatively, these positions may be conserved without the aspartate side chains directly interacting with the substrate. Neither possibility is excluded by the results of these experiments. Also interesting in the PiT family sequence analysis is the lack of any noted conserved basic residues. In comparison, the bacterial outer membrane protein OmpP, a phosphate selective porin, has an arginine ladder which is believed to attract the anion to the transporter active site (173). As yet no basic motif is known in the PiT family to similarly attract phosphate, though further functional study or sequence analysis may clarify the means of attracting the substrate to the P_i binding site. Finally, while CysP may belong to the PiT phosphate transporter family there may be positions, either inside or outside the motifs, which confer sulfate selectivity and this mechanism must be mutated for phosphate transport.

As phosphate is an essential nutrient in *E. coli* growth, an alternative unbiased means of identifying the mutations needed for selectivity between sulfate and phosphate is possible. Leveraging the phosphate transporter deficient CE1491 strain previously used, a library of randomly mutagenized CysP genes could be screened for phosphate transporter activity, either by positive selection on inorganic phosphate only minimal media or negative selection by replica plating onto arsenate spiked and arsenate free plates. These screens could identified mutations which at a minimum are non-selective between sulfate and phosphate, clarifying the amino-acids critical for oxyanion discrimination. The growth assay with inorganic phosphate only media has the advantage of being a positive selection assay, while the arsenate cell death assay may avoid false negatives by being less stringent of P_i transport capability.

Appendix 2. Data Collection and Refinement Statistics.

	NaK2K	MthK _T59A	NaK _D66Y	NaK _N68D	NaK2K _Y66F	NaK2K _Y55W
Data Collection						
Space group	I4	$P42_12$	I4	I4	I4	I4
Cell dimensions a=b, c (Å)	67.9, 89.6	63.6, 44.0	68.2, 89.2	68.1, 89.1	67.6, 89.1	68.4, 86.5
Resolution (Å)	50-1.55	50-1.7 5	50-1.80	50-1.95	50-1.90	30-1.90
Rsym (%)	4.8 (97.6)	7.2 (100)	4.6 (92.7)	7.7 (92.3)	8.2 (47.6)	8.6 (48.1)
I/σI	35.0 (1.0)	27.6 (1.5)	43.0 (1.75)	27.4 (1.17)	22.4 (3.53)	19.1 (1.13)
No. reflections-total (unique)	191,495 (28,703)	86,388 (9484)	140,667 (18,824)	102,342 (14,516)	83,891 (15,737)	70,382 (14,653)
Completeness	97.2 (77.0)	98.9 (99.8)	99.9 (100)	98.2 (84.5)	99.6 (100)	94.1 (74.5)
Redundancy	6.7 (2.8)	9.1 (7.9)	7.5 (7.3)	7.1 (4.9)	5.3 (5.2)	4.8 (3.6)
Refinement						
Resolution(Å)	1.55	1.75	1.80	1.95	1.90	1.90
Rwork/Rfree	20.0 / 21.5	21.2 / 23.6	21.2 / 23.3	19.1 / 22.3	20.6 / 23.8	22.6 / 24.1
No. atoms						
Protein	1487	639	1485	1477	1485	1489
MPD/ion	40/9	-/5	-/10	-/7	-/8	-/8
Water	72	67	4	9	23	37
RMSD						
Bond angles (Å)	1.088	1.072	0.563	0.713	1.123	0.730
Bond lengths (Å)	0.0051	0.0054	0.005	0.005	0.010	0.003

	NaK2K _Y55F	NaK2K _D68E	NaK2K-Ba^{+2}	NaK2K-Rb^{+}	NaK2K-Cs^{+}
Data Collection					
Space group	I4	I4	I4	I4	I4
Cell dimensions a=b, c (Å)	67.4, 83.6	67.4, 84.0	68.1, 89.6	68.0, 89.3	68.1, 89.6
Resolution (Å)	50-1.70	15-1.75	32.8-1.83	34.0-1.58	34.1-1.73
Rsym (%)	4.9 (100)	6.9 (72.0)	5.5 (87.2)	5.4 (78.7)	4.4 (76.2)
I/σI	30.3 (1.59)	43.7 (1.21)	16.56 (2.05)	18.48 (2.16)	17.82 (2.10)
No. reflections-total (unique)	114,794 (20,479)	115,372 (18,720)	126,218 (17,886)	205,064 (27,777)	158,119 (21,270)
Completeness	99.3 (93.7)	98.6 (87.1)	99.57 (100)	99.86 (99.93)	99.9 (99.8)
Redundancy	5.6 (5.1)	6.2 (2.5)	7.1 (7.2)	7.4 (7.3)	7.4 (7.2)
Refinement					
Resolution(Å)	1.70	1.75	32.8-2.0	34.01-1.8	32.8-1.83
Rwork/Rfree	19.5 / 22.5	20.2 / 22.5	20.2/25.6	20.2/23.2	21.6/25.2
No. atoms					
Protein	1492	1490	1464	1424	1457
MPD/ion	-/8	-/8	16/9	8/6	8/9
Water	38	52	47	66	41
RMSD					
Bond angles (Å)	0.837	0.975	0.98	1.14	1.35
Bond lengths (Å)	0.004	0.005	0.007	0.011	0.013

Bibliography

1. Hauser H, Stubbs M, & Phillips MC (1972) Ion Permeability of Phospholipid Bilayers. *Nature* 239(5371):342-344.

2. Stryer L (1995) *Biochemistry* (W.H. Freeman and Company, New York) Fourth Edition Ed.

3. Hille B (2001) *Ion Channels of Excitable Membranes*.

4. Singer SJ & Nicolson GL (1972) Fluid Mosaic Model of Structure of Cell-Membranes. *Science* 175(4023):720-731.

5. Almen MS, Nordstrom KJV, Fredriksson R, & Schioth HB (2009) Mapping the human membrane proteome: a majority of the human membrane proteins can be classified according to function and evolutionary origin. *Bmc Biol* 7.

6. Mitchell P (2011) Chemiosmotic coupling in oxidative and photosynthetic phosphorylation. 1966. *Biochim Biophys Acta* 1807(12): 1507-1538.

7. Cramer WA*, et al.* (1995) Structure-Function of the Channel-Forming Colicins. *Annual Review of Biophysics and Biomolecular Structure* 24:611-641.

8. Hancock REW & Chapple DS (1999) Peptide antibiotics. *Antimicrob Agents Ch* 43(6):1317-1323.

9. Cao Y*, et al.* (2011) Crystal structure of a potassium ion transporter, TrkH. *Nature* 471(7338):336-340.

10. Holland IB & Blight MA (1999) ABC-ATPases, adaptable energy generators fuelling transmembrane movement of a variety of molecules organisms from bacteria to humans. *Journal of Molecular Biology* 293(2): 381-399.

11. Skou JC & Esmann M (1992) The Na,K-Atpase. *J Bioenerg Biomembr* 24(3):249-261.

12. Ueda K*, et al.* (1987) The Human Multidrug Resistance (Mdr1) Gene - Cdna Cloning and Transcription Initiation. *Journal of Biological Chemistry* 262(2):505-508.

13. Heginbotham L, Abramson T, & Mackinnon R (1992) A Functional Connection between the Pores of Distantly Related Ion Channels as Revealed by Mutant K+ Channels. *Science* 258(5085):1152-1155.

14. Craven KB & Zagotta WN (2006) CNG and HCN Channels: Two peas, One pod. *Annual Review of Physiology* 68:375-401.

15. Choi M*, et al.* (2011) K+ Channel Mutations in Adrenal Aldosterone-Producing Adenomas and Hereditary Hypertension. *Science* 331(6018): 768-772.

16. Sanguinetti MC & Tristani-Firouzi M (2006) hERG potassium channels and cardiac arrhythmia. *Nature* 440(7083):463-469.

17. Trankner D*, et al.* (2004) Molecular basis of an inherited form of incomplete achromatopsia. *J Neurosci* 24(1):138-147.

18. Ravens U & Cerbai E (2008) Role of potassium currents in cardiac arrhythmias. *Europace* 10(10):1133-1137.

19. Schrempf H*, et al.* (1995) A prokaryotic potassium ion channel with two predicted transmembrane segments from Streptomyces lividans. *The EMBO journal* 14(21):5170-5178.

20. Plugge B*, et al.* (2000) A potassium channel protein encoded by chlorella virus PBCV-1. *Science* 287(5458):1641-1644.

21. Jan LY & Jan YN (1997) Cloned Potassium Channels from Eukaryotes and Prokaryotes. *Annual Review of Neuroscience* 20:91-123.

22. Martinac B, Saimi Y, & Kung C (2008) Ion channels in microbes. *Physiol Rev* 88(4):1449-1490.

23. MacKinnon R & Doyle DA (1997) Prokaryotes offer hope for potassium channel structural studies. *Nat Struct Biol* 4(11):877-879.

24. Kuo MM-C, Hayes WJ, Loukin SH, Kung C, & Saimi Y (2005) Prokaryotic K+ channels: From crystal structures to diversity. *FEMS Microbiology Reviews* 29:961-985.

25. Saier MH (2000) Families of transmembrane transporters selective for amino acids and their derivatives. *Microbiology* 146:1775-1795.

26. Yu FH, Yarov-Yarovoy V, Gutman GA, & Catterall WA (2005) Overview of molecular relationships in the voltage-gated ion channel superfamily. *Pharmacol Rev* 57(4):387-395.

27. MacKinnon R (1995) Pore Loops: An Emerging Theme in Ion-Channel Structure. *Neuron* 14(5):889-892.

28. Liman ER, Tytgat J, & Hess P (1992) Subunit Stoichiometry of a Mammalian K+ Channel Determined by Construction of Multimeric Cdnas. *Neuron* 9(5):861-871.

29. Saier MH (2003) Tracing pathways of transport protein evolution. *Mol Microbiol* 48(5):1145-1156.

30. Heginbotham L, Lu Z, Abramson T, & MacKinnon R (1994) Mutations in the K+ Channel Signature Sequence. *Biophysical Journal* 66(4):1061-1067.

31. Gutman GA*, et al.* (2005) International Union of Pharmacology. LIII. Nomenclature and molecular relationships of voltage-gated potassium channels. *Pharmacol Rev* 57(4):473-508.

32. Wei AD, *et al.* (2005) International Union of Pharmacology. LII. Nomenclature and molecular relationships of calcium-activated potassium channels. *Pharmacol Rev* 57(4):463-472.

33. Kubo Y, *et al.* (2005) International Union of Pharmacology. LIV. Nomenclature and molecular relationships of inwardly rectifying potassium channels. *Pharmacol Rev* 57(4):509-526.

34. Goldstein SAN, *et al.* (2005) International Union of Pharmacology. LV. Nomenclature and molecular relationships of two-P potassium channels. *Pharmacol Rev* 57(4):527-540.

35. Cortes DM, Cuello LG, & Perozo E (2001) Molecular architecture of full-length KcsA: role of cytoplasmic domains in ion permeation and activation gating. *J Gen Physiol* 117(2):165-180.

36. Jiang YX, *et al.* (2002) Crystal structure and mechanism of a calcium-gated potassium channel. *Nature* 417(6888):515-522.

37. Brohawn SG, del Marmol J, & MacKinnon R (2012) Crystal structure of the human K2P TRAAK, a lipid- and mechano-sensitive K+ ion channel. *Science* 335(6067):436-441.

38. Miller AN & Long SB (2012) Crystal structure of the human two-pore domain potassium channel K2P1. *Science* 335(6067):432-436.

39. Long SB, Campbell EB, & Mackinnon R (2005) Crystal Structure of a Mammalian Voltage-Dependent Shaker Family K+ Channel. *Science* 309(5736):897-903.

40. Jiang YX, *et al.* (2003) X-ray structure of a voltage-dependent K+ channel. *Nature* 423(6935):33-41.

41. Clayton GM, Altieri S, Heginbotham L, Unger VM, & Morais-Cabral JH (2008) Structure of the transmembrane regions of a bacterial cyclic

nucleotide-regulated channel. *Proceedings of the National Academy of Sciences of the United States of America* 105(5):1511-1515.

42. Wu YK, Yang Y, Ye S, & Jiang YX (2010) Structure of the gating ring from the human large-conductance Ca2+-gated K+ channel. *Nature* 466(7304):393-397.

43. Warmke J, Drysdale R, & Ganetzky B (1991) A Distinct Potassium Channel Polypeptide Encoded by the Drosophila-eag Locus. *Science* 252(5012):1560-1562.

44. Morais-Cabral JH, Zhou YF, & MacKinnon R (2001) Energetic optimization of ion conduction rate by the K+ selectivity filter. *Nature* 414(6859):37-42.

45. Eisenman G & Horn R (1983) Ionic Selectivity Revisited - the Role of Kinetic and Equilibrium Processes in Ion Permeation through Channels. *J Membrane Biol* 76(3):197-225.

46. Bezanilla F & Armstrong CM (1972) Negative Conductance Caused by Entry of Sodium and Cesium Ions into Potassium Channels of Squid Axons. *Journal of General Physiology* 60(5):588-608.

47. Doyle DA*, et al.* (1998) The Structure of the Potassium Channel: Molecular Basis of K+ Conduction and Selectivity. *Science* 280(5360):69-77.

48. Zhou YF, Morais-Cabral JH, Kaufman A, & MacKinnon R (2001) Chemistry of ion coordination and hydration revealed by a K+ channel-Fab complex at 2.0 angstrom resolution. *Nature* 414(6859):43-48.

49. Valiyaveetil FI, Leonetti M, Muir TW, & MacKinnon R (2006) Ion Selectivity in a Semisynthetic K+ Channel Locked in the Conductive Conformation. *Science* 314(5801):1004-1007.

50. Valiyaveetil FI, Sekedat M, MacKinnon R, & Muir TW (2004) Glycine as a D-amino acid surrogate in the K+-selectivity filter. *Proceedings of the National Academy of Sciences of the United States of America* 101(49): 17045-17049.

51. Tao X, Avalos JL, Chen JY, & MacKinnon R (2009) Crystal Structure of the Eukaryotic Strong Inward-Rectifier K+ Channel Kir2.2 at 3.1 angstrom Resolution. *Science* 326(5960):1668-1674.

52. Kuo AL*, et al.* (2003) Crystal structure of the potassium channel KirBac1.1 in the closed state. *Science* 300(5627):1922-1926.

53. Shi N, Ye S, Alam A, Chen LP, & Jiang YX (2006) Atomic structure of a Na+- and K+-conducting channel. *Nature* 440(7083):570-574.

54. Alam A & Jiang YX (2009) Structural analysis of ion selectivity in the NaK channel. *Nature Structural & Molecular Biology* 16(1):35-41.

55. Ye S, Li Y, & Jiang YX (2010) Novel insights into K+ selectivity from high-resolution structures of an open K+ channel pore. *Nature Structural & Molecular Biology* 17(8):1019-1865.

56. Payandeh J, Scheuer T, Zheng N, & Catterall WA (2011) The crystal structure of a voltage-gated sodium channel. *Nature* 475(7356):353-358.

57. Alam A & Jiang YX (2011) Structural studies of ion selectivity in tetrameric cation channels. *Journal of General Physiology* 137(5):397-403.

58. Andersen OS (2011) Perspectives on: Ion selectivity. *Journal of General Physiology* 137(5):393-395.

59. Dixit PD & Asthagiri D (2011) Thermodynamics of ion selectivity in the KcsA K+ channel. *Journal of General Physiology* 137(5):427-433.

60. Nimigean CM & Allen TW (2011) Origins of ion selectivity in potassium channels from the perspective of channel block. *Journal of General Physiology* 137(5):405-413.

61. Roux B, *et al.* (2011) Ion selectivity in channels and transporters. *Journal of General Physiology* 137(5):415-426.

62. Varma S, Rogers DM, Pratt LR, & Rempe SB (2011) Design principles for K+ selectivity in membrane transport. *Journal of General Physiology* 137(6):479-488.

63. Mullins LJ (1960) An Analysis of Pore Size in Excitable Membranes. *Journal of General Physiology* 43:105-117.

64. Noskov SY, Berneche S, & Roux B (2004) Control of ion selectivity in potassium channels by electrostatic and dynamic properties of carbonyl ligands. *Nature* 431(7010):830-834.

65. Noskov SY & Roux B (2007) Importance of Hydration and Dynamics on the Selectivity of the KcsA and NaK Channels. *Journal of General Physiology* 129(2):135-143.

66. Bostick DL & Brooks CL (2007) Selectivity in K+ channels is due to topological control of the permeant ion's coordinated state. *Proceedings of the National Academy of Sciences of the United States of America* 104(22): 9260-9265.

67. Nimigean CM & Miller C (2002) Na+ block and permeation in a K+ channel of known structure. *Journal of General Physiology* 120(3):323-335.

68. Thompson AN, *et al.* (2009) Mechanism of potassium-channel selectivity revealed by Na+ and Li+ binding sites within the KcsA pore. *Nature Structural & Molecular Biology* 16(12):1317-1324.

69. Yang J, Yu M, Jan YN, & Jan LY (1997) Stabilization of ion selectivity filter by pore loop ion pairs in an inwardly rectifying potassium channel. *Proceedings of the National Academy of Sciences of the United States of America* 94(4):1568-1572.

70. Alam A, Shi N, & Jiang YX (2007) Structural insight into Ca2+ specificity in tetrameric cation channels. *Proceedings of the National Academy of Sciences of the United States of America* 104(39):15334-15339.

71. Derebe MG, Zeng W, Li Y, Alam A, & Jiang Y (2011) Structural studies of ion permeation and Ca2+ blockage of a bacterial channel mimicking the cyclic nucleotide-gated channel pore. *Proceedings of the National Academy of Sciences of the United States of America* 108(2):592-597.

72. Cordero-Morales JF, *et al.* (2006) Molecular determinants of gating at the potassium-channel selectivity filter. *Nature Structural & Molecular Biology* 13(4):311-318.

73. Cordero-Morales JF, *et al.* (2007) Molecular driving forces determining potassium channel slow inactivation. *Nature Structural & Molecular Biology* 14(11):1062-1069.

74. Chatelain FC, *et al.* (2009) Selection of Inhibitor-Resistant Viral Potassium Channels Identifies a Selectivity Filter Site that Affects Barium and Amantadine Block. *PLoS ONE* 4(10):e7496.

75. Alam A & Jiang YX (2009) High-resolution structure of the open NaK channel. *Nature Structural & Molecular Biology* 16(1):30-34.

76. Finn RD, *et al.* (2010) The Pfam protein families database. *Nucleic Acids Res* 38:D211-D222.

77. Pei JM, Kim BH, & Grishin NV (2008) PROMALS3D: a tool for multiple protein sequence and structure alignments. *Nucleic Acids Res* 36(7): 2295-2300.

78. Sauer DB, Zeng WZ, Raghunathan S, & Jiang YX (2011) Protein interactions central to stabilizing the K(+) channel selectivity filter in a four-sited configuration for selective K(+) permeation. *Proceedings of the National Academy of Sciences of the United States of America* 108(40):16634-16639.

79. Chang AB, Lin R, Keith Studley W, Tran CV, & Saier MH, Jr. (2004) Phylogeny as a guide to structure and function of membrane transport proteins. *Molecular membrane biology* 21(3):171-181.

80. Thompson JD, Higgins DG, & Gibson TJ (1994) CLUSTAL W: improving the sensitivity of progressive multiple sequence alignment through sequence weighting, position-specific gap penalties and weight matrix choice. *Nucleic Acids Res* 22(22):4673-4680.

81. Waterhouse AM, Procter JB, Martin DMA, Clamp M, & Barton GJ (2009) Jalview Version 2-a multiple sequence alignment editor and analysis workbench. *Bioinformatics* 25(9):1189-1191.

82. Schneider TD & Stephens RM (1990) Sequence Logos - a New Way to Display Consensus Sequences. *Nucleic Acids Res* 18(20):6097-6100.

83. Crooks GE, Hon G, Chandonia JM, & Brenner SE (2004) WebLogo: A sequence logo generator. *Genome Res* 14(6):1188-1190.

84. Bernstein FC, *et al.* (1977) Protein Data Bank - Computer-Based Archival File for Macromolecular Structures. *Journal of Molecular Biology* 112(3):535-542.

85. Holland RCG, *et al.* (2008) BioJava: an open-source framework for bioinformatics. *Bioinformatics* 24(18):2096-2097.

86. Derebe MG, *et al.* (2011) Tuning the ion selectivity of tetrameric cation channels by changing the number of ion binding sites. *Proceedings of the National Academy of Sciences of the United States of America* 108(2): 598-602.

87. Otwinowski Z & Minor W (1997) Processing of X-Ray Diffraction Data Collected in Oscillation Mode. *Method Enzymol* 276:307-326.

88. Emsley P, Lohkamp B, Scott LR, & Cowtan K (2010) Features and Development of Coot. *Acta Crystallogr D* 66:486-501.

89. Adams PD*, et al.* (2010) PHENIX: a comprehensive Python-based system for macromolecular structure solution. *Acta Crystallogr D* 66:213-221.

90. Schrodinger, LLC (2010) The PyMOL Molecular Graphics System, Version 1.3r1.

91. Pettersen EF*, et al.* (2004) UCSF chimera - A visualization system for exploratory research and analysis. *J Comput Chem* 25(13):1605-1612.

92. Giorgetti A, Carloni P, Mistrik P, & Torre V (2005) A Homology Model of the Pore Region of HCN Channels. *Biophysical Journal* 89(2):932-944.

93. Shin N, Soh H, Chang S, Kim DH, & Park CS (2005) Sodium permeability of a cloned small-conductance calcium-activated potassium channel. *Biophysical Journal* 89(5):3111-3119.

94. Kuner T, Seeburg PH, & Guy HR (2003) A common architecture for K+ channels and ionotropic glutamate receptors? *Trends Neurosci* 26(1):27-32.

95. Chapman ML, Krovetz HS, & VanDongen AMJ (2001) GYGD pore motifs in neighbouring potassium channel subunits interact to determine ion selectivity. *Journal of Physiology-London* 530(1):21-33.

96. Chapman M, Blanke M, Krovetz H, & VanDongen A (2006) Allosteric effects of external K+ ions mediated by the aspartate of the GYGD signature sequence in the Kv2.1 K+ channel. *Pflugers Archiv-European Journal of Physiology* 451(6):776-792.

97. Haug T, Olcese R, Toro L, & Stefani E (2004) Regulation of K+ Flow by a Ring of Negative Charges in the Outer Pore of BKCa Channels. Part II: Neutralization of Aspartate 292 Reduces Long Channel Openings and Gating Current Slow Component. *Journal of General Physiology* 124(2):185-197.

98. Haug T*, et al.* (2004) Regulation of K+ Flow by a Ring of Negative Charges in the Outer Pore of BKCa Channels. Part I: Aspartate 292 modulates K+ Conduction by External Surface Charge Effect. *Journal of General Physiology* 124(2):173-184.

99. Roller A*, et al.* (2005) In the yeast potassium channel, Tok1p, the external ring of aspartate residues modulates both gating and conductance. *Pflugers Archiv-European Journal of Physiology* 451(2):362-370.

100. Bucher D, Guidoni L, & Rothlisberger U (2007) The Protonation State of the Glu-71/Asp-80 Residues in the KcsA Potassium Channel: A First-Principles QM/MM Molecular Dynamics Study. *Biophysical Journal* 93(7): 2315-2324.

101. Shealy RT, Murphy AD, Ramarathnam R, Jakobsson E, & Subramaniam S (2003) Sequence-Function Analysis of the K+-Selective Family of Ion Channels Using a Comprehensive Alignment and the KcsA Channel Structure. *Biophysical Journal* 84(5):2929-2942.

102. Kumpf RA & Dougherty DA (1993) A Mechanism for Ion Selectivity in Potassium Channels - Computational Studies of Cation-Pi Interactions. *Science* 261(5129):1708-1710.

103. Kirsch GE, Pascual JM, & Shieh CC (1995) Functional-Role of a Conserved Aspartate in the External Mouth of Voltage-Gated Potassium Channels. *Biophysical Journal* 68(5):1804-1813.

104. Nishida M, Cadene M, Chait BT, & MacKinnon R (2007) Crystal structure of a Kir3.1-prokaryotic Kir channel chimera. *EMBO Journal* 26(17): 4005-4015.

105. Clarke OB*, et al.* (2010) Domain Reorientation and Rotation of an Intracellular Assembly Regulate Conduction in Kir Potassium Channels. *Cell* 141(6):1018-1029.

106. Horton JR, Upadhyay AK, Hashimoto H, Zhang X, & Cheng X (2011) Structural basis for human PHF2 Jumonji domain interaction with metal ions. *J Mol Biol* 406(1):1-8.

107. Schipke CG, Goodin DB, McRee DE, & Stout CD (1999) Oxidized and reduced Azotobacter vinelandii ferredoxin I at 1.4 A resolution: conformational change of surface residues without significant change in the [3Fe-4S]+/0 cluster. *Biochemistry* 38(26):8228-8239.

108. Ricagno S, de Rosa M, Aliverti A, Zanetti G, & Bolognesi M (2007) The crystal structure of FdxA, a 7Fe ferredoxin from Mycobacterium smegmatis. *Biochem Biophys Res Commun* 360(1):97-102.

109. Warmke JW & Ganetzky B (1994) A family of potassium channel genes related to eag in Drosophila and mammals. *Proceedings of the National Academy of Sciences of the United States of America* 91(8):3438-3442.

110. Mullins FM, Stepanovic SZ, Desai RR, George AL, & Balser JR (2002) Extracellular sodium interacts with the HERG channel at an outer pore site. *Journal of General Physiology* 120(4):517-537.

111. Bruggemann A, Pardo LA, Stuhmer W, & Pongs O (1993) Ether-a-go-go encodes a voltage-gated channel permeable to K+ and Ca2+ and modulated by cAMP. *Nature* 365(6445):445-448.

112. Chakrapani S, Cordero-Morales JF, & Perozo E (2007) A quantitative description of KcsA Gating II: Single-channel currents. *Journal of General Physiology* 130(5):479-496.

113. Chapman ML & VanDongen AMJ (2005) K channel subconductance levels result from heteromeric pore conformations. *Journal of General Physiology* 126(2):87-103.

114. Zheng J & Sigworth FJ (1997) Selectivity changes during activation of mutant Shaker potassium channels. *Journal of General Physiology* 110(2): 101-117.

115. Bett GCL, Dinga-Madou I, Zhou QL, Bondarenko VE, & Rasmusson RL (2011) A Model of the Interaction between N-type and C-type Inactivation in Kv1.4 Channels. *Biophysical Journal* 100(1):11-21.

116. Baukrowitz T & Yellen G (1995) Modulation of K+ Current by Frequency and External [K+] - a Tale of 2 Inactivation Mechanisms. *Neuron* 15(4):951-960.

117. Starkus JG, Kuschel L, Rayner MD, & Heinemann SH (1997) Ion Conduction through C-type Inactivated Shaker Channels. *Journal of General Physiology* 110(5):539-550.

118. Starkus JG, Kuschel L, Rayner MD, & Heinemann SH (1998) Macroscopic Na+ Currents in the "Nonconducting" Shaker Potassium Channel Mutant W434F. *Journal of General Physiology* 112(1):85-93.

119. Cheng WWL, Mccoy JG, Thompson AN, Nichols CG, & Nimigean CM (2011) Mechanism for selectivity-inactivation coupling in KcsA potassium channels. *Proceedings of the National Academy of Sciences of the United States of America* 108(13):5272-5277.

120. Cordero-Morales JF, Jogini V, Chakrapani S, & Perozo E (2011) A Multipoint Hydrogen-Bond Network Underlying KcsA C-Type Inactivation. *Biophysical Journal* 100(10):2387-2393.

121. Cuello LG, Jogini V, Cortes DM, & Perozo E (2010) Structural mechanism of C-type inactivation in K+ channels. *Nature* 466(7303): 203-208.

122. Cuello LG, *et al.* (2010) Structural basis for the coupling between activation and inactivation gates in K(+) channels. *Nature* 466(7303):272-U154.

123. Chakrapani S, *et al.* (2011) On the structural basis of modal gating behavior in K+ channels. *Nature Structural & Molecular Biology* 18(1):67-74.

124. Migeon MB, *et al.* (1992) Cloning, Sequence and Chromosomal Localization of Mk6, a Murine Potassium Channel Gene. *Epilepsy Res*:173-181.

125. Yang YS, Yan YY, & Sigworth FJ (1997) How Does the W434F Mutation Block Current in Shaker Potassium Channels? *Journal of General Physiology* 109(6):779-789.

126. Proks P, Capener CE, Jones P, & Ashcroft FM (2001) Mutations within the P-loop of Kir6.2 modulate the intraburst kinetics of the ATP-sensitive potassium channel. *Journal of General Physiology* 118(4):341-353.

127. Zhou YF & MacKinnon R (2003) The Occupancy of Ions in the K+ Selectivity Filter: Charge Balance and Coupling of Ion Binding to a Protein Conformational Change Underlie High Conduction Rates. *Journal of Molecular Biology* 333(5):965-975.

128. Lockless SW, Zhou M, & MacKinnon R (2007) Structural and Thermodynamic Properties of Selective Ion Binding in a K+ Channel. *PLoS Biology* 5(5):1079-1088.

129. Neyton J & Miller C (1988) Potassium Blocks Barium Permeation through a Calcium-Activated Potassium Channel. *Journal of General Physiology* 92(5):549-567.

130. Neyton J & Miller C (1988) Discrete Ba2+ Block as a Probe of Ion Occupancy and Pore Structure in the High-Conductance Ca2+-Activated K+ Channel. *Journal of General Physiology* 92(5):569-586.

131. Jiang YX & MacKinnon R (2000) The Barium Site in a Potassium Channel by X-ray Crystallography. *Journal of General Physiology* 115(3): 269-272.

132. Einsle O*, et al.* (2002) Nitrogenase MoFe-protein at 1.16 angstrom resolution: A central ligand in the FeMo-cofactor. *Science* 297(5587): 1696-1700.

133. Piasta KN, Theobald DL, & Miller C (2011) Potassium-selective block of barium permeation through single KcsA channels. *Journal of General Physiology* 138(4):421-436.

134. Margolskee RF (2002) Molecular mechanisms of bitter and sweet taste transduction. *Journal of Biological Chemistry* 277(1):1-4.

135. Richter TA, Dvoryanchikov GA, Chaudhari N, & Roper SD (2004) Acid-sensitive two-pore domain potassium (K2P) channels in mouse taste buds. *J Neurophysiol* 92(3):1928-1936.

136. Ashcroft FM (2005) ATP-sensitive potassium channelopathies: focus on insulin secretion. *J Clin Invest* 115(8):2047-2058.

137. Giebisch G (1998) Renal potassium transport: mechanisms and regulation. *Am J Physiol-Renal* 274(5):F817-F833.

138. Simon DB*, et al.* (1996) Genetic heterogeneity of Bartter's syndrome revealed by mutations in the K+ channel, ROMK. *Nat Genet* 14(2):152-156.

139. Graves TD (2006) Ion channels and epilepsy. *Qjm-Int J Med* 99(4): 201-217.

140. Zhou M & MacKinnon R (2004) A Mutant KcsA K+ Channel with Altered Conduction Properties and Selectivity Filter Ion Distribution. *Journal of Molecular Biology* 338(4):839-846.

141. Kang M*, et al.* (2004) Small potassium ion channel proteins encoded by chlorella viruses. *Proceedings of the National Academy of Sciences of the United States of America* 101(15):5318-5324.

142. Wolfe-Simon F*, et al.* (2011) Response to Comments on "A Bacterium That Can Grow Using Arsenic Instead of Phosphorus". *Science* 332(6034): 1163-1166.

143. Rhoades RA & Tanner GA (1995) *Medical Physiology* (Little, Brown and Company, New York) 1st Edition Ed p 839.

144. Murer H, Forster I, & Biber J (2004) The sodium phosphate cotransporter family SLC34. *Pflugers Arch* 447(5):763-767.

145. Werner A & Kinne RK (2001) Evolution of the Na-P(i) cotransport systems. *Am J Physiol Regul Integr Comp Physiol* 280(2):R301-312.

146. Bellocchio EE, Reimer RJ, Fremeau RT, & Edwards RH (2000) Uptake of glutamate into synaptic vesicles by an inorganic phosphate transporter. *Science* 289(5481):957-960.

147. Virkki LV, Biber J, Murer H, & Forster IC (2007) Phosphate transporters: a tale of two solute carrier families. *Am J Physiol-Renal* 293(3):F643-F654.

148. Runswick MJ, Powell SJ, Nyren P, & Walker JE (1987) Sequence of the bovine mitochondrial phosphate carrier protein: structural relationship to

ADP/ATP translocase and the brown fat mitochondria uncoupling protein. *The EMBO journal* 6(5):1367-1373.

149. Palmieri F (2004) The mitochondrial transporter family (SLC25): physiological and pathological implications. *Pflugers Arch* 447(5):689-709.

150. Pebay-Peyroula E*, et al.* (2003) Structure of mitochondrial ADP/ATP carrier in complex with carboxyatractyloside. *Nature* 426(6962):39-44.

151. Collins JF, Bai L, & Ghishan FK (2004) The SLC20 family of proteins: dual functions as sodium-phosphate cotransporters and viral receptors. *Pflugers Arch* 447(5):647-652.

152. Saliba KJ*, et al.* (2006) Sodium-dependent uptake of inorganic phosphate by the intracellular malaria parasite. *Nature* 443(7111):582-585.

153. Rosenberg H, Gerdes RG, & Chegwidden K (1977) 2 Systems for Uptake of Phosphate in Escherichia-Coli. *Journal of bacteriology* 131(2): 505-511.

154. Raghothama KG & Karthikeyan AS (2005) Phosphate acquisition. *Plant Soil* 274(1-2):37-49.

155. Persson BL*, et al.* (1999) Phosphate permeases of Saccharomyces cerevisiae: structure, function and regulation. *Biochim Biophys Acta* 1422(3): 255-272.

156. Rausch C*, et al.* (2001) A phosphate transporter expressed in arbuscule-containing cells in potato. *Nature* 414(6862):462-470.

157. Paszkowski U, Kroken S, Roux C, & Briggs SP (2002) Rice phosphate transporters include an evolutionarily divergent gene specifically activated in arbuscular mycorrhizal symbiosis. *Proceedings of the National Academy of Sciences of the United States of America* 99(20):13324-13329.

158. Quiocho FA & Ledvina PS (1996) Atomic structure and specificity of bacterial periplasmic receptors for active transport and chemotaxis: Variation of common themes. *Mol Microbiol* 20(1):17-25.

159. Quiocho FA (1996) Atomic basis of the exquisite specificity of phosphate and sulfate transport receptors. *Kidney Int* 49(4):943-946.

160. Wang ZM, Choudhary A, Ledvina PS, & Quiocho FA (1994) Fine-Tuning the Specificity of the Periplasmic Phosphate-Transport Receptor - Site-Directed Mutagenesis, Ligand-Binding, and Crystallographic Studies. *Journal of Biological Chemistry* 269(40):25091-25094.

161. Ziegler C, Ressl S, van Scheltinga ACT, Vonrhein C, & Ott V (2009) Molecular basis of transport and regulation in the Na(+)/betaine symporter BetP. *Nature* 458(7234):47-52.

162. Toyoshima C, Nakasako M, Nomura H, & Ogawa H (2000) Crystal structure of the calcium pump of sarcoplasmic reticulum at 2.6 angstrom resolution. *Nature* 405(6787):647-655.

163. Ziegler C*, et al.* (2011) Substrate specificity and ion coupling in the Na(+)/betaine symporter BetP. *Embo Journal* 30(7):1221-1229.

164. Axelsen KB & Palmgren MG (1998) Evolution of substrate specificities in the P-type ATPase superfamily. *J Mol Evol* 46(1):84-101.

165. Kavanaugh MP*, et al.* (1994) Cell-surface receptors for gibbon ape leukemia virus and amphotropic murine retrovirus are inducible sodium-dependent phosphate symporters. *Proc Natl Acad Sci U S A* 91(15): 7071-7075.

166. Salaun C, Rodrigues P, & Heard JM (2001) Transmembrane topology of PiT-2, a phosphate transporter-retrovirus receptor. *J Virol* 75(12): 5584-5592.

167. Bottger P & Pedersen L (2002) Two highly conserved glutamate residues critical for type III sodium-dependent phosphate transport revealed by uncoupling transport function from retroviral receptor function. *The Journal of biological chemistry* 277(45):42741-42747.

168. Bottger P & Pedersen L (2005) Evolutionary and experimental analyses of inorganic phosphate transporter PiT family reveals two related signature sequences harboring highly conserved aspartic acids critical for sodium-dependent phosphate transport function of human PiT2. *The FEBS journal* 272(12):3060-3074.

169. Mansilla MC & de Mendoza D (2000) The Bacillus subtilis cysP gene encodes a novel sulphate permease related to the inorganic phosphate transporter (Pit) family. *Microbiology (Reading, England)* 146 (Pt 4): 815-821.

170. Johns S TOPO2, Transmembrane protein display software.

171. Hoffer SM, Schoondermark P, van Veen HW, & Tommassen J (2001) Activation by gene amplification of pitB, encoding a third phosphate transporter of Escherichia coli K-12. *Journal of bacteriology* 183(15): 4659-4663.

172. Hughes MF (2002) Arsenic toxicity and potential mechanisms of action. *Toxicol Lett* 133(1):1-16.

173. Moraes TF, Bains M, Hancock RE, & Strynadka NC (2007) An arginine ladder in OprP mediates phosphate-specific transfer across the outer membrane. *Nat Struct Mol Biol* 14(1):85-87.